https://ntrs.nasa.gov/search.jsp?R=19830002748 2020-03-21T06:35:35+00:00Z

[redacted]

[redacted]

NASA TECHNICAL MEMORANDUM

NASA TM X-3355

[redacted]

NASA TM X-3355

[redacted] CLASSIFIED
BY Security Classification Officer, NASA LaRC
SUBJECT TO GENERAL DECLASSIFICATION SCHEDULE OF EXECUTIVE ORDER 11652 AUTOMATICALLY DOWNGRADED AT TWO YEAR INTERVALS AND DECLASSIFIED ON DEC 31 1982

INVESTIGATION OF SOME EFFECTS OF HUMIDITY ON AERODYNAMIC CHARACTERISTICS OF A 10-PERCENT-THICK NASA SUPERCRITICAL AIRFOIL (U)

Frank L. Jordan, Jr.

Langley Research Center
Hampton, Va. 23665

NATIONAL AERONAUTICS AND SPACE ADMINISTRATION • WASHINGTON, D. C. • MARCH 1976

[redacted]

[redacted]

1. Report No.	2. Government Accession No.	3. Recipient's Catalog No.
NASA TM X-3355		

4. Title and Subtitle	5. Report Date
INVESTIGATION OF SOME EFFECTS OF HUMIDITY ON AERODYNAMIC CHARACTERISTICS OF A 10-PERCENT-THICK NASA SUPERCRITICAL AIRFOIL (U)	March 1976
	6. Performing Organization Code
7. Author(s)	8. Performing Organization Report No.
Frank L. Jordan, Jr.	L-10606
	10. Work Unit No.
9. Performing Organization Name and Address	505-06-31-02
NASA Langley Research Center Hampton, Va. 23665	11. Contract or Grant No.
	13. Type of Report and Period Covered
12. Sponsoring Agency Name and Address	Technical Memorandum
National Aeronautics and Space Administration Washington, D.C. 20546	14. Sponsoring Agency Code

15. Supplementary Notes

16. Abstract

(U) An investigation has been conducted in the Langley 8-foot transonic pressure tunnel to determine the effects of wind-tunnel humidity on the aerodynamic characteristics of a 10-percent-thick NASA supercritical airfoil. Effects of dewpoint variation from 267 K (20° F) to 294 K (70° F) were investigated. The tunnel stagnation temperature was 322 K (120° F) and the stagnation pressure was 0.1013 MN/m^2 (1 atm).

17. Key Words (Suggested by Author(s))

Supercritical airfoil
Humidity effects
Wind-tunnel testing

19. Security Classif. (of this report)	20. Security Classif. (of this page)	21. No. of Pages	22. Price
[redacted]	Unclassified	67	

INVESTIGATION OF SOME EFFECTS OF HUMIDITY ON AERODYNAMIC CHARACTERISTICS OF A 10-PERCENT-THICK NASA SUPERCRITICAL AIRFOIL (U)

Frank L. Jordan, Jr.
Langley Research Center

(U) SUMMARY

(U) An investigation has been conducted in the Langley 8-foot transonic pressure tunnel to determine the effects of wind-tunnel humidity on the aerodynamic characteristics of a 10-percent-thick NASA supercritical airfoil. Effects of dewpoint variation from 267 K (20° F) to 294 K (70° F) were investigated. The tunnel stagnation temperature was 322 K (120° F) and the stagnation pressure was 0.1013 MN/m^2 (1 atm).

(U) Effects of condensation originating principally in the local region of supersonic flow over the airfoil upper surface were small for conditions well beyond local saturation but became significant for some test conditions before free-stream saturation. For airfoil normal-force coefficients near design value, these effects were small, but for relatively high normal-force coefficients, they were significant. Airfoil upper-surface pressures increased in the region of supersonic flow and resulted in a decrease in lift coefficient. Local condensation generally decreased stagnation pressures in the airfoil wake and thus increased drag coefficient.

(U) The occurrence of condensation in the free stream corresponded approximately to the onset of estimated free-stream saturation. It was accompanied by further effects on airfoil test data similar to those caused by local condensation.

(U) INTRODUCTION

(U) The present investigation of the effects of humidity on a 10-percent-thick NASA supercritical airfoil is a continuation of an earlier humidity investigation (ref. 1) conducted on a representative model incorporating an NASA supercritical wing. Results obtained during the earlier investigation demonstrated that condensation originating only in the local expansion regions around the model can cause significant effects on model test data. Wing upper-surface pressures were increased in the region of supersonic flow beginning near the leading edge. These effects on wing pressure, believed to be caused by condensation in the local regions of supersonic flow over the wings, resulted in significant reductions in lift coefficient.

(U) The present two-dimensional investigation was conducted to provide additional information on the effects of humidity on the aerodynamic characteristics of NASA supercritical wings. A representative 10-percent-thick NASA supercritical airfoil with a chord of 63.5 cm (25.0 in.) was used. (See refs. 2 and 3.) Effects of both local and free-stream condensation on model chordwise pressure distributions, wake profiles, and resulting aerodynamic force and moment coefficients are presented. Tunnel humidity corresponding to significant effects in data is compared with tunnel humidities corresponding to local and free-stream saturation conditions.

(U) SYMBOLS

(U) Values are given in both the International System of Units (SI) and U.S. Customary Units. Measurements and calculations are made in U.S. Customary Units.

(U) The terms, equations, and charts used to describe the properties of humid air can be found in the existing literature (refs. 4 and 5, for example) and are not included in the present report.

C_p pressure coefficient, $\frac{p_l - p_\infty}{q_\infty}$

$C_{p,sat}$ pressure coefficient corresponding to saturation Mach number M_{sat}

$C_{p,sonic}$ pressure coefficient corresponding to local Mach number of 1.0

c chord of airfoil, 63.5 cm (25.0 in.)

c_d section drag coefficient, $\sum_{\text{Wake}} c_d' \frac{\Delta z}{c}$

c_d' point drag coefficient (ref. 6)

c_m section pitching-moment coefficient about the quarter-chord point,

$$\sum_{\substack{\text{Lower}\\ \text{surface}}} C_p\left(0.25 - \frac{x}{c}\right)\frac{\Delta x}{c} - \sum_{\substack{\text{Upper}\\ \text{surface}}} C_p\left(0.25 - \frac{x}{c}\right)\frac{\Delta x}{c}$$

c_n section normal-force coefficient, $\sum_{\substack{\text{Lower}\\ \text{surface}}} C_p \frac{\Delta x}{c} - \sum_{\substack{\text{Upper}\\ \text{surface}}} C_p \frac{\Delta x}{c}$

K surface curvature, reciprocal of local radius of curvature

M Mach number

M_{sat} Mach number of a given isentropic expansion of moist air where partial pressure of water vapor in the flow is equal to saturation pressure of water vapor at flow temperature (see ref. 4)

m slope of airfoil surface, $\frac{dy}{dx}$

p static pressure, N/m^2 (lb/ft^2)

Δp_t total-pressure loss, N/m^2 (lb/ft^2)

q dynamic pressure, N/m^2 (lb/ft^2)

R Reynolds number based on airfoil chord

s tunnel test-section semispan at slot origin, 1.087 m (3.563 ft)

T_{dp} tunnel dewpoint measured at pressure of 0.1013 MN/m^2 (1 atm), K $(^{\circ}F)$

$T_{dp,sat}$ dewpoint at pressure of 0.1013 MN/m^2 (1 atm) corresponding to saturated flow at a specified Mach number

x coordinate along airfoil reference line measured from airfoil leading edge; coordinate along test-section center line measured from test-section slot origin; cm (in.)

Δx incremental distance along airfoil reference line, cm (in.)

y ordinate normal to airfoil reference line, cm (in.)

z vertical distance in wake profile measured from bottom of rake, cm (in.)

Δz incremental vertical distance in wake profile, cm (in.)

α angle of attack of airfoil reference line relative to test-section center line, deg

Subscripts:

L lower surface

l	local point on airfoil
max	maximum
U	upper surface
∞	free stream

Abbreviations:

L.E.	leading edge
T.E.	trailing edge

APPARATUS AND PROCEDURES

(U) Wind Tunnel

(U) The investigation was conducted in the Langley 8-foot transonic pressure tunnel (ref. 7). This continuous-flow, variable-pressure wind tunnel has a 2.16-m-square (7.1-ft-square) test section with filleted corners so that the total cross-sectional area is equivalent to a 2.44-m-diameter (8-ft-diameter) circle. The upper and lower test-section walls are axially slotted to permit testing through the transonic speed range. The total slot width at the position of the model averaged about 5 percent of the width of the upper and lower walls. The solid side walls and slotted upper and lower walls make this tunnel relatively well suited to the investigation of two-dimensional models since the side walls act as end plates while the slots permit development of the flow field in the vertical direction.

(U) The tunnel controls allow independent variation of Mach number, stagnation pressure, temperature, and specific humidity. Since atmospheric dewpoints above approximately 283 K (50° F) cannot be obtained except on very humid days, water was injected into the airflow downstream of the test section. Once introduced into the closed circuit of the tunnel, the added moisture remained in the flow and raised the dewpoint to the desired test level.

(U) The interior of the test section can be observed through windows in the side walls. Observations were made of the amount and distribution of condensation in the test-section flow for all test conditions.

[redacted] Model

[redacted] The two-dimensional model had a chord length of 63.5 cm (25.0 in.) and a 10-percent-thick NASA supercritical airfoil section. During the supercritical airfoil development program a numbering system was used for identifying each airfoil tested as the program progressed. The airfoil used in the present investigation was designated number 22. It was developed during a recent stage of the program in which a supercritical airfoil optimized for a normal-force coefficient of about 0.55 was being sought. (See refs. 2 and 3.)

[redacted] A sketch of the airfoil is shown in figure 1, and coordinates are presented in table I. Chordwise distributions of the airfoil surface slopes and curvatures are presented in figures 2 and 3, respectively. Photographs of the airfoil and the profile drag rake mounted in the tunnel are shown in figure 4. The airfoil included a trailing-edge cavity (see the insert in fig. 1 and the photographs of fig. 4) which had a favorable effect on the wake as discussed in reference 8. The model was mounted in an inverted position and spanned the width of the tunnel with a span-to-chord ratio of 3.4. Angle of attack was changed manually by rotating the model about pivots in the tunnel side walls. Further details of the airfoil mounted in the tunnel and the profile drag rake are shown in figure 5.

([redacted] Boundary-Layer Transition

([redacted] On the basis of the technique discussed in reference 9, boundary-layer transition was fixed along the 28-percent chord line on the upper and lower surfaces of the model in an attempt to simulate full-scale Reynolds numbers ranging from about 23×10^6 to 28×10^6 by providing the same relative trailing-edge boundary-layer displacement thickness at model scale as would exist at full-scale flight conditions. The transition trips consisted of 0.25-cm-wide (0.10-in.-wide) bands of No. 90 carborundum grains.

[redacted] It is recognized that this simulation technique is not valid for test conditions at which the shock wave on the airfoil upper surface is located ahead of the transition trip, since the technique requires that laminar flow be maintained ahead of the trip. This, however, is not believed to be a serious limitation to the investigation of effects of humidity on airfoil pressure profiles.

([redacted] Measurements

[redacted] Airfoil surface pressure measurements.- Normal forces and pitching moments acting on the airfoil were determined from surface static-pressure measurements. Surface pressure measurements were obtained from a chordwise row of orifices located approximately 0.32c from the tunnel center line. (See fig. 5.) Orifices were concentrated near the leading and trailing edges of the airfoil to define the severe pressure gradients in these regions. In addition, a rearward facing orifice was included in the cavity at the

trailing edge (identified at an airfoil upper-surface x/c location of 1.00). The transducers used in the differential-pressure scanning valves used to measure the static pressure at the airfoil surface had a range of ±68.9 kN/m^2 (10 lb/in^2).

(U) Wake measurements.- Drag forces acting on the airfoil, as measured by the momentum loss within the wake, were derived from vertical variations of the total and static pressures measured across the wake with the profile drag rake shown in figure 5. The profiles, schematically illustrated in figure 6, represent the momentum losses as indicated by stagnation-pressure deficits across the wake. The peak or center section of these profiles reflects primarily viscous losses in the boundary layer, whereas the outer portions of the profile reflect separation losses and direct losses in stagnation pressure across the airfoil shock waves. The rake was positioned in the vertical center-line plane of the tunnel, approximately one chord length rearward of the trailing edge of the airfoil. The total-pressure tubes were flattened horizontally and closely spaced vertically (0.36 percent of the airfoil chord apart) in the region of the wake associated with skin-friction boundary-layer losses. Outside this region the tube vertical spacing progressively widened until, in the region above the wing where only shock losses were anticipated, the total-pressure tubes were spaced about 7.2 percent of the chord apart. Static-pressure tubes were distributed as shown in figure 5. The rake was attached to the conventional center-line sting mount of the tunnel which permitted it to be moved vertically to center the concentration of tubes on the boundary-layer wake. Total and static pressure across the wake were measured with differential-pressure scanning valves. The transducer [redacted] the differential-pressure scanning valve connected to total-pressure tubes intended to measure boundary-layer losses had a range of ±17.2 kN/m^2 (2.5 lb/in^2), and the transducers in the valves for measuring shock losses and static pressure had a range of ±6.9 kN/m^2 (1 lb/in^2).

(U) Mach number measurements in the test section.- Axial Mach number distributions along the top and side walls of the test section were determined from surface static pressures. These static pressures were also measured by means of differential-pressure scanning valves. Transducers in the valves used to measure tunnel-wall pressures had ranges of ±34.4 kN/m^2 (5.0 lb/in^2) and ±6.9 kN/m^2 (1.0 lb/in^2). The row of static-pressure orifices in the side wall of the test section was located 0.26 m (10.4 in.) above the test-section center line.

(U) Reduction of Data

(U) Section normal-force and pitching-moment coefficients were obtained by numerical integration (based on the trapezoidal method) of the local surface pressure coefficient measured at each orifice multiplied by an appropriate weighting factor (incremental area). To obtain section drag coefficients, point drag coefficients were computed for each total- and static-pressure measurement in the wake by means of the procedure of reference 6.

The point drag coefficients were then summed by numerical integration across the wake, again based on the trapezoidal method.

TEST CONDITIONS

Tests were conducted at Mach numbers from 0.60 to 0.83 at a tunnel stagnation pressure of 0.1013 MN/m^2 (1 atm) with resultant Reynolds numbers based on the airfoil chord as shown in figure 7. Data were taken at dewpoints from 267 K (20° F) to 294 K (70° F) at a stagnation temperature of 322 K (120° F). The airfoil was set at angles of attack of 1.0°, 2.0°, and 3.5° relative to the test-section center line.

(U) Dewpoint corresponding to free-stream saturation $T_{dp,sat,\infty}$ and dewpoint corresponding to local saturation in the region of supersonic flow over the airfoil $T_{dp,sat,l}$ are listed in table II for each test condition. Saturation dewpoint in the supersonic region was determined from maximum local Mach number $M_{l,max}$ at each test condition.

RESULTS AND DISCUSSION

(U) Observation of Condensation in Test-Section Flow

(U) Condensation originating in local expansion region.- As expected, condensation was first seen in the region of supersonic flow over the airfoil upper surface. Appearing as a thin layer at the airfoil surface and uniformly distributed across the span, it followed the airfoil curvature to the trailing edge and trailed downstream into the tunnel diffuser. The thickness of this condensation layer and the amount of condensation increased with increasing dewpoint, Mach number, and airfoil angle of attack. A moderate amount of condensation was observed in nearly the entire region of supersonic flow before the appearance of any condensation in the free stream ahead of the airfoil.

(U) Condensation originating in the free stream.- Condensation in the free stream ahead of the model was first seen as a very thin fog originating upstream of the tunnel test section. The amount of condensation increased with increasing dewpoint and Mach number and its density was relatively uniform across the test-section span. Its appearance corresponded approximately to the onset of saturation conditions, a result which agrees with observations made in this wind tunnel at near-sonic Mach numbers and reported in reference 1. This result implies that condensation was formed by heterogeneous nucleation. According to reference 5, this type of condensation process normally occurs in nozzles of large wind tunnels, such as the Langley 8-foot transonic pressure tunnel. In such a large nozzle the rates of temperature change are sufficiently small to allow condensation to take place on foreign nuclei.

[redacted] Effects of Condensation in Test-Section Flow

[redacted] Wind-tunnel-wall Mach number distributions.- Effects of condensation on the axial Mach number distributions along the top and side walls of the test section with the tunnel at a nominal Mach number of 0.820 and the model at a[redacted]ngle of attack of 2.0° are presented in figure 8. Included in the key of this figure are the free-stream Mach number, at which each wall Mach number distribution was measured, and the estimated saturat[redacted] Mach number $M_{sat,\infty}$ for each humidity condition.

(U) A very small reduction is seen in the Mach number upstream of test-section station $x/s = 0.8$ at the highest dewpoint. This decrease in Mach number is considered insignificant, since it is practically within the repeatability of data. A considerable amount of condensation was observed upstream of the model for this humidity condition. Similar, but larger, effects of condensation on the wall Mach number distributions at near-sonic speed in this wind tunnel were reported in reference 1.

(U) Chordwise pressure distributions.- Effects of dewpoint variation on chordwise pressure distributions are presented in figure 9. The pressure coefficient corresponding to saturation for each humidity condition is listed, and the pr[redacted]sure coefficient corresponding to local sonic speed is indicated.

(U) The most noticeable effect of condensation on the chordwise pressure distributions is an increase in the pressures in the region of supersonic flow over the upper surface. (See fig. 9(p), for instance.) This is an expected result, since heat addition, due to condensation, reduces Mach number and increases stream pressure in supersonic flow. The effect usually begins near the leading edge and becomes more severe further downstream where more condensation is forming. (See fig. 9(j), for instance.) A comparison of the pressure distributions with the airfoil at different angles of attack shows that at higher angles of attack the effect appears at lower dewpoints. This occurs, of course, because of the lower local stream temperatures over the airfoil at higher angles of attack.

(U) Another effect of condensation on the pressure distributions is to cause a forward movement of the recompression shock when the airfoil is operating at near-design conditions (near the design normal-force coefficient). (See figs. 9(b) to 9(d).) This occurs principally with free-stream condensation and is believed to be associated with a reduction in Mach number in the region of supersonic flow. Both these results agree qualitatively with the results of reference 1.

[redacted] A characteristic of NASA supercritical airfoils (ref. 2) is the existence of extensive local regions of supersonic flow when operating at design conditions. Because an effect of condensation, mentioned previously, is to increase the pressures in the regions of supersonic flow over the airfoil upper surface, the lift characteristics of NASA supercritical airfoils may be particularly sensitive to wind-tunnel humidity at design conditions.

(U) Wake profiles.- Effects of dewpoint variation on the wake profiles are presented in figure 10. The main effect of condensation is an increase in the measured stagnation-pressure deficit in those sections of the profile associated with regions in the stream where condensation is occurring. Condensation in wind-tunnel flow is known to be accompanied by a reduction in stagnation pressure (ref. 4), and this effect of condensation on wake profiles has been observed in other investigations. (See ref. 10, for example.) The measurement of stagnation pressure is difficult to interpret quantitatively because some vaporization of the condensate usually takes place during recompression at the total-pressure tubes. The measured pressure is always less than it was before condensation occurred, however.

(U) Another effect of condensation on the wake profiles is large decreases in the shock losses at the higher angles of attack. (See figs. 10(n) to 10(p).) This occurs with local and free-stream condensation and is believed to result from a reduction in Mach number in the region of supersonic flow with its associated decrease in shock-wave intensity.

(U) The first effects of local condensation appear in the peak of the profile in the region associated with viscous losses in the boundary layer. (See figs. 10(n) to 10(p).) If shock losses exist, they may be decreased as discussed previously. As the amount of local condensation increases, the region associated with boundary-layer losses becomes wider. With the airfoil at an angle of attack of 3.5°, at the highest dewpoints and Mach numbers, the condensate was observed to separate from the airfoil surface at about the shock location and to follow less contoured streamlines to the rake. Large increases in wake losses occurred in this region of the profile. (See figs. 10(o) and 10(p).)

(U) When condensation occurs in the free stream, the effects generally spread beyond the airfoil wake as a nearly constant pressure deficit, and the losses within the wake suffer a further increase. If shock losses exist, this further increase in pressure deficit with free-stream condensation tends to offset the decrease in the shock losses related to the effect of condensation on shock intensity discussed previously.

Force and moment characteristics.- Effects of dewpoint variation on the normal-force, pitching-moment, and drag characteristics are presented in figures 11, 12, and 13, respectively. It should be mentioned that the highest test Mach numbers of 0.83 and 0.82 are beyond the drag-divergence Mach numbers for this airfoil at normal-force coefficients of 0.5 and 0.7, respectively (ref. 3). Data at these Mach numbers are, therefore, beyond the range of primary interest but are still included since the general trends resulting from the effects of condensation at the lower Mach numbers are not significantly different in these data.

(U) It should be pointed out that the stagnation-pressure deficit across the test section, resulting from condensation occurring principally in the free stream, will result in large errors in calculated drag if the pressure integration across the profile rake is carried

beyond the airfoil wake. This effect of condensation on the drag coefficients is contingent on airfoil characteristics to only a limited degree, of course, because it is caused by condensation in the free stream. It is included in the drag characteristics presented herein, however, to demonstrate the large errors that result in these data when the effects of free-stream condensation are included.

(U) The normal-force coefficients generally show the loss of lift apparent in the pressure distributions, and the drag coefficients generally show the increase in momentum deficit apparent in the wake profiles. The pitching-moment coefficients show less definite trends since the pressure distributions are affected both ahead and aft of the pitch center.

[redacted] Effects of Local Condensation

[redacted] Effects on the airfoil pressure distributions and wake profiles of local condensation, that is, condensation that occurs before free-stream saturation is reached, are small for conditions well beyond local saturation. With the airfoil at the highest angle of attack of 3.5°, effects are generally small up to dewpoints about 40 K (72° F) higher than estimated local saturation dewpoints. (Refer to table II for estimated local and free-stream saturation dewpoints corresponding to test conditions.) With the airfoil at lower angles of attack (1.0° and 2.0°), corresponding to near-design normal-force coefficients, effects are generally small at all dewpoints lower than estimated free-stream saturation dewpoints.

[redacted] These effects of local condensation do become significant, however, at some test conditions before free-stream saturation is reached. With the airfoil at the highest angle of attack of 3.5°, corresponding to relatively high normal-force coefficients, significant effects appear in data at the highest dewpoints and Mach numbers, although the dewpoints corresponding to free-stream saturation are not reached. (See fig. 9(p), for instance.) Condensation originating principally in the local region of supersonic flow over the airfoil upper surface is believed to be responsible for these effects.

(U) CONCLUDING REMARKS [redacted]

(U) An investigation has been conducted in the Langley 8-foot transonic pressure tunnel to determine the effects of wind-tunnel humidity on the aerodynamic characteristics of a 10-percent-thick NASA supercritical airfoil. Effects of dewpoint variation from 267 K (20° F) to 294 K (70° F) were investigated. The tunnel stagnation temperature was 322 K (120° F) and the stagnation pressure was 0.1013 MN/m^2 (1 atm).

(U) Effects of condensation originating principally in the local region of supersonic flow over the airfoil upper surface were small for conditions well beyond local saturation but became significant for some test conditions before free-stream saturation. For airfoil normal-force coefficients near design value, these effects were small, but for relatively

high normal-force coefficients, they were significant. Airfoil upper-surface pressures increased in the region of supersonic flow and resulted in a decrease in lift coefficient. Local condensation generally decreased stagnation pressures in the airfoil wake and thus increased drag coefficient.

(U) The occurrence of condensation in the free stream corresponded approximately to the onset of estimated free-stream saturation. It was accompanied by further effects on airfoil test data similar to those caused by local condensation.

Langley Research Center
National Aeronautics and Space Administration
Hampton, Va. 23665
January 20, 1976

(U) REFERENCES

1. Jordan, Frank L., Jr.: Investigation at Near-Sonic Speed of Some Effects of Humidity on the Longitudinal Aerodynamic Characteristics of an NASA Supercritical-Wing Research Airplane Model. NASA TM X-2618, 1972.
2. Harris, Charles D.: Aerodynamic Characteristics of an Improved 10-Percent-Thick NASA Supercritical Airfoil. NASA TM X-2978, 1974.
3. Harris, Charles D.: Aerodynamic Characteristics of 10-Percent-Thick NASA Supercritical Airfoils With Different Aft Camber. NASA TM X-72007, 1975.
4. Wegener, P. P.; and Mack, L. M.: Condensation in Supersonic and Hypersonic Wind Tunnels. Advances in Applied Mechanics, Volume V, H. L. Dryden and Th. von Kármán, eds., Academic Press, Inc., 1958, pp. 307-447.
5. Wegener, Peter P.: Gasdynamics of Expansion Flows With Condensation, and Homogeneous Nucleation of Water Vapor. Nonequilibrium Flows – Part I, Peter P. Wegener, ed., Marcel Dekker, Inc., 1969, pp. 163-243.
6. Baals, Donald D.; and Mourhess, Mary J.: Numerical Evaluation of the Wake-Survey Equations for Subsonic Flow Including the Effect of Energy Addition. NACA WR L-5, 1945. (Formerly NACA ARR L5H27.)
7. Schaefer, William T., Jr.: Characteristics of Major Active Wind Tunnels at the Langley Research Center. NASA TM X-1130, 1965.
8. Harris, Charles D.: Wind-Tunnel Investigation of Effects of Trailing-Edge Geometry on a NASA Supercritical Airfoil Section. NASA TM X-2336, 1971.
9. Blackwell, James A., Jr.: Preliminary Study of Effects of Reynolds Number and Boundary-Layer Transition Location on Shock-Induced Separation. NASA TN D-5003, 1969.
10. Pearcey, H. H.: The Effect of the Condensation of Atmospheric Water Vapour on Total Head and Other Measurements in the N.P.L. High Speed Tunnels. R. & M. No. 2249, British A.R.C., 1951.

[redacted]

TABLE I.- AIRFOIL SECTION COORDINATES

[c = 63.5 cm (25.0 in.); leading-edge radius, 0.0203c]

x/c	$(y/c)_U$	$(y/c)_L$	x/c	$(y/c)_U$	$(y/c)_L$	x/c	$(y/c)_U$	$(y/c)_L$
0	0	0	0.33	0.0492	-0.0498	0.67	0.0437	-0.0264
.005	.0136	-.0131	.34	.0494	-.0499	.68	.0431	-.0245
.01	.0177	-.0178	.35	.0495	-.0499	.69	.0425	-.0226
.02	.0225	-.0228	.36	.0496	-.0499	.70	.0419	-.0207
.03	.0257	-.0261	.37	.0497	-.0499	.71	.0413	-.0188
.04	.0281	-.0285	.38	.0498	-.0498	.72	.0407	-.0169
.05	.0302	-.0306	.39	.0499	-.0497	.73	.0400	-.0150
.06	.0319	-.0324	.40	.0500	-.0495	.74	.0393	-.0131
.07	.0335	-.0340	.41	.0500	-.0493	.75	.0386	-.0113
.08	.0349	-.0355	.42	.0500	-.0491	.76	.0378	-.0095
.09	.0361	-.0368	.43	.0500	-.0489	.77	.0370	-.0077
.10	.0373	-.0380	.44	.0499	-.0486	.78	.0361	-.0060
.11	.0383	-.0391	.45	.0498	-.0483	.79	.0352	-.0044
.12	.0392	-.0401	.46	.0497	-.0480	.80	.0343	-.0028
.13	.0401	-.0410	.47	.0496	-.0476	.81	.0333	-.0013
.14	.0409	-.0419	.48	.0495	-.0472	.82	.0323	.0001
.15	.0417	-.0427	.49	.0494	-.0467	.83	.0312	.0014
.16	.0424	-.0434	.50	.0493	-.0462	.84	.0301	.0026
.17	.0431	-.0441	.51	.0492	-.0456	.85	.0289	.0036
.18	.0437	-.0448	.52	.0490	-.0449	.86	.0277	.0045
.19	.0443	-.0454	.53	.0488	-.0442	.87	.0264	.0052
.20	.0449	-.0460	.54	.0486	-.0434	.88	.0250	.0057
.21	.0454	-.0465	.55	.0483	-.0426	.89	.0235	.0060
.22	.0459	-.0470	.56	.0480	-.0417	.90	.0220	.0061
.23	.0463	-.0474	.57	.0477	-.0407	.91	.0204	.0061
.24	.0467	-.0478	.58	.0474	-.0396	.92	.0186	.0058
.25	.0471	-.0482	.59	.0471	-.0385	.93	.0169	.0053
.26	.0475	-.0485	.60	.0468	-.0373	.94	.0149	.0046
.27	.0478	-.0488	.61	.0464	-.0360	.95	.0129	.0035
.28	.0481	-.0490	.62	.0460	-.0346	.96	.0108	.0022
.29	.0484	-.0492	.63	.0456	-.0332	.97	.0086	.0007
.30	.0486	-.0494	.64	.0452	-.0316	.98	.0062	-.0012
.31	.0488	-.0496	.65	.0447	-.0299	.99	.0037	-.0035
.32	.0490	-.0497	.66	.0442	-.0282	1.00	-----	-.0061

[redacted]

[redacted]

TABLE II.- DEWPOINTS CORRESPONDING TO SATURATED FLOW AT TEST M_∞ AND $M_{l,max}$

α, deg	M_∞	$T_{dp,sat,\infty}$ (at M_∞)		$T_{dp,sat,l}$ (at $M_{l,max}$)	
		K	°F	K	°F
1.0	0.74	296	73	262	12
1.0	.78	293	68	261	10
1.0	.80	292	66	261	10
1.0	.81	291	64	260	8
1.0	.82	290	63	260	8
1.0	.83	290	62	257	2
2.0	.70	298	77	251	-8
2.0	.74	296	73	250	-9
2.0	.78	293	68	253	-5
2.0	.80	292	66	254	-3
2.0	.81	291	64	253	-5
2.0	.82	290	63	250	-9
3.5	.60	304	88	244	-20
3.5	.70	298	77	236	-35
3.5	.74	296	73	237	-34
3.5	.76	295	71	238	-32

[redacted]

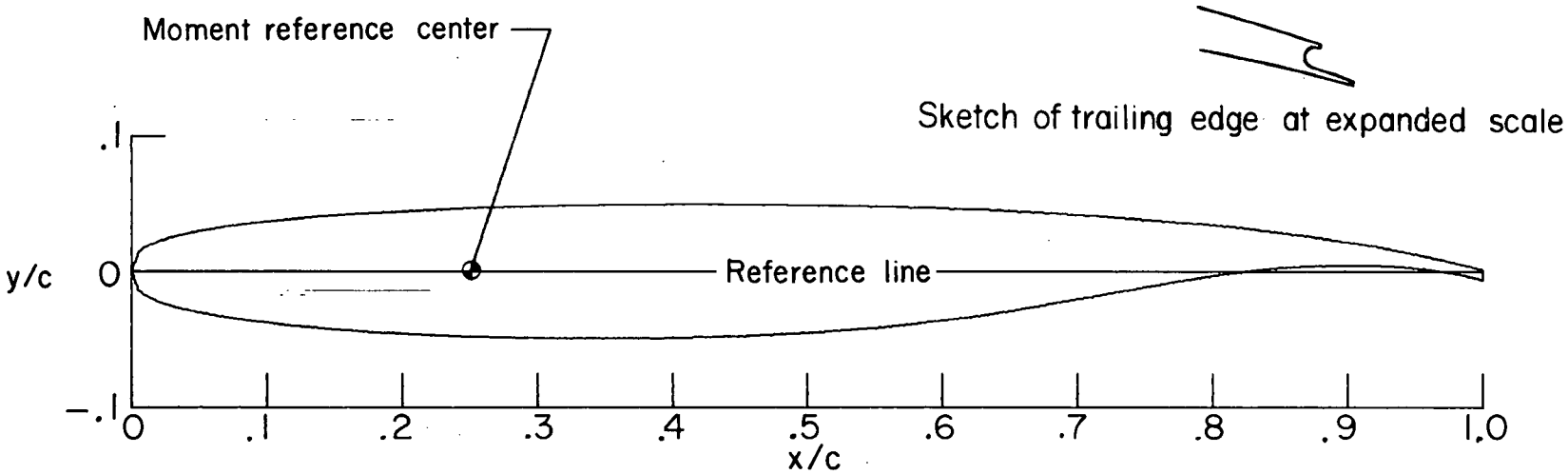

Figure 1.- Airfoil sketch.

[redacted]

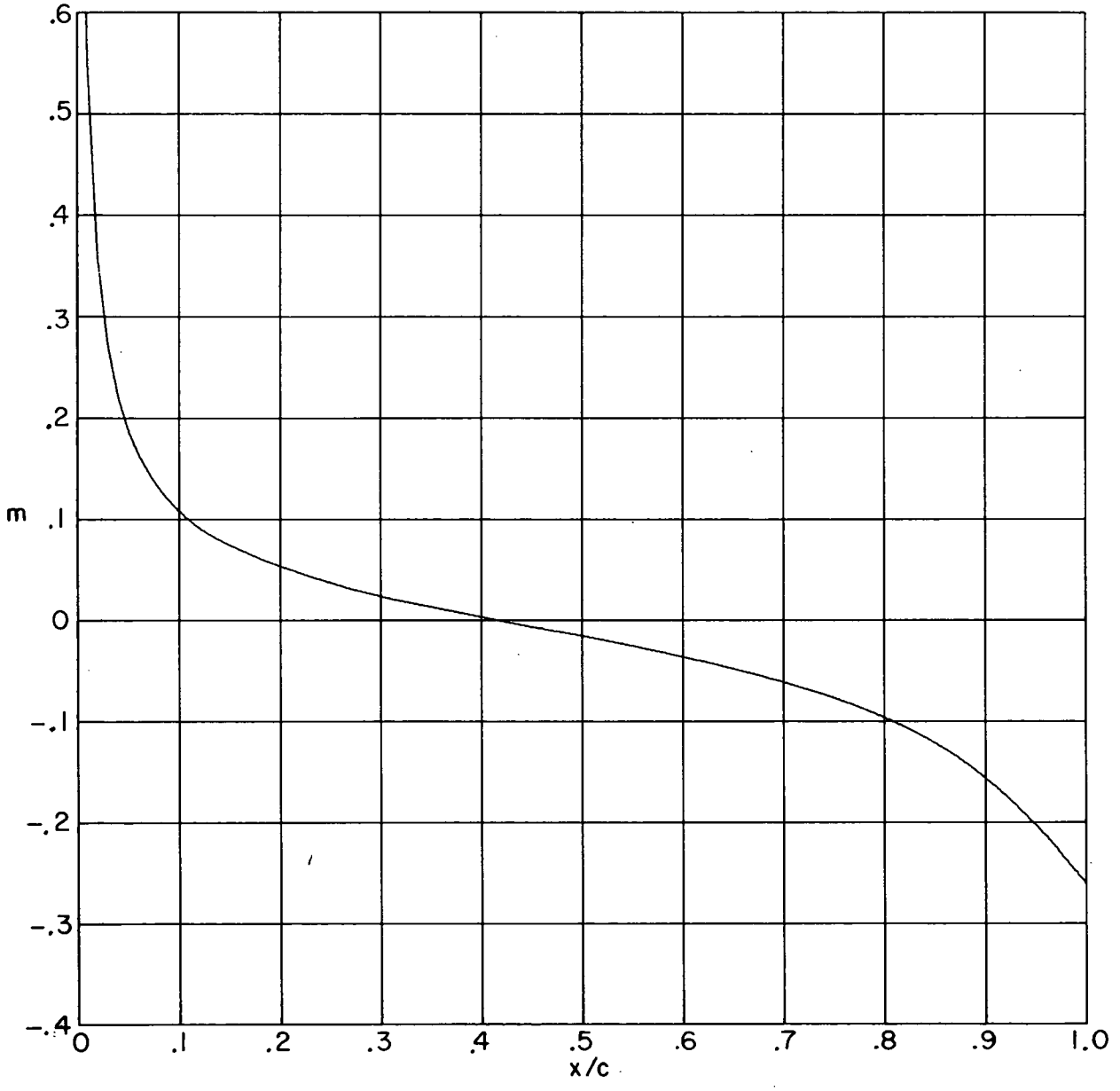

(a) Upper surface.

Figure 2.- Chordwise distribution of airfoil surface slopes.

[redacted]

[redacted]

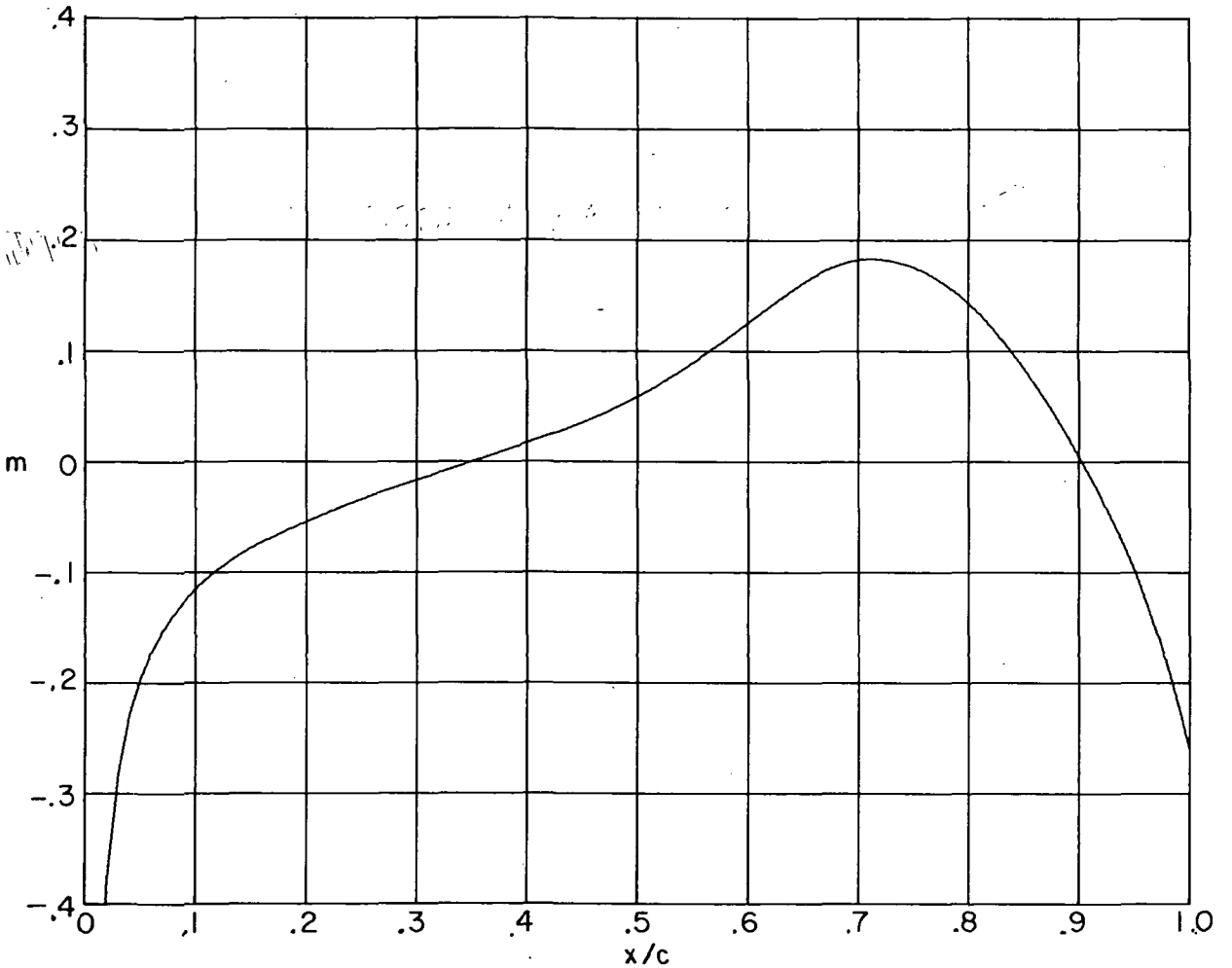

(b) Lower surface.

Figure 2.- Concluded.

[redacted]

[redacted]

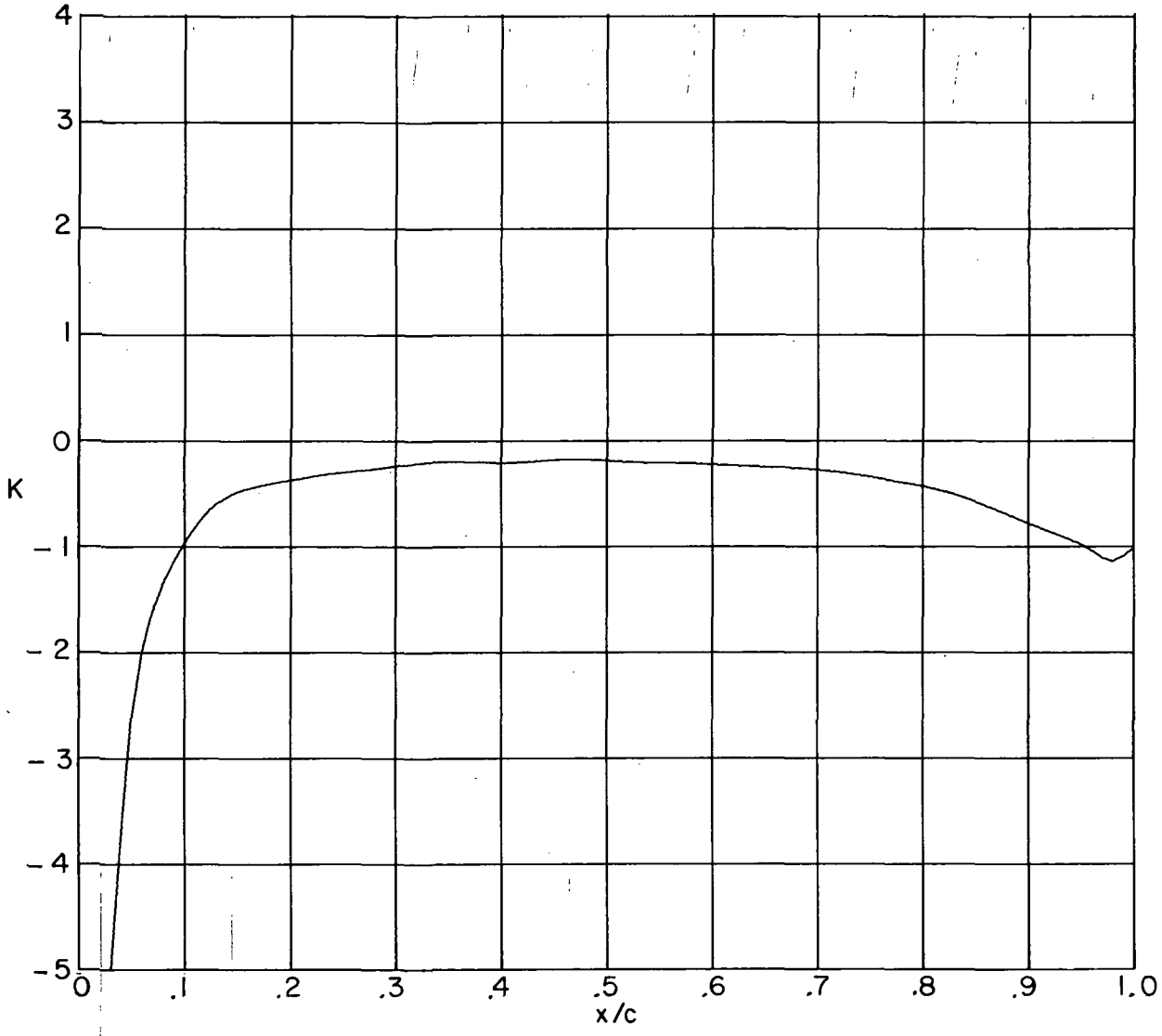

(a) Upper surface.

Figure 3.- Chordwise distribution of airfoil surface curvatures.

[redacted]

[redacted]

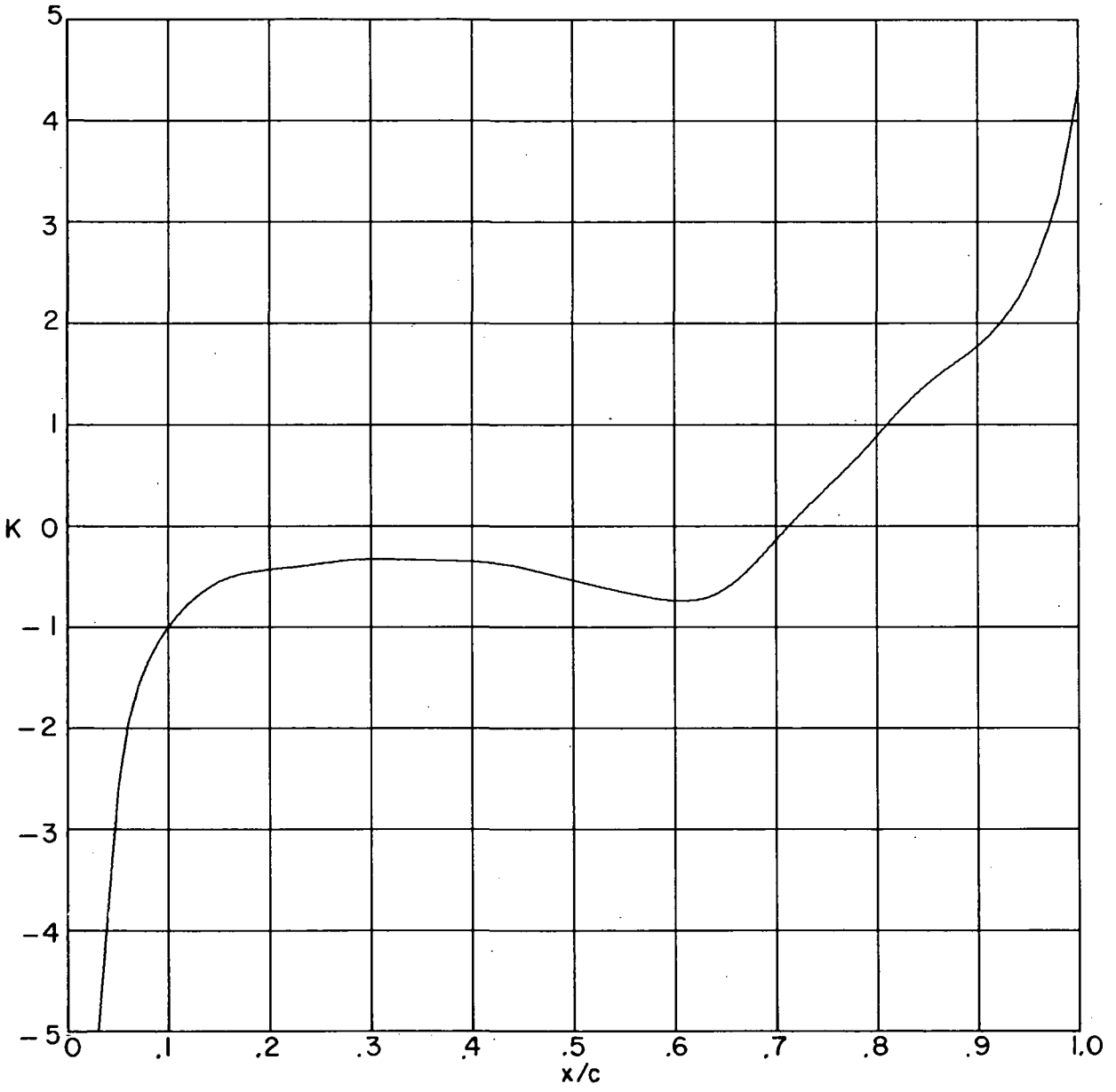

(b) Lower surface.

Figure 3.- Concluded.

[redacted]

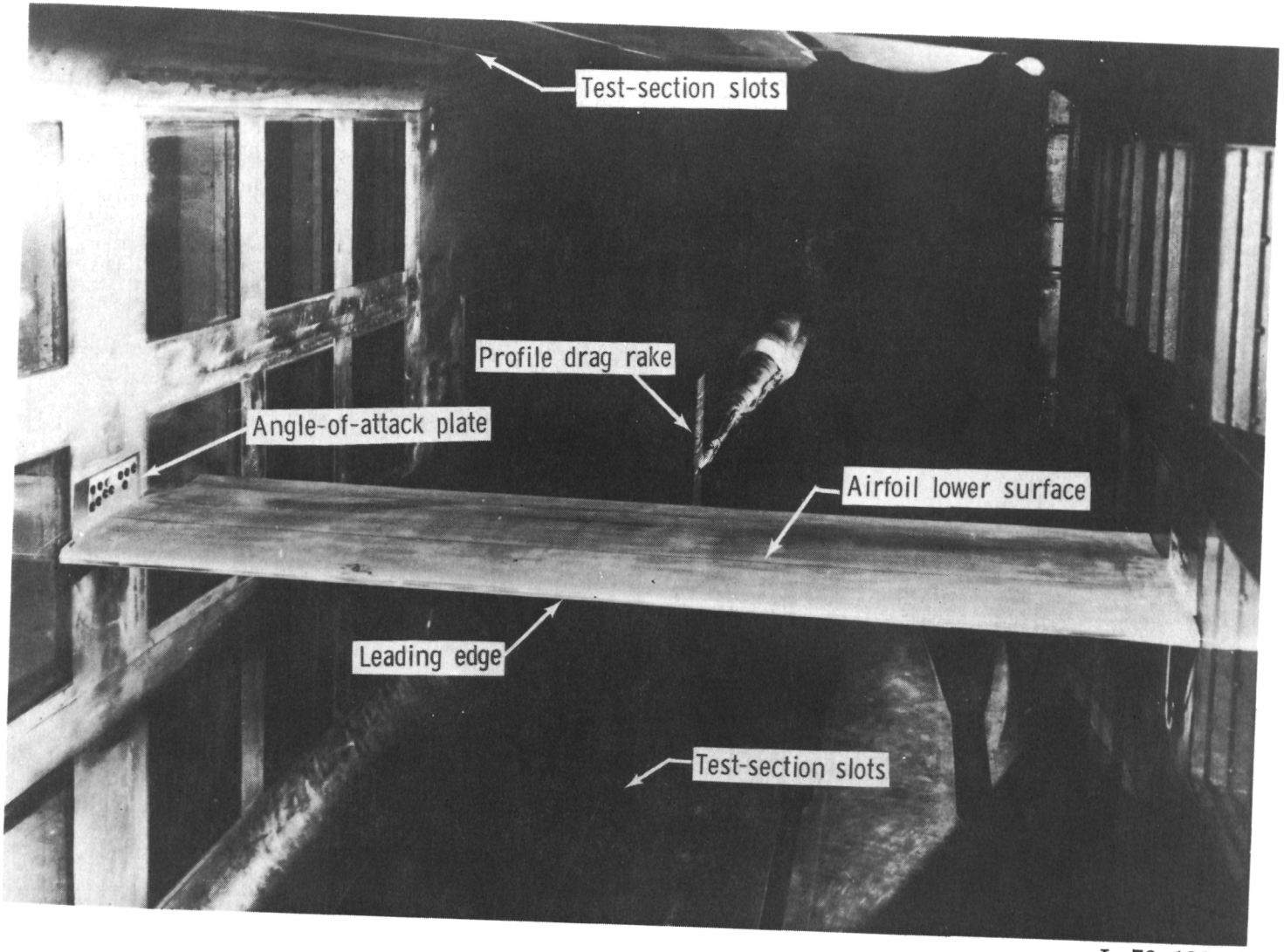

L-73-1225.2

(a) Supercritical airfoil and profile drag rake mounted in tunnel.

Figure 4.- Photographs.

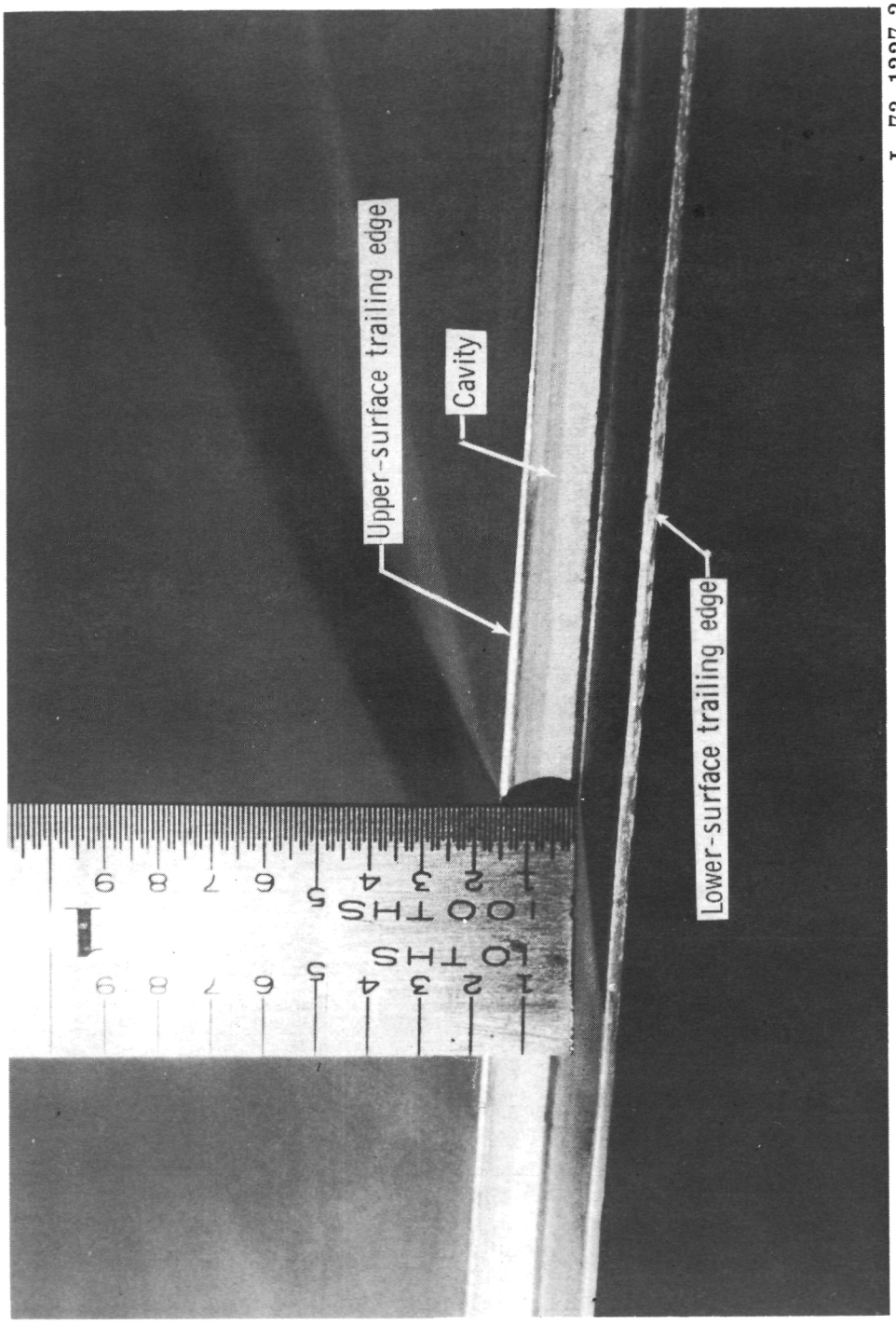

L-73-1227.2

(b) Trailing-edge cavity of airfoil.

Figure 4.- Concluded.

[redacted]

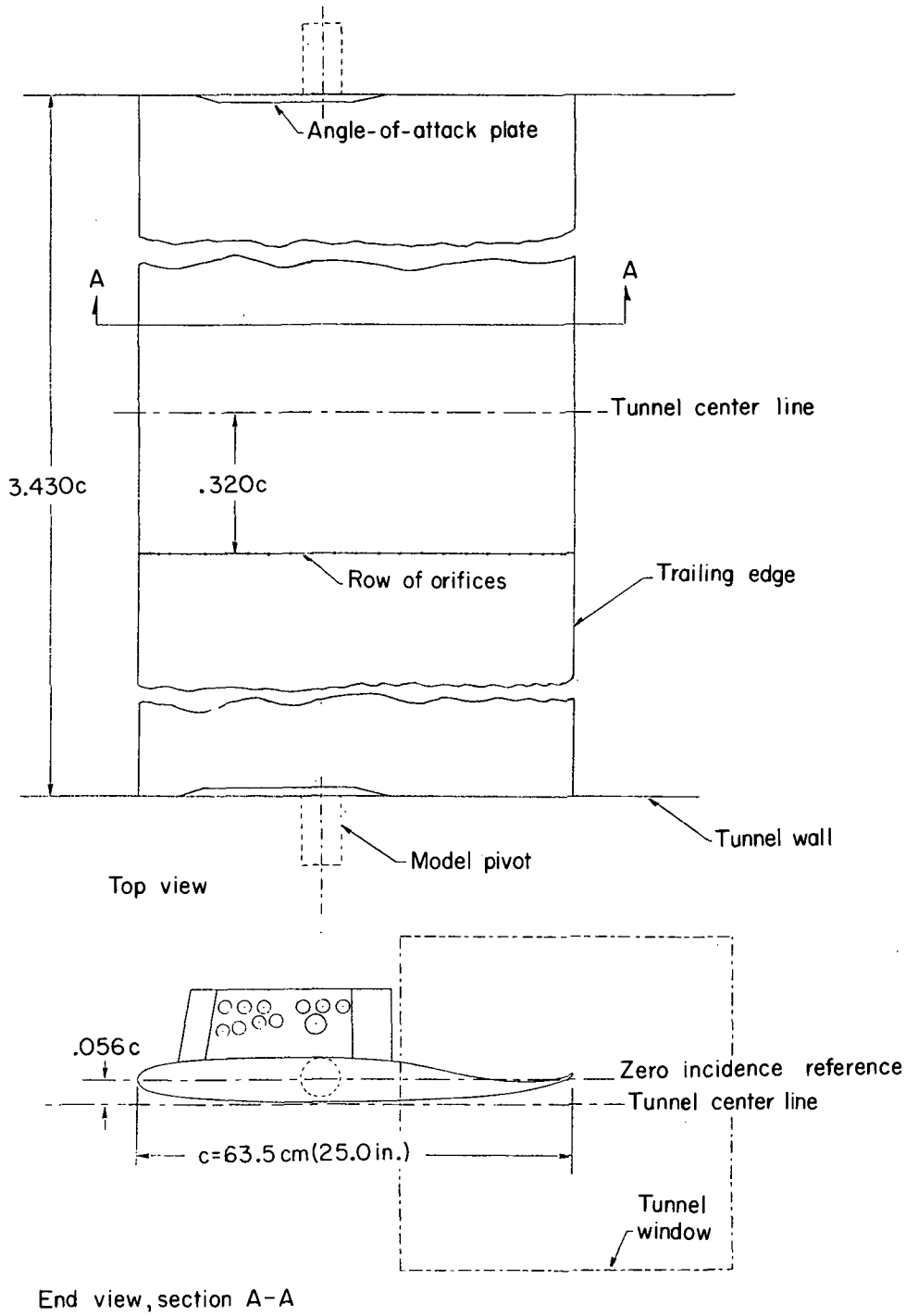

(a) Airfoil mounted in tunnel.

Figure 5.- Apparatus. Dimensions in terms of chord c = 63.5 cm (25.0 in.).

[redacted]

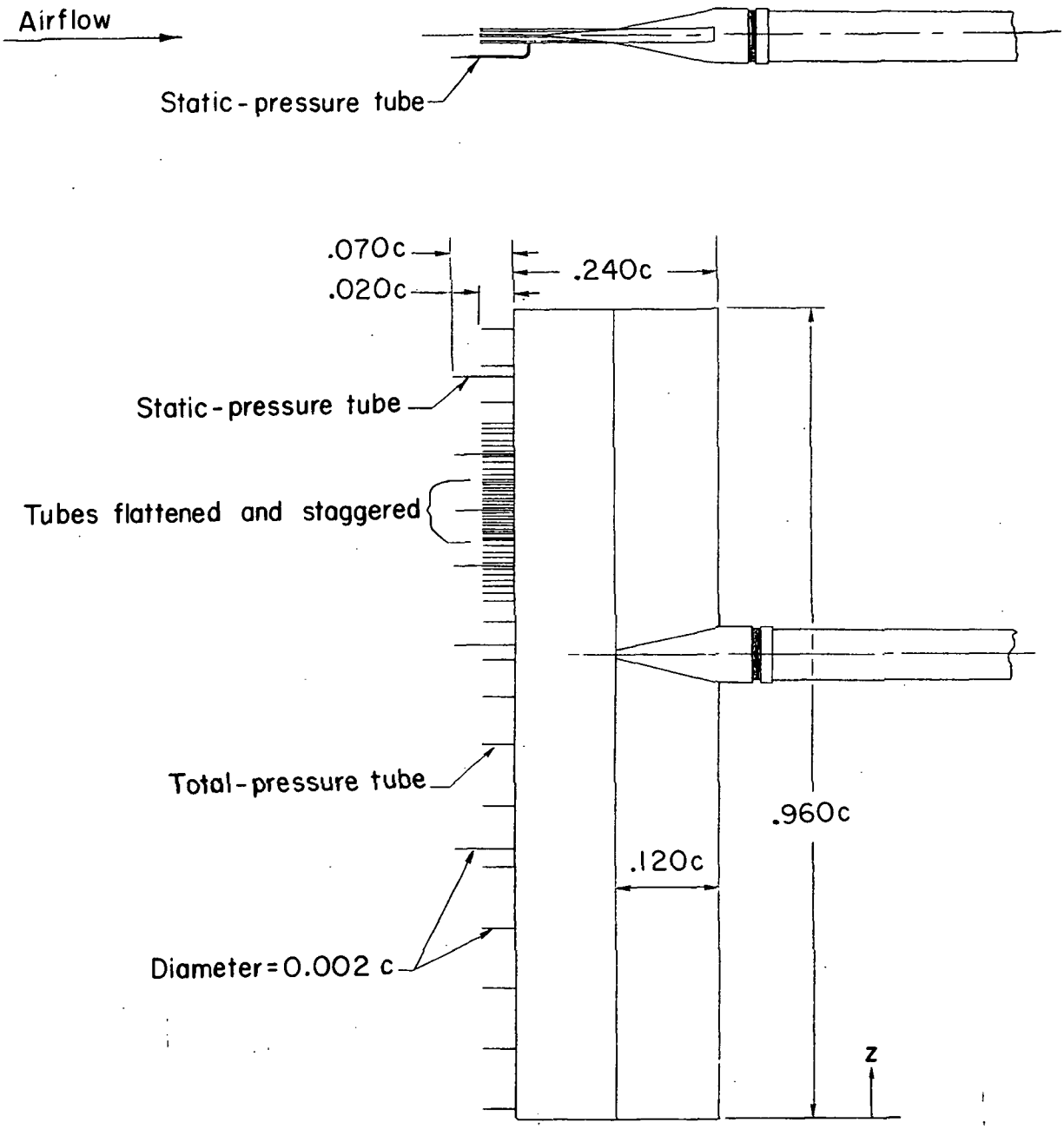

(b) Profile drag rake.

Figure 5.- Concluded.

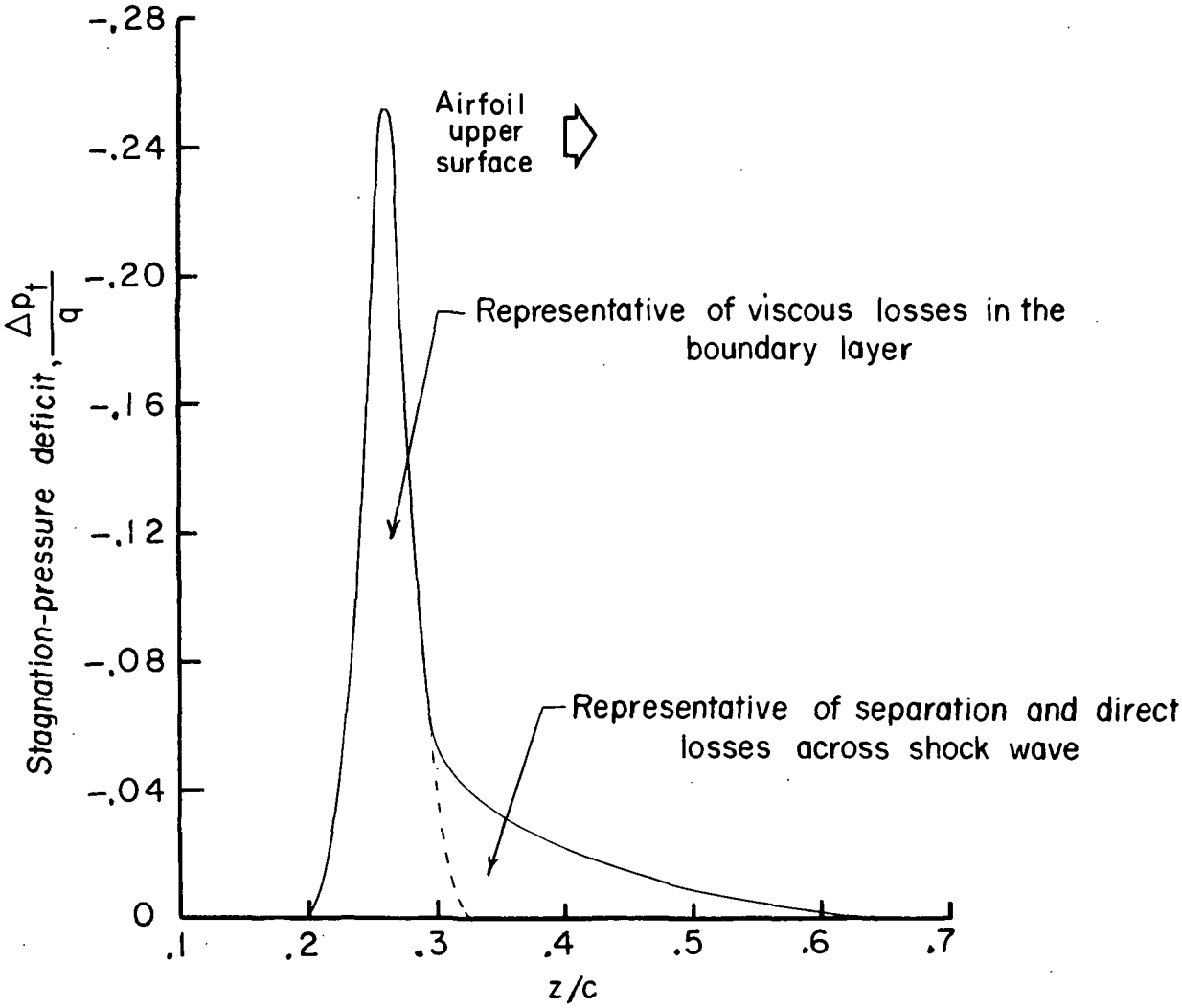

Figure 6.- Schematic of wake profiles.

[redacted]

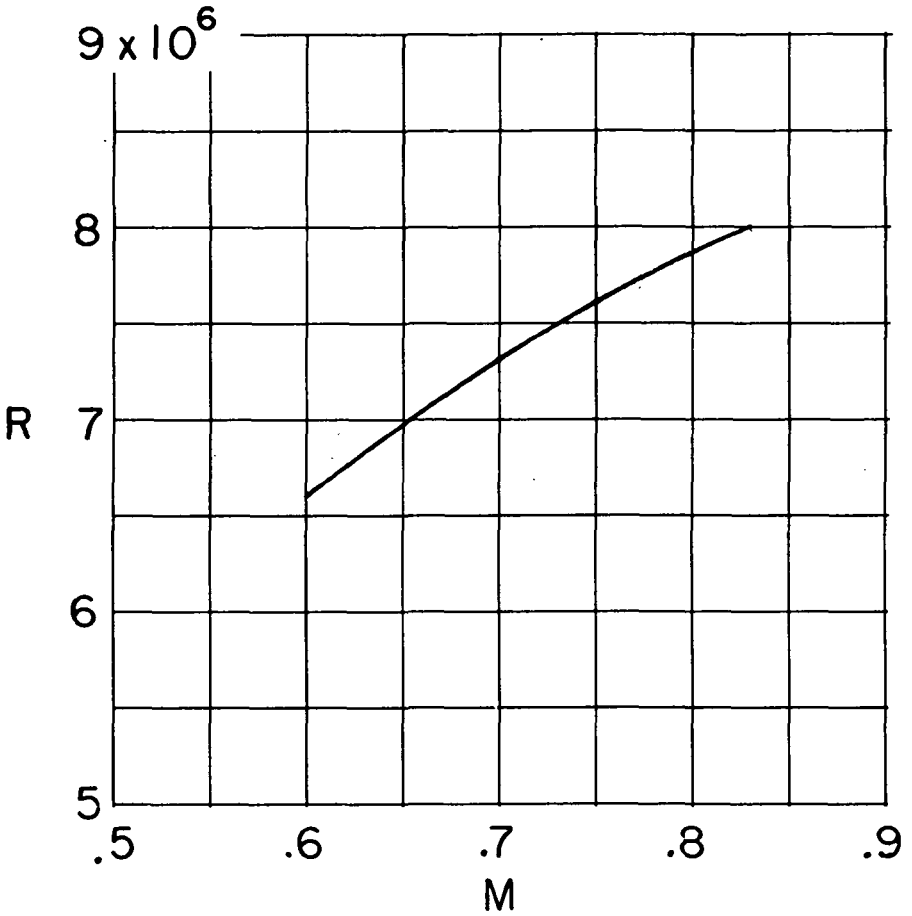

Figure 7.- Variation with Mach number of test wind-tunnel Reynolds number.

[redacted]

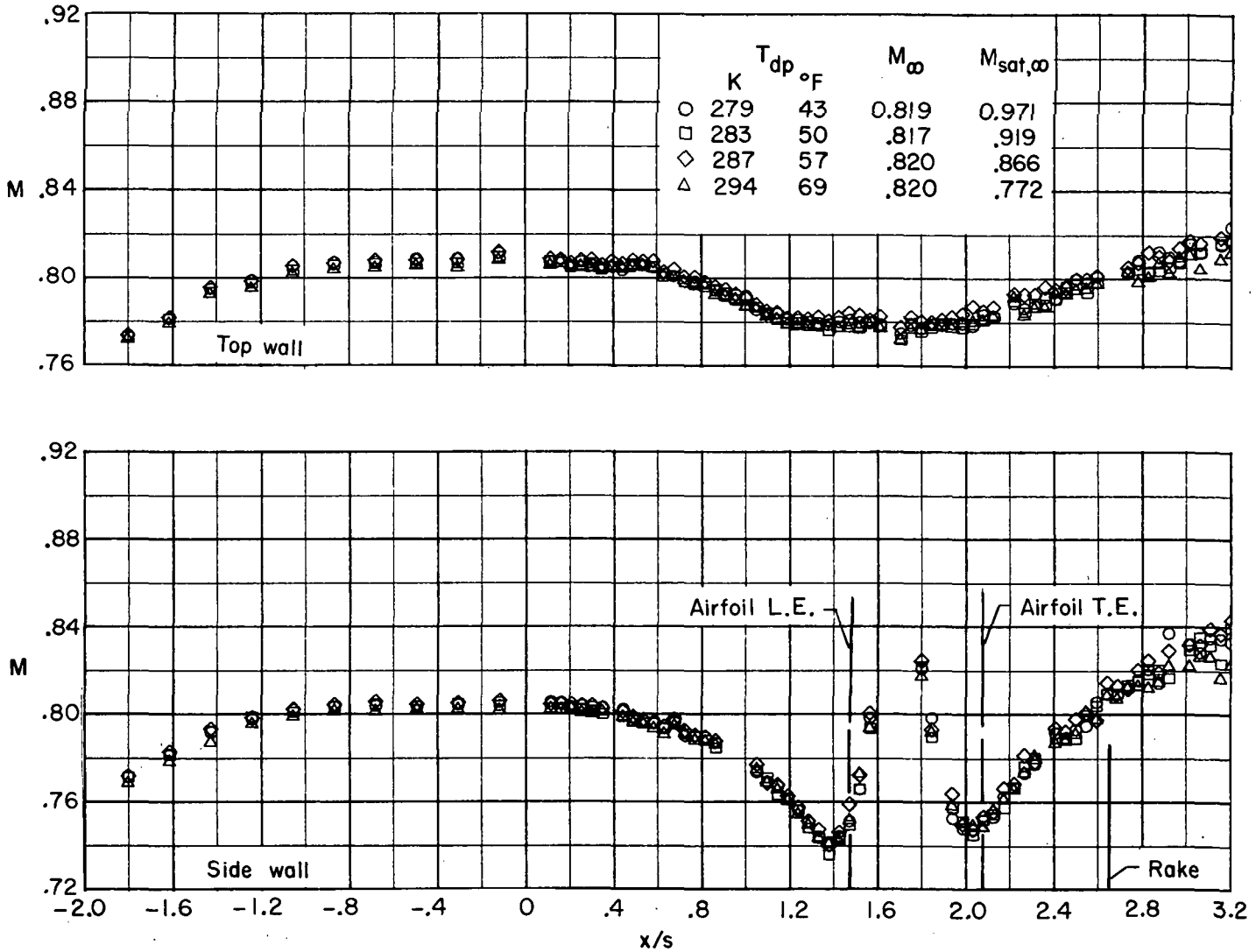

Figure 8.- Effect of wind-tunnel humidity on axial Mach number distribution along wall of test section. $\alpha = 2.0^{\circ}$.

[redacted]

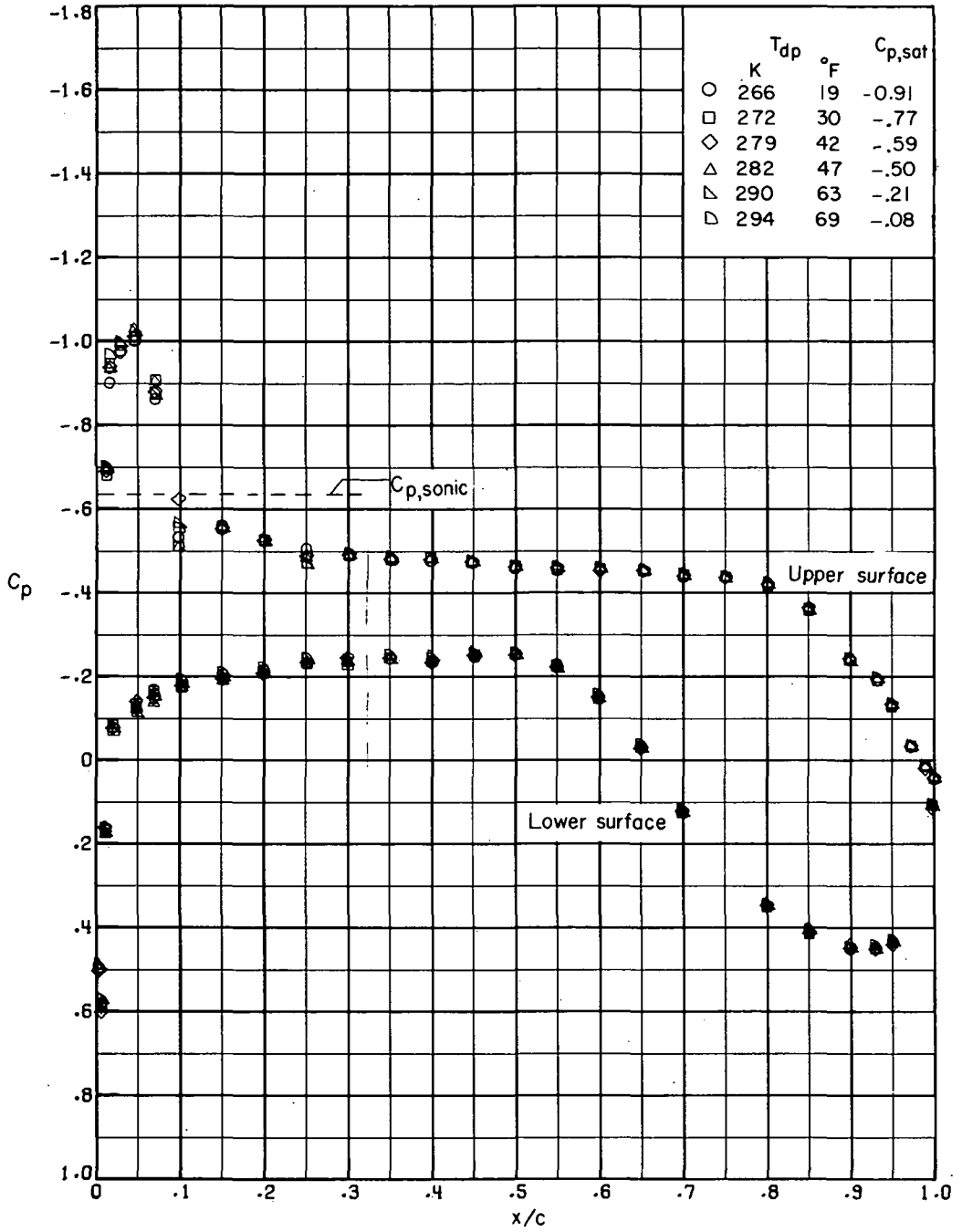

(a) M = 0.74; α = 1.0°.

Figure 9.- Effect of wind-tunnel humidity on chordwise pressure distributions. Lower curves correspond to lower surface; upper curves, to upper surface.

[redacted]

[redacted]

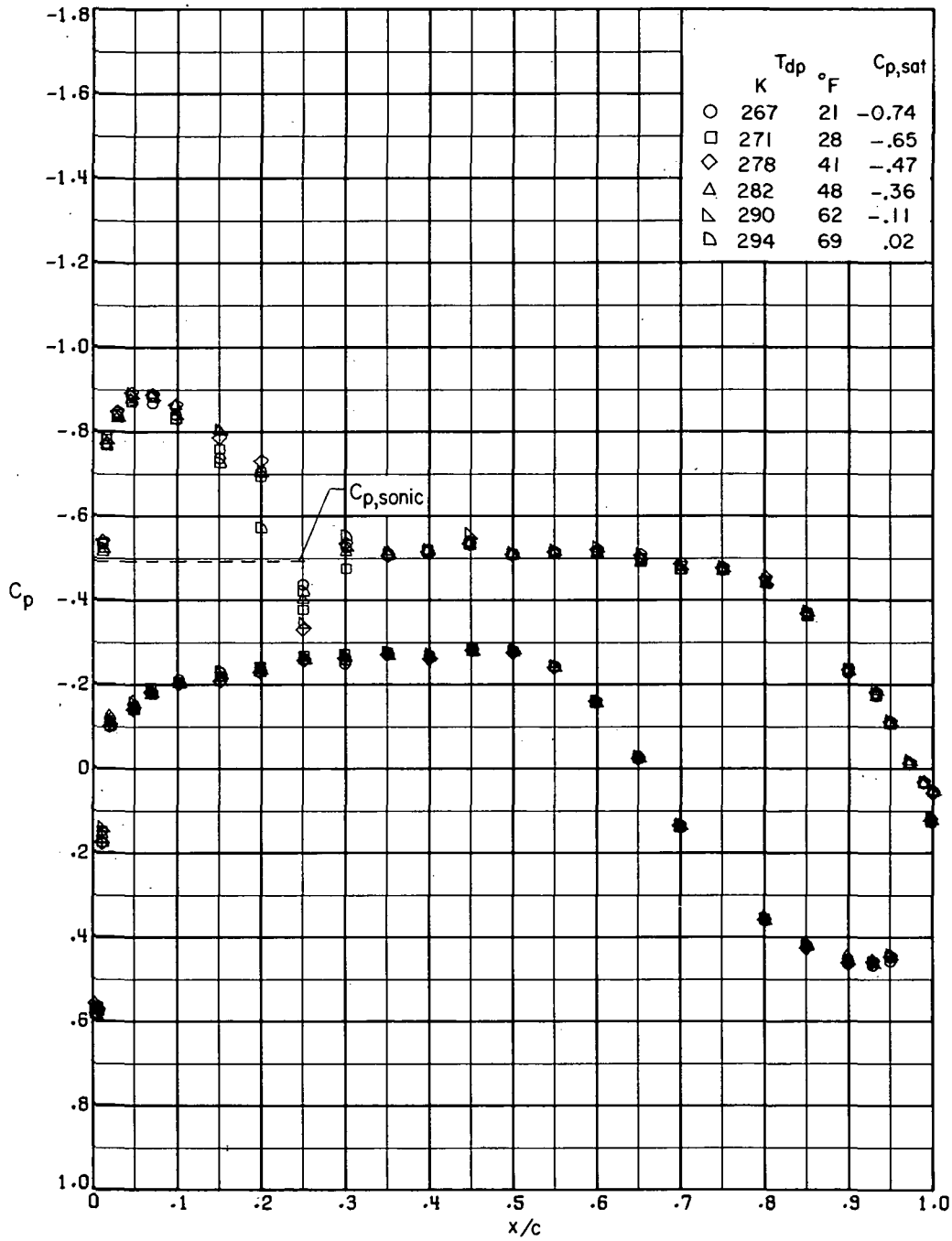

(b) M = 0.78; α = 1.0°.

Figure 9.- Continued.

[redacted]

[redacted]

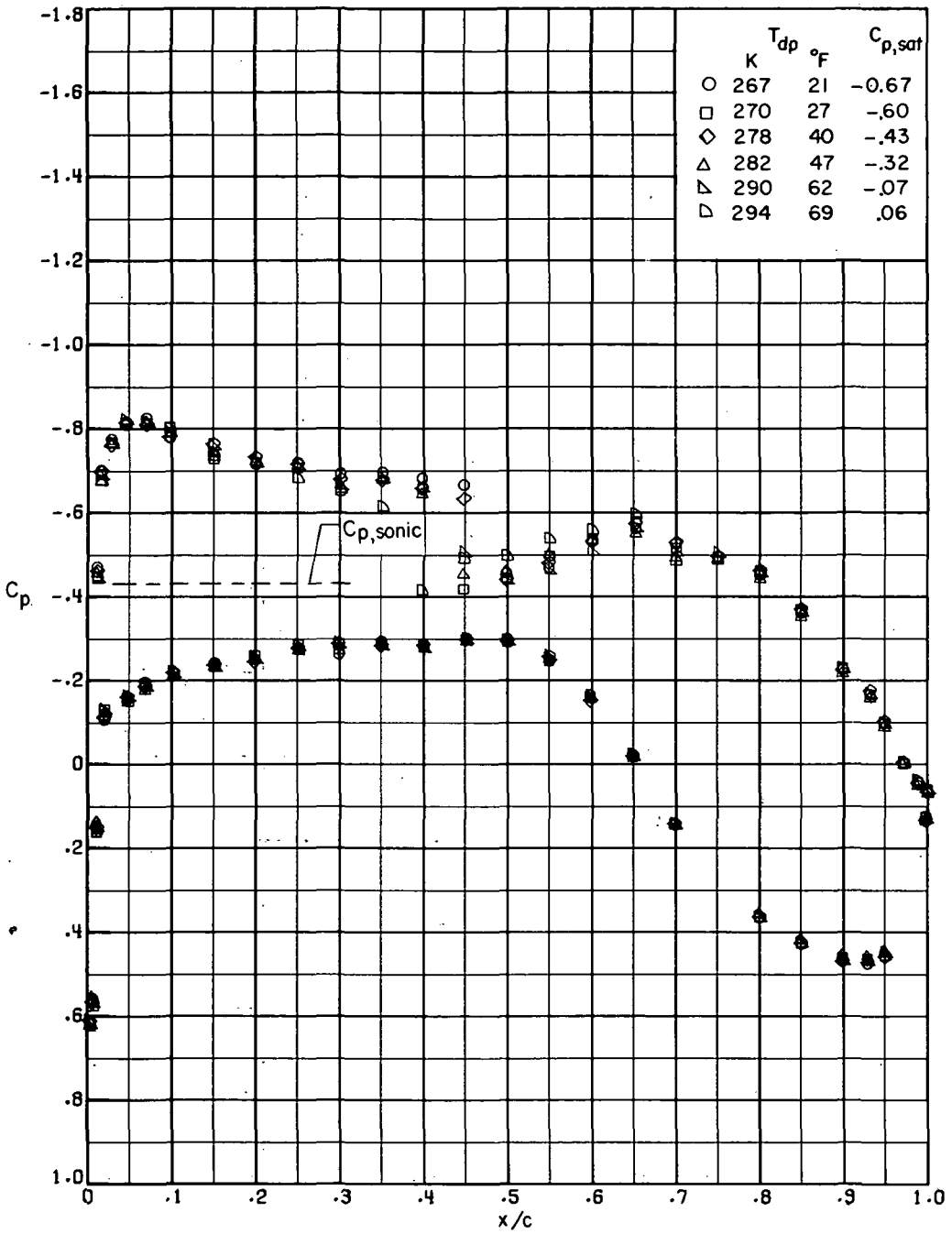

(c) M = 0.80; α = 1.0°.

Figure 9.- Continued.

[redacted]

[redacted]

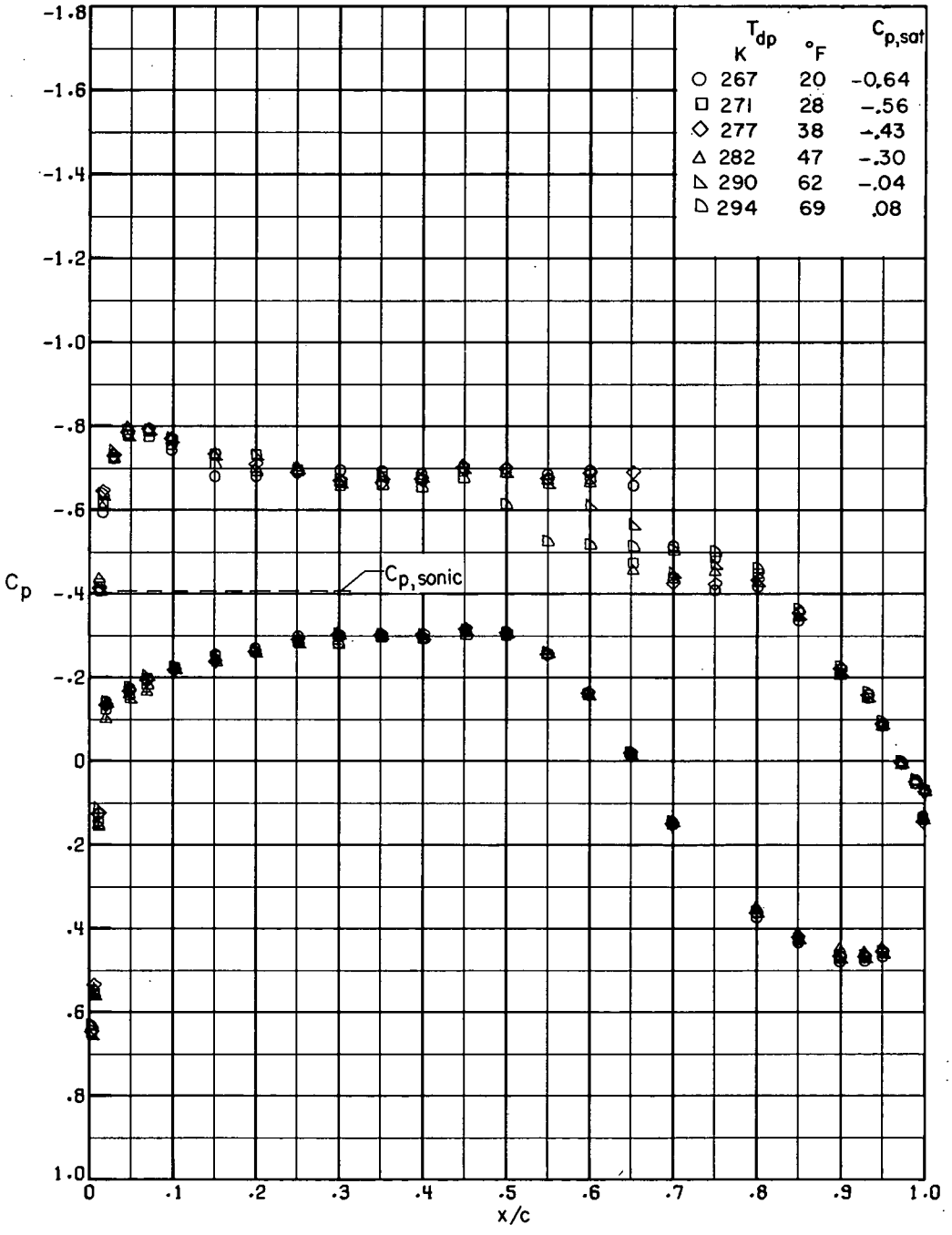

(d) M = 0.81; α = 1.0°.

Figure 9.- Continued.

[redacted]

[redacted]

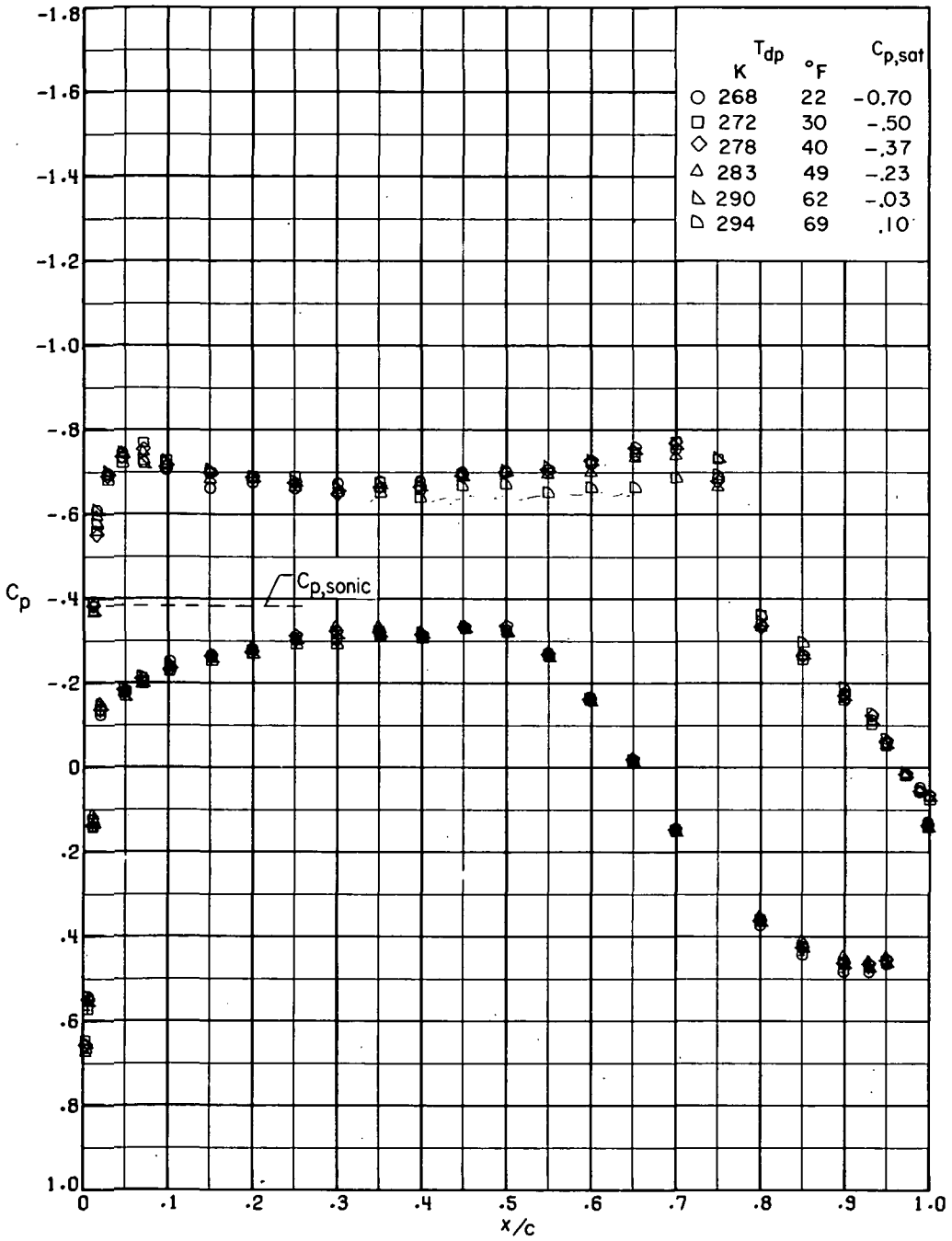

(e) M = 0.82; α = 1.0°.

Figure 9.- Continued.

[redacted]

[redacted]

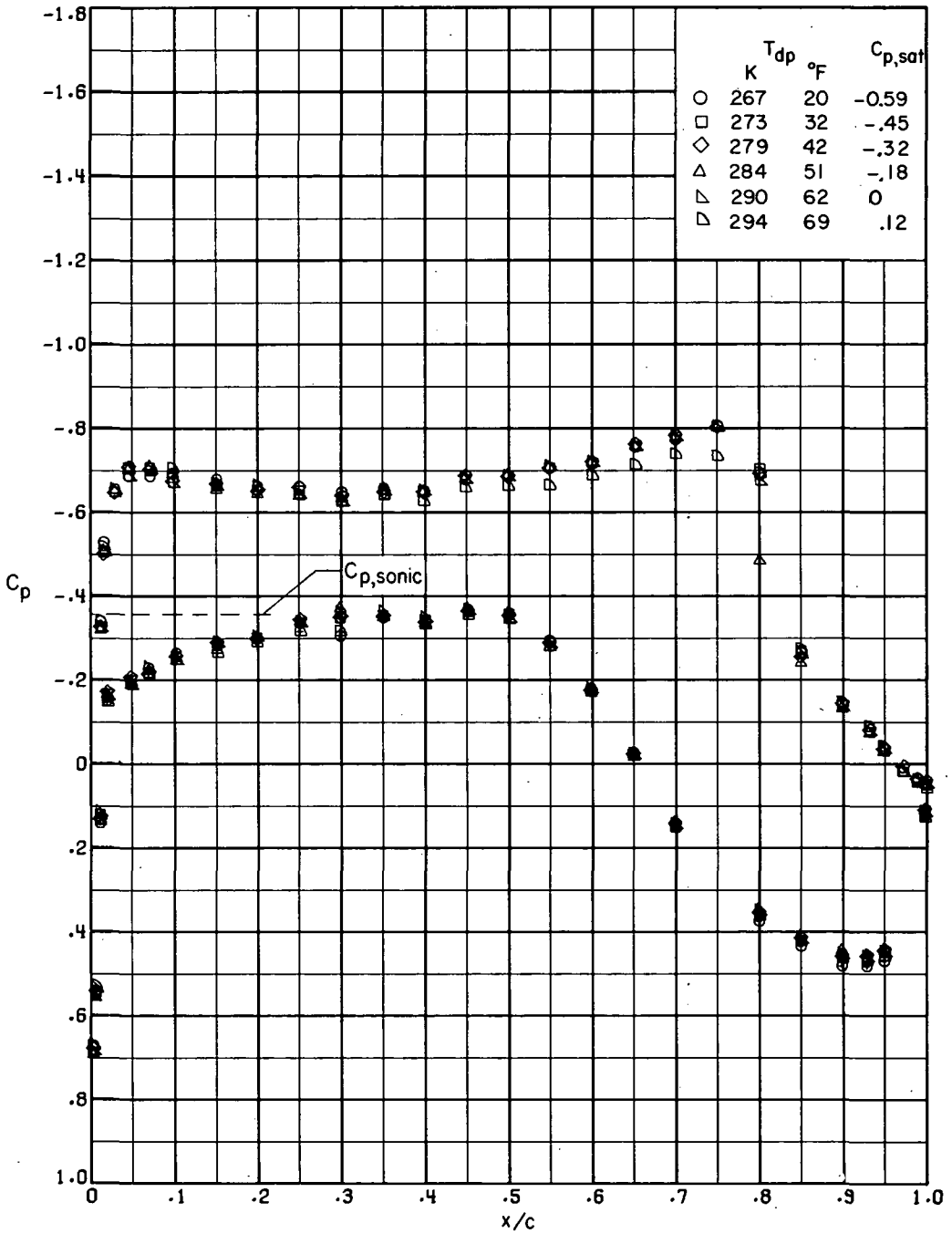

(f) M = 0.83; $\alpha = 1.0^{\circ}$.

Figure 9.- Continued.

[redacted]

[redacted]

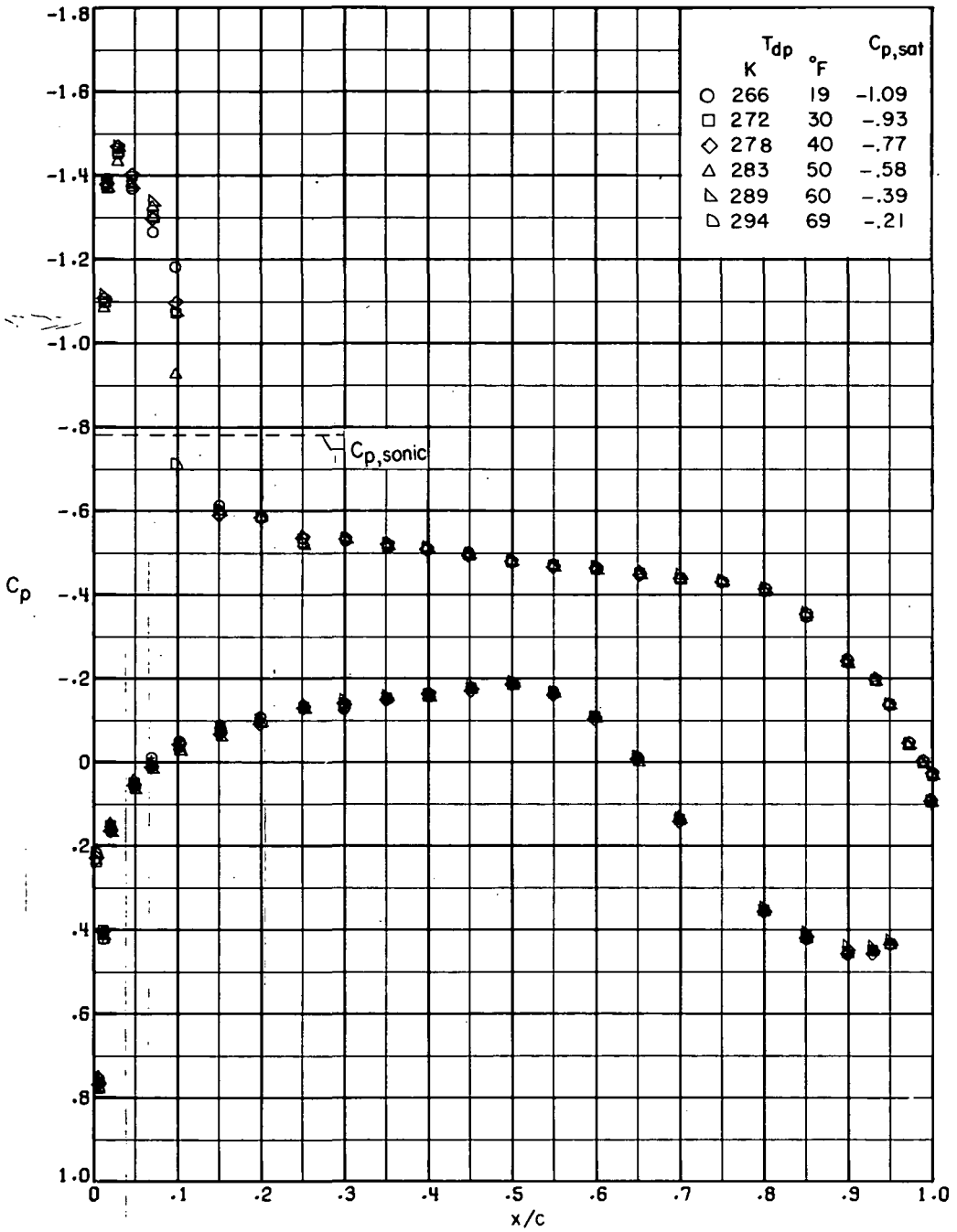

(g) M = 0.70; $\alpha = 2.0^{\circ}$.

Figure 9.- Continued.

[redacted]

[redacted]

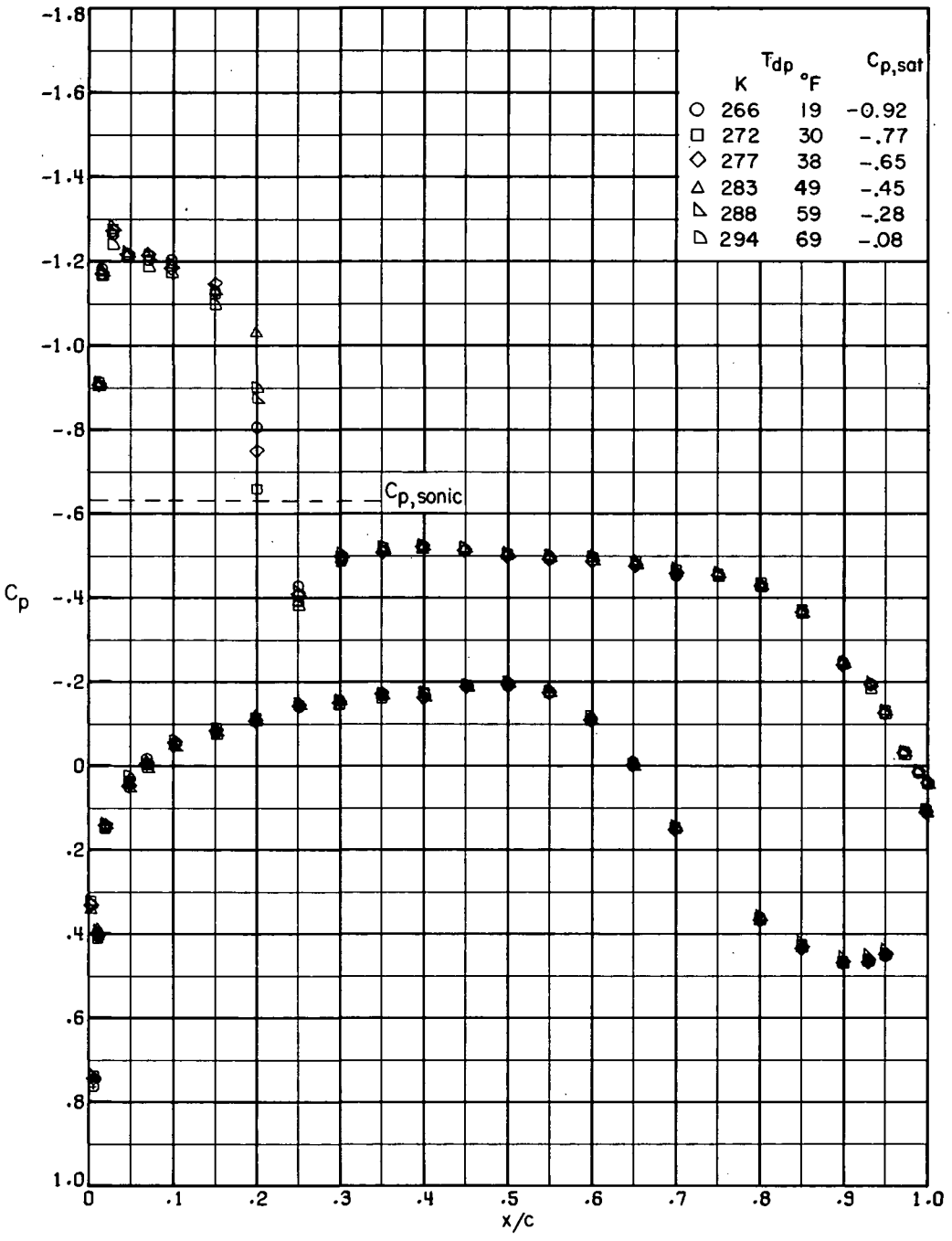

(h) M = 0.74; $\alpha = 2.0^{\circ}$.

Figure 9.- Continued.

[redacted]

[redacted]

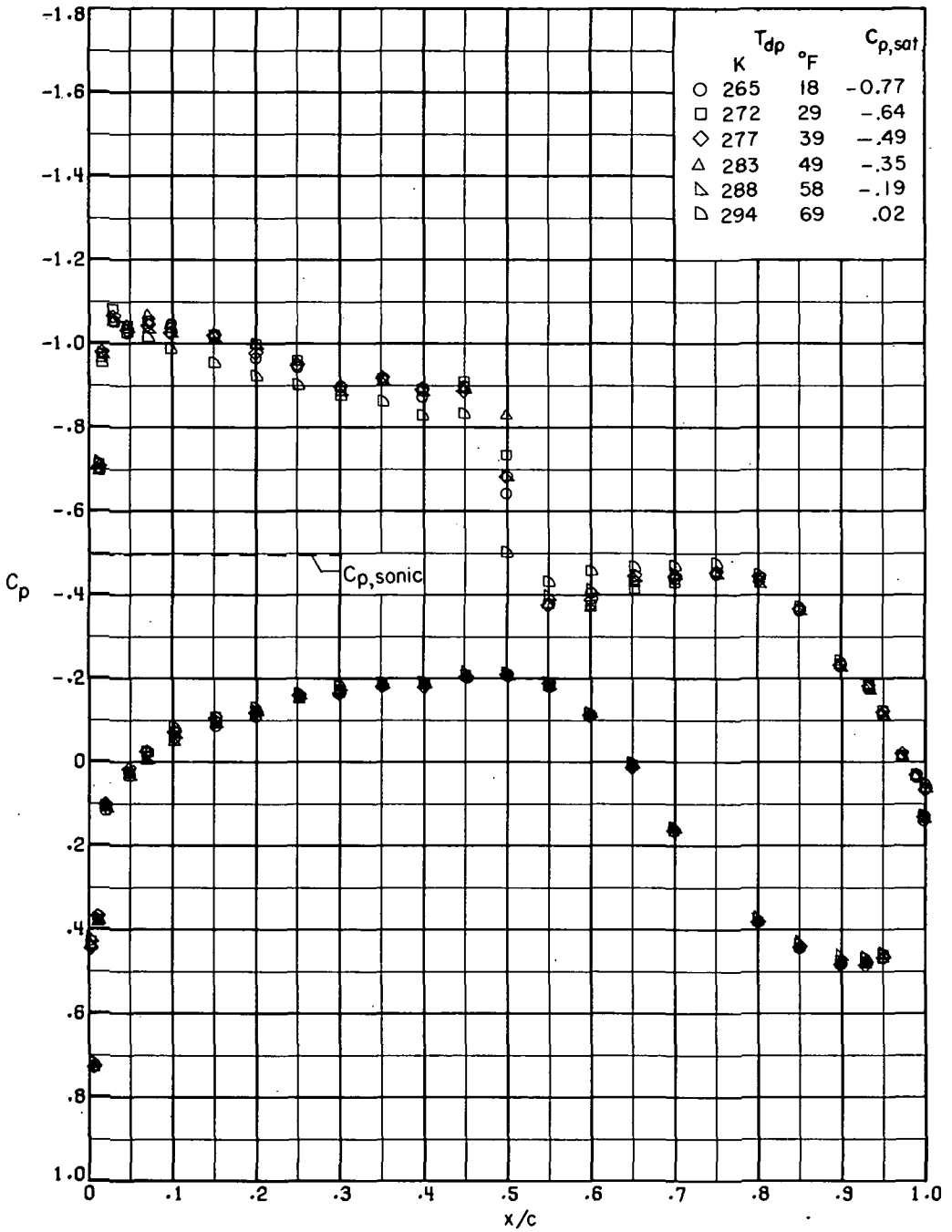

(i) M = 0.78; $\alpha = 2.0^{\circ}$.

Figure 9.- Continued.

[redacted]

[redacted]

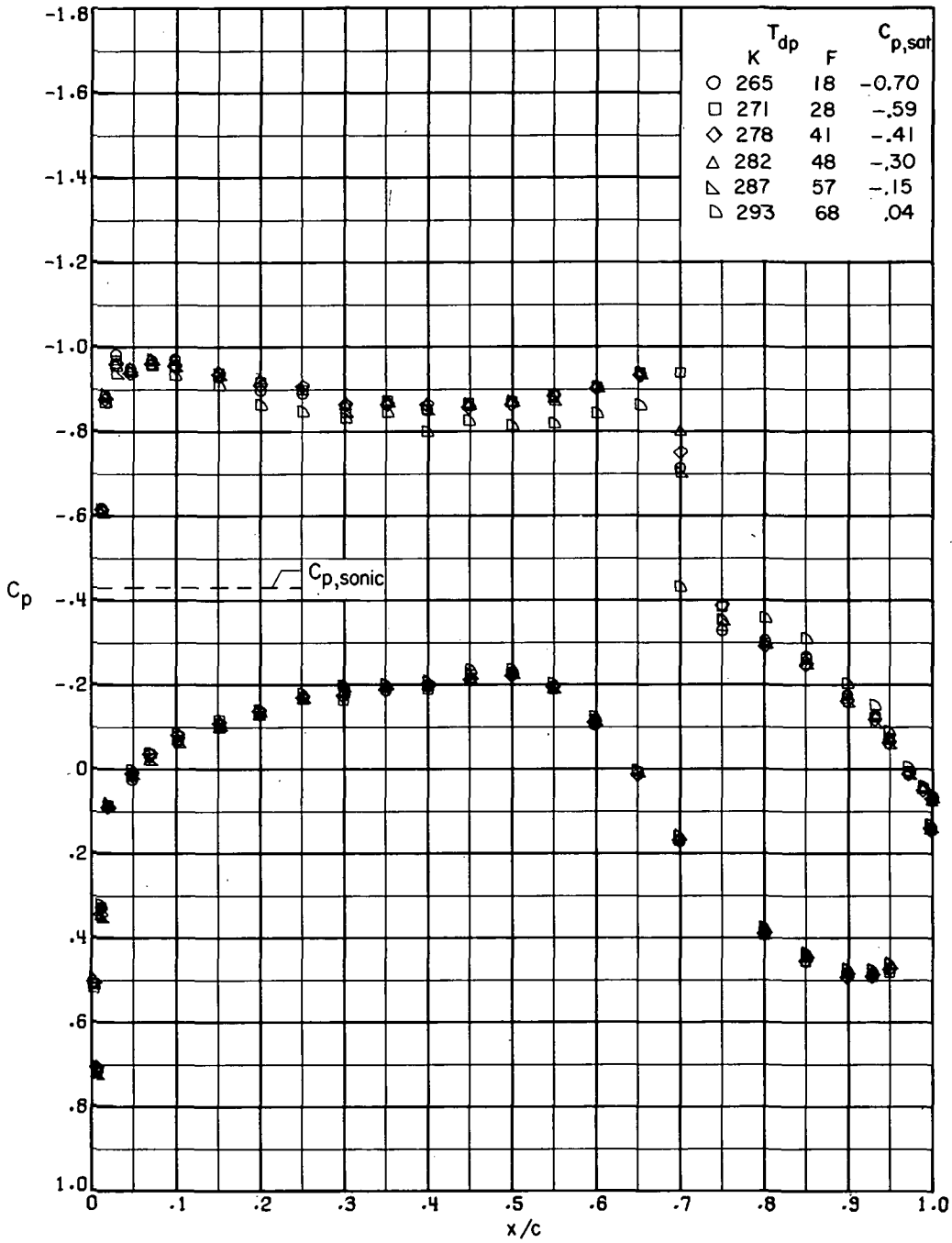

(j) M = 0.80; $\alpha = 2.0^{\circ}$.

Figure 9.- Continued.

[redacted]

[redacted]

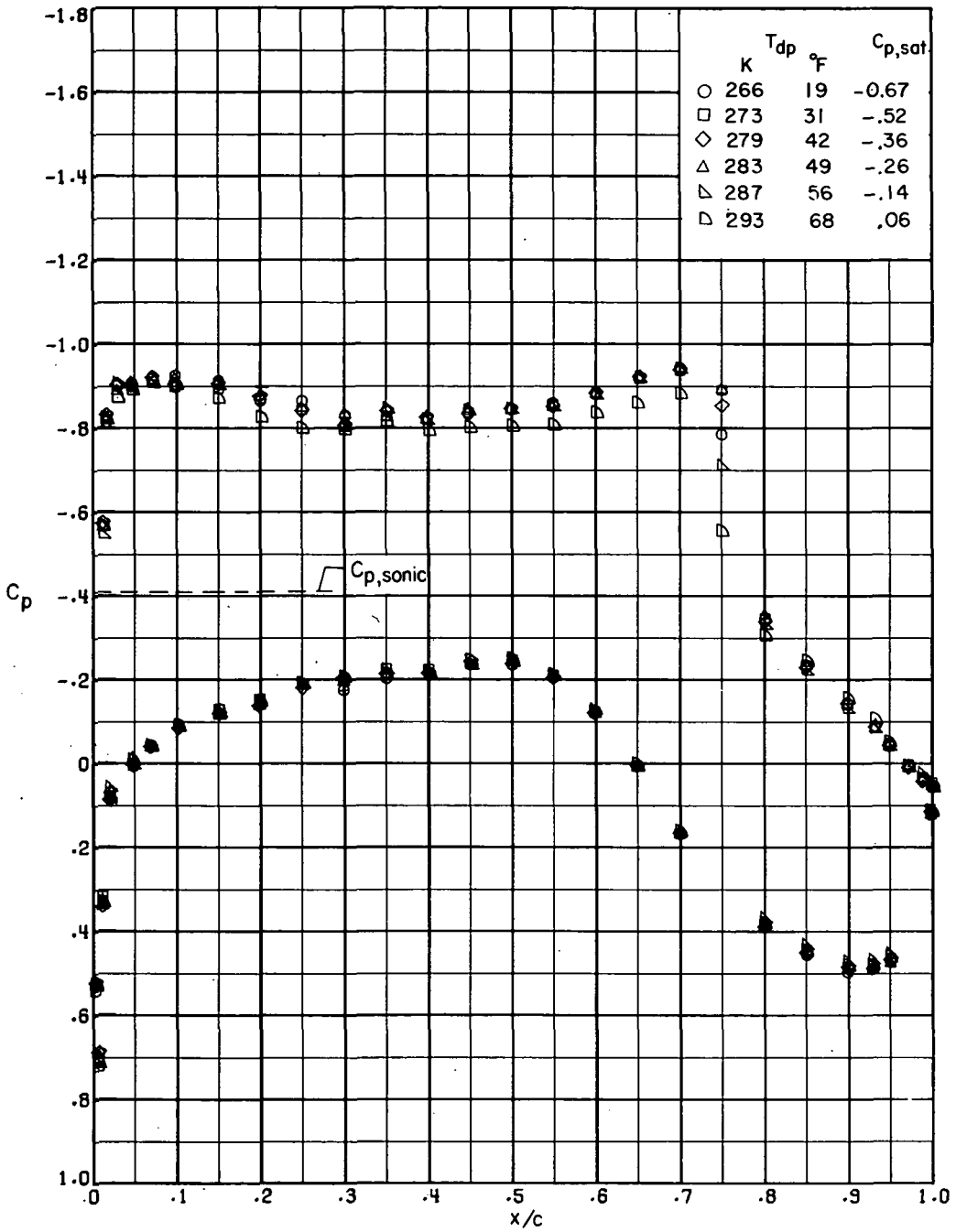

(k) M = 0.81; $\alpha = 2.0^{\circ}$.

Figure 9.- Continued.

[redacted]

[redacted]

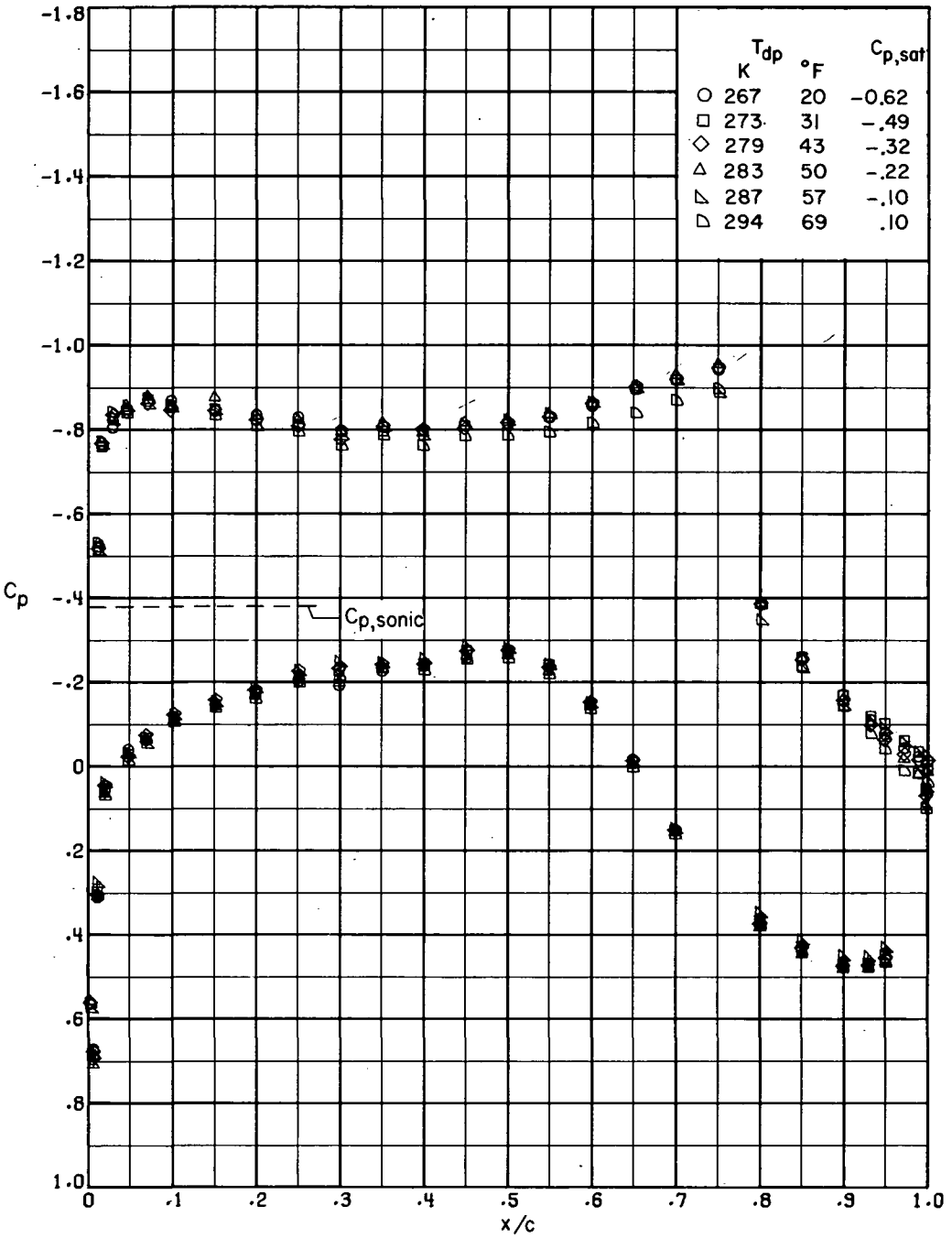

(l) M = 0.82; $\alpha = 2.0^{\circ}$.

Figure 9.- Continued.

[redacted]

[redacted]

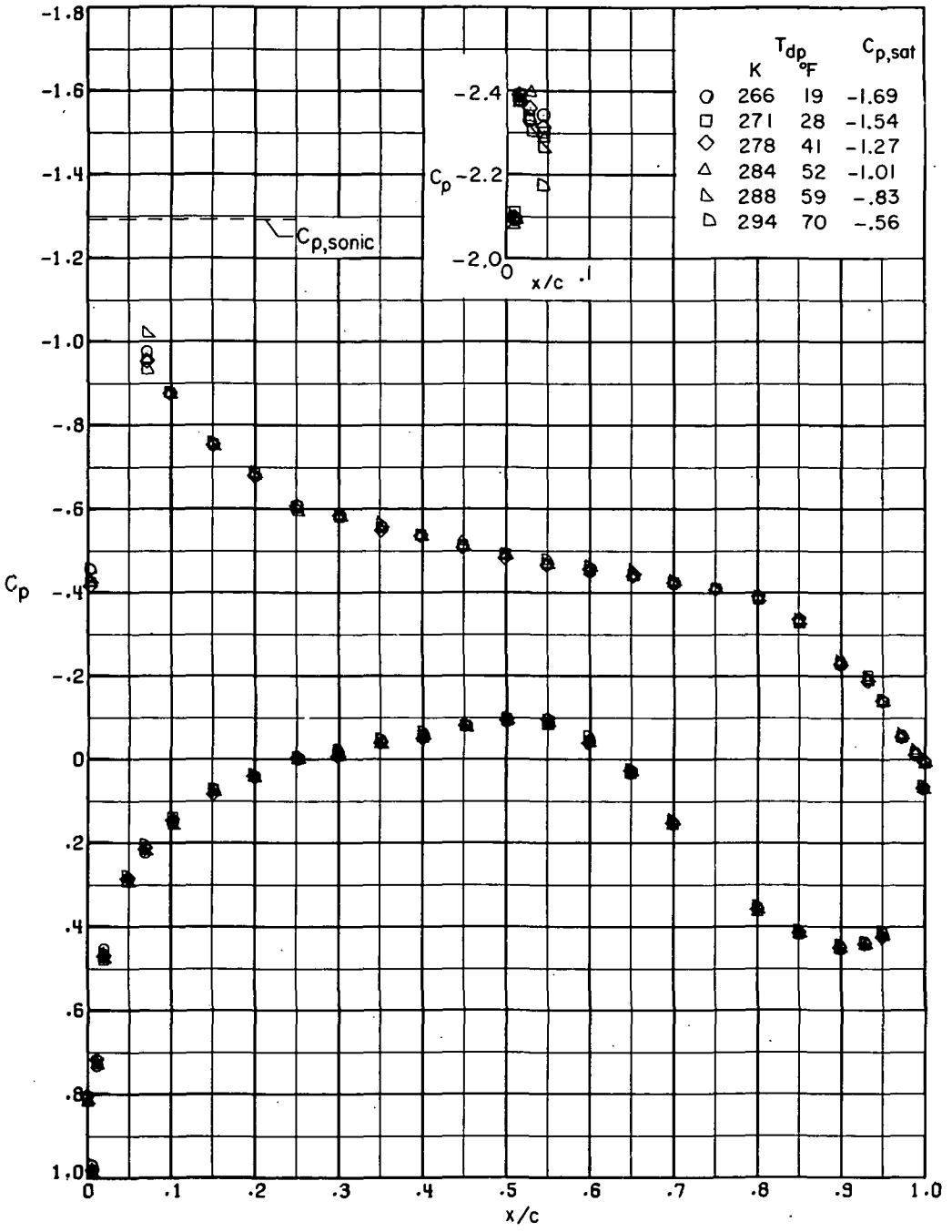

(m) M = 0.60; α = 3.5°.

Figure 9.- Continued.

[redacted]

[redacted]

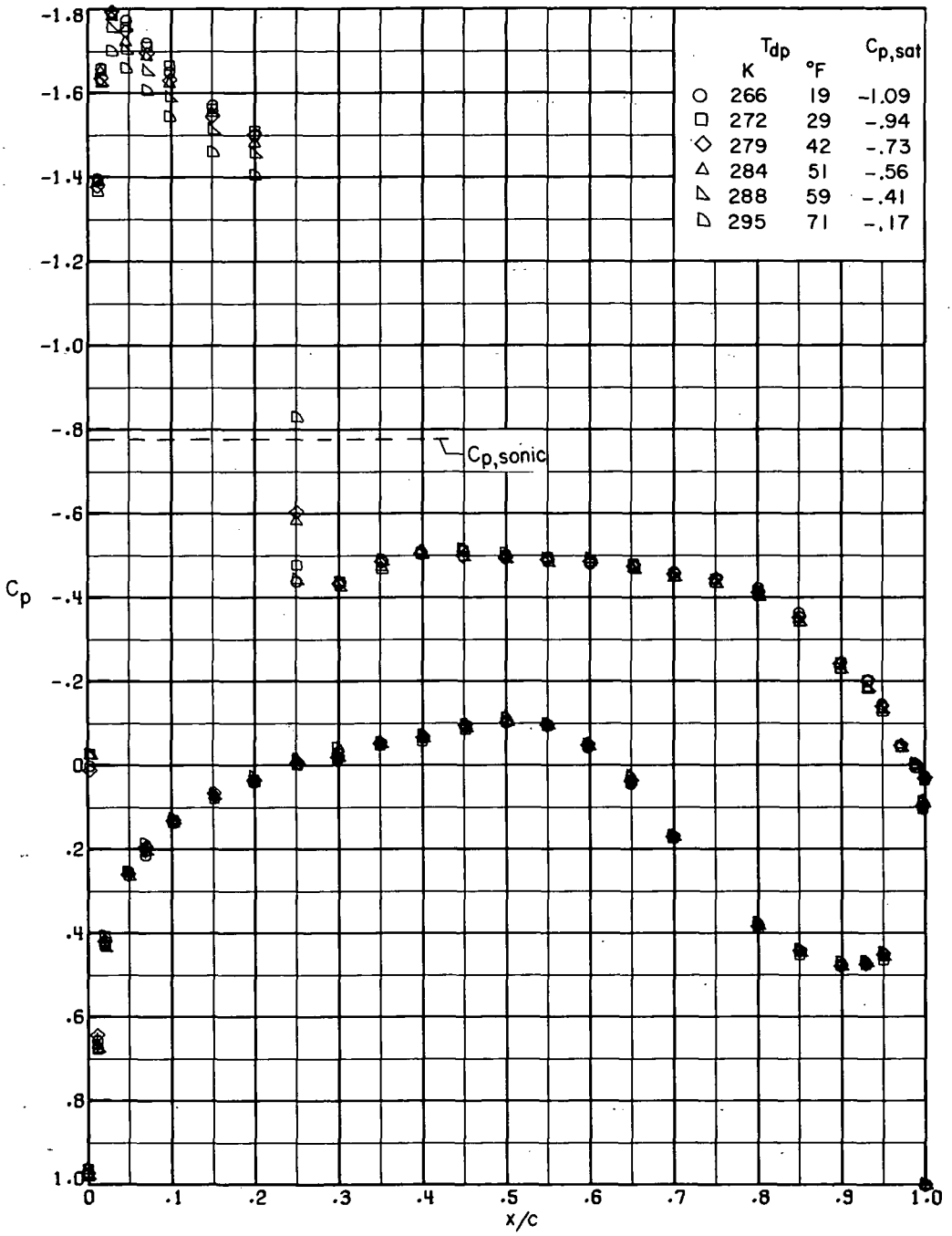

(n) M = 0.70; $\alpha = 3.5^{\circ}$.

Figure 9.- Continued.

[redacted]

[redacted]

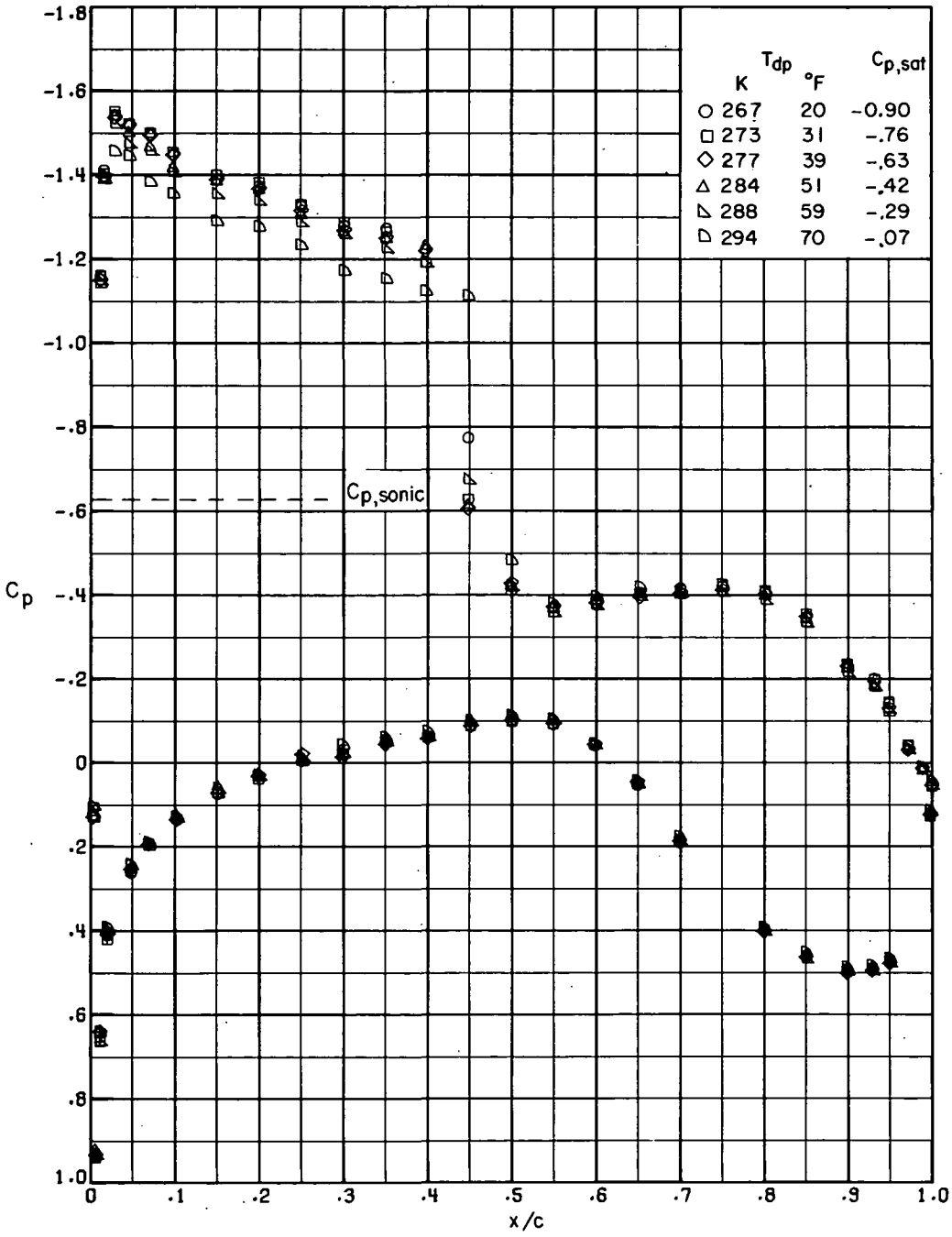

(o) M = 0.74; $\alpha = 3.5^{\circ}$.

Figure 9.- Continued.

[redacted]

[redacted]

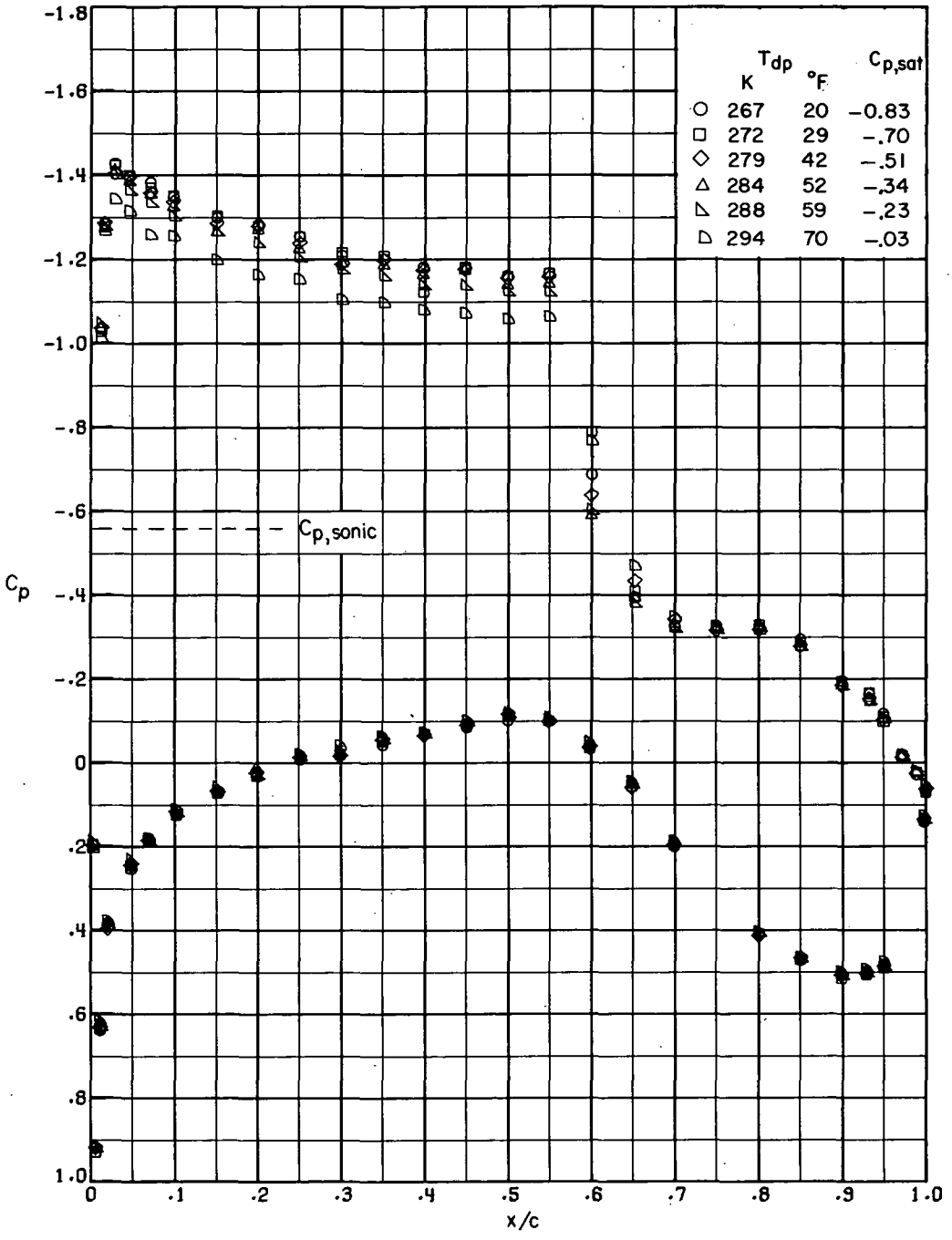

(p) M = 0.76; $\alpha = 3.5^{\circ}$.

Figure 9.- Concluded.

[redacted]

[redacted]

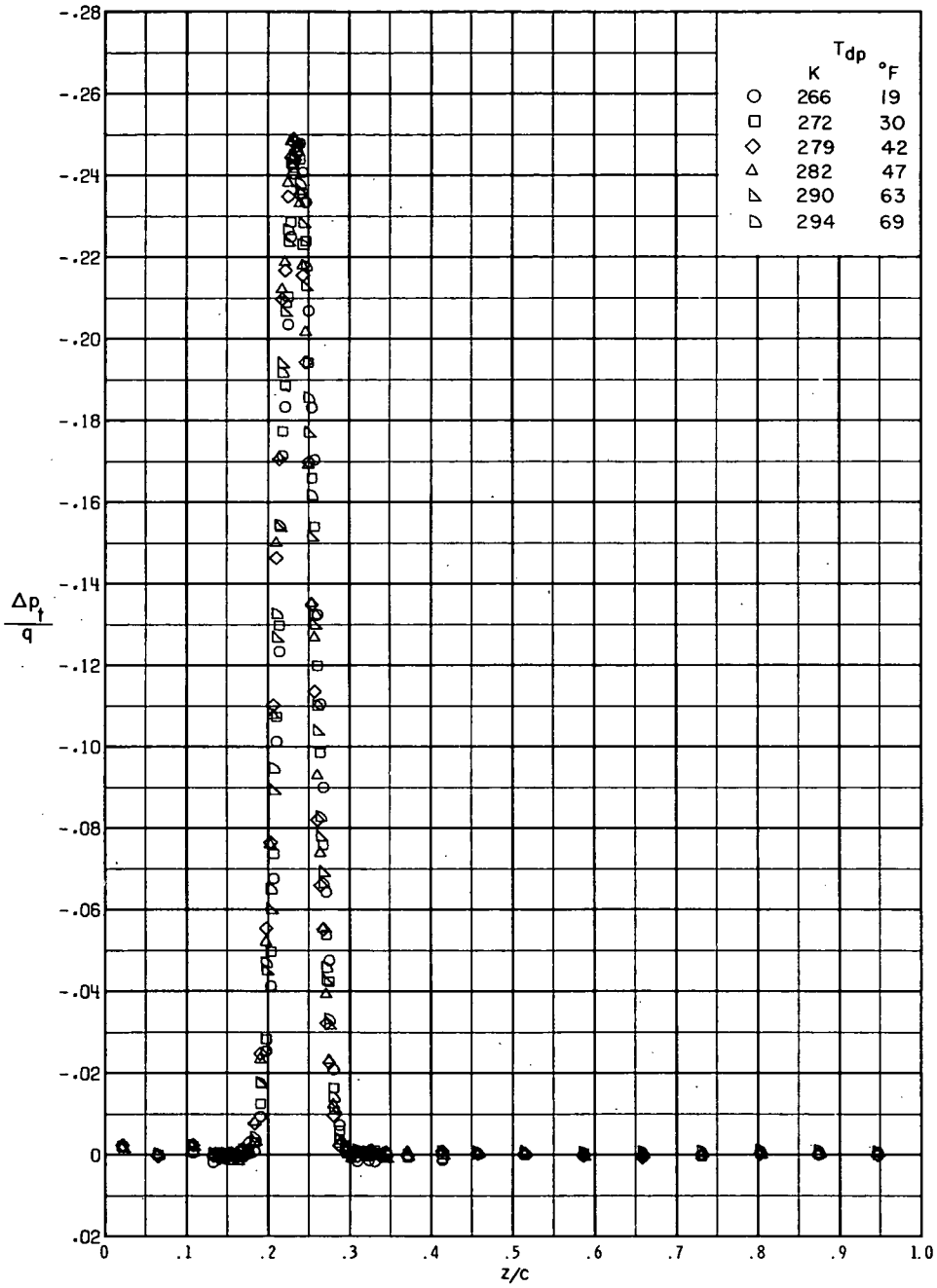

(a) M = 0.74; α = 1.0°.

Figure 10.- Effect of wind-tunnel humidity on wake profiles.

[redacted]

[redacted]

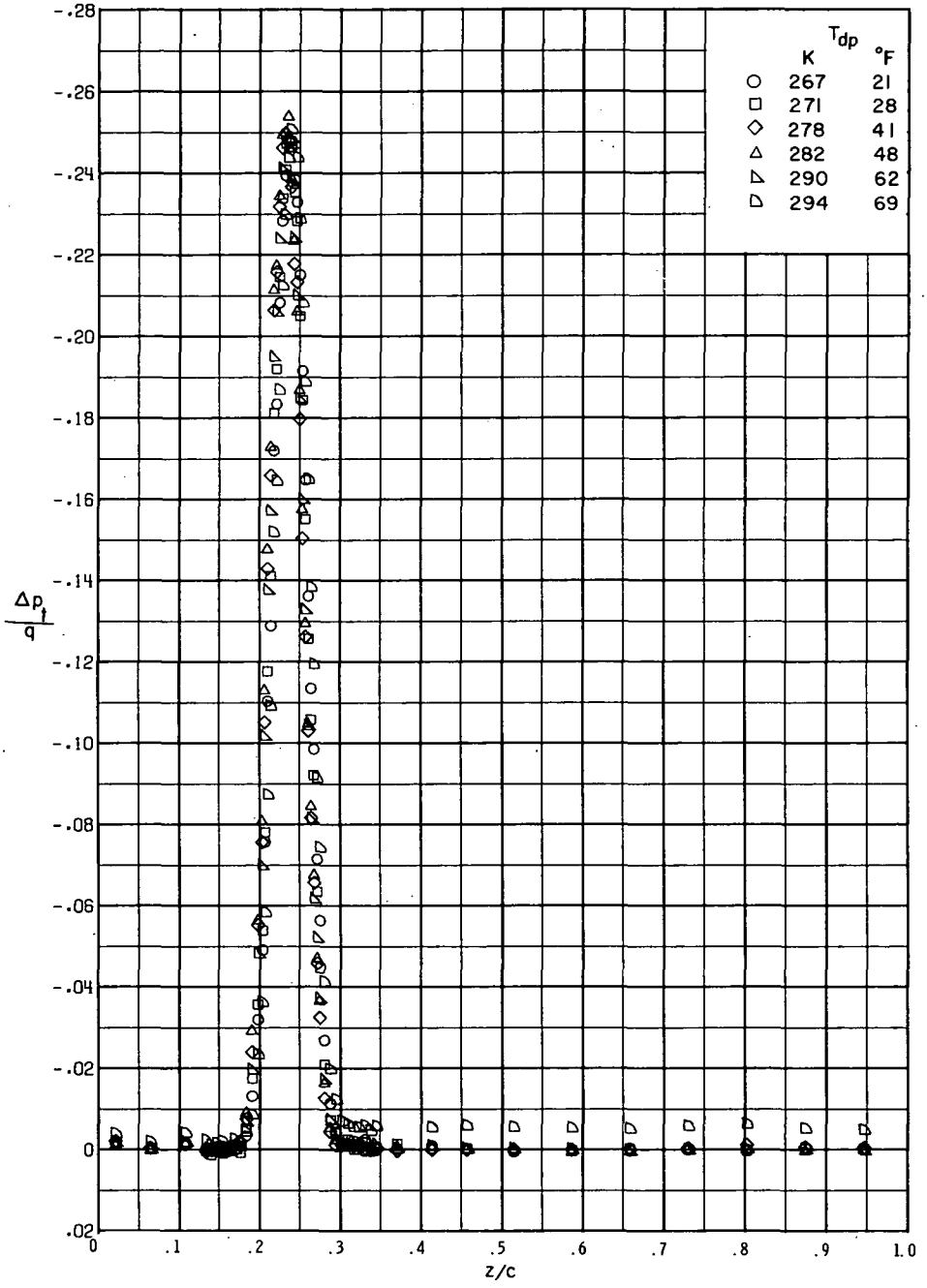

(b) M = 0.78; α = 1.0°.

Figure 10.- Continued.

[redacted]

[redacted]

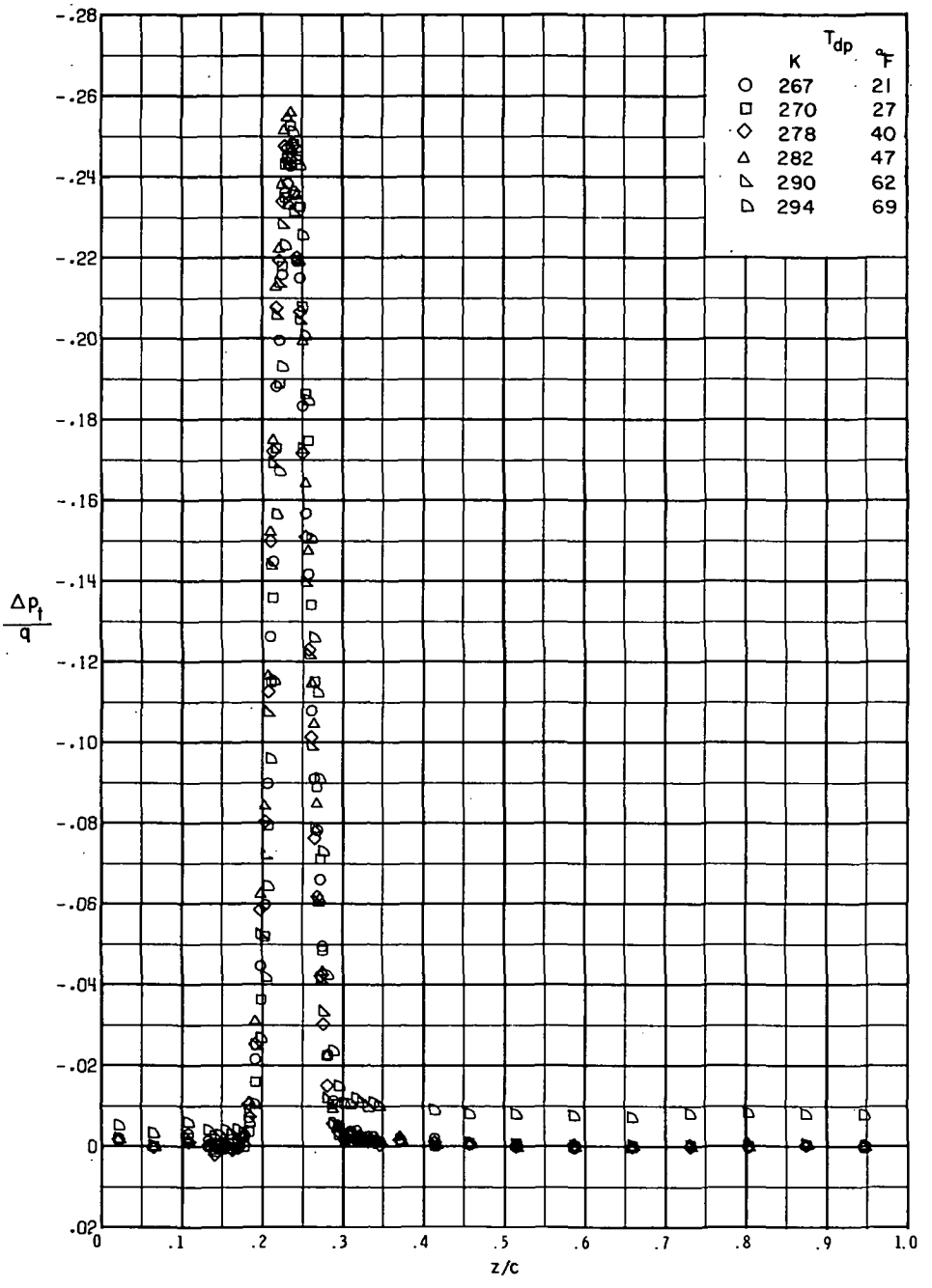

(c) M = 0.80; α = 1.0°.

Figure 10.- Continued.

[redacted]

[redacted]

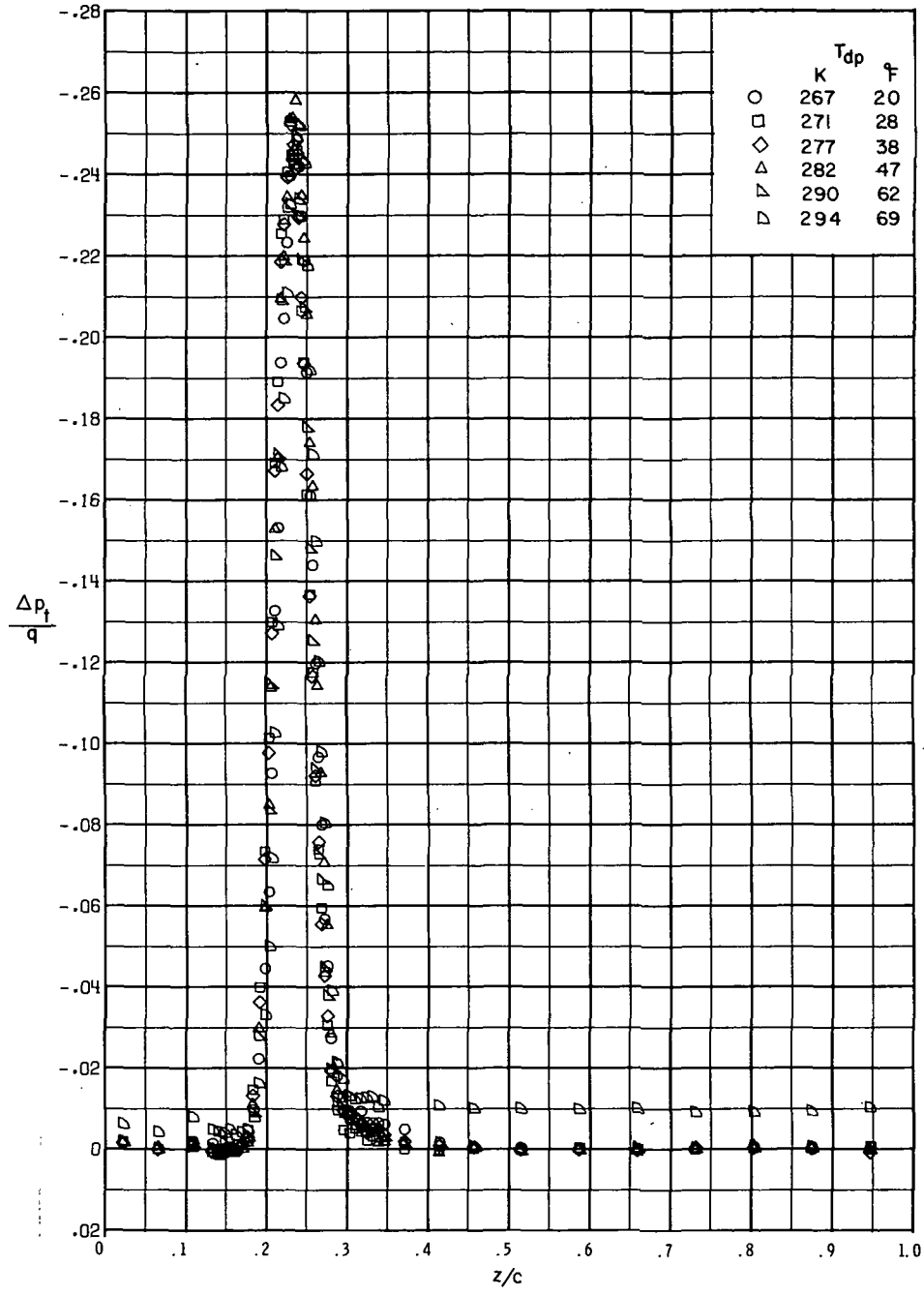

(d) M = 0.81; α = 1.0°.

Figure 10.- Continued.

[redacted]

[redacted]

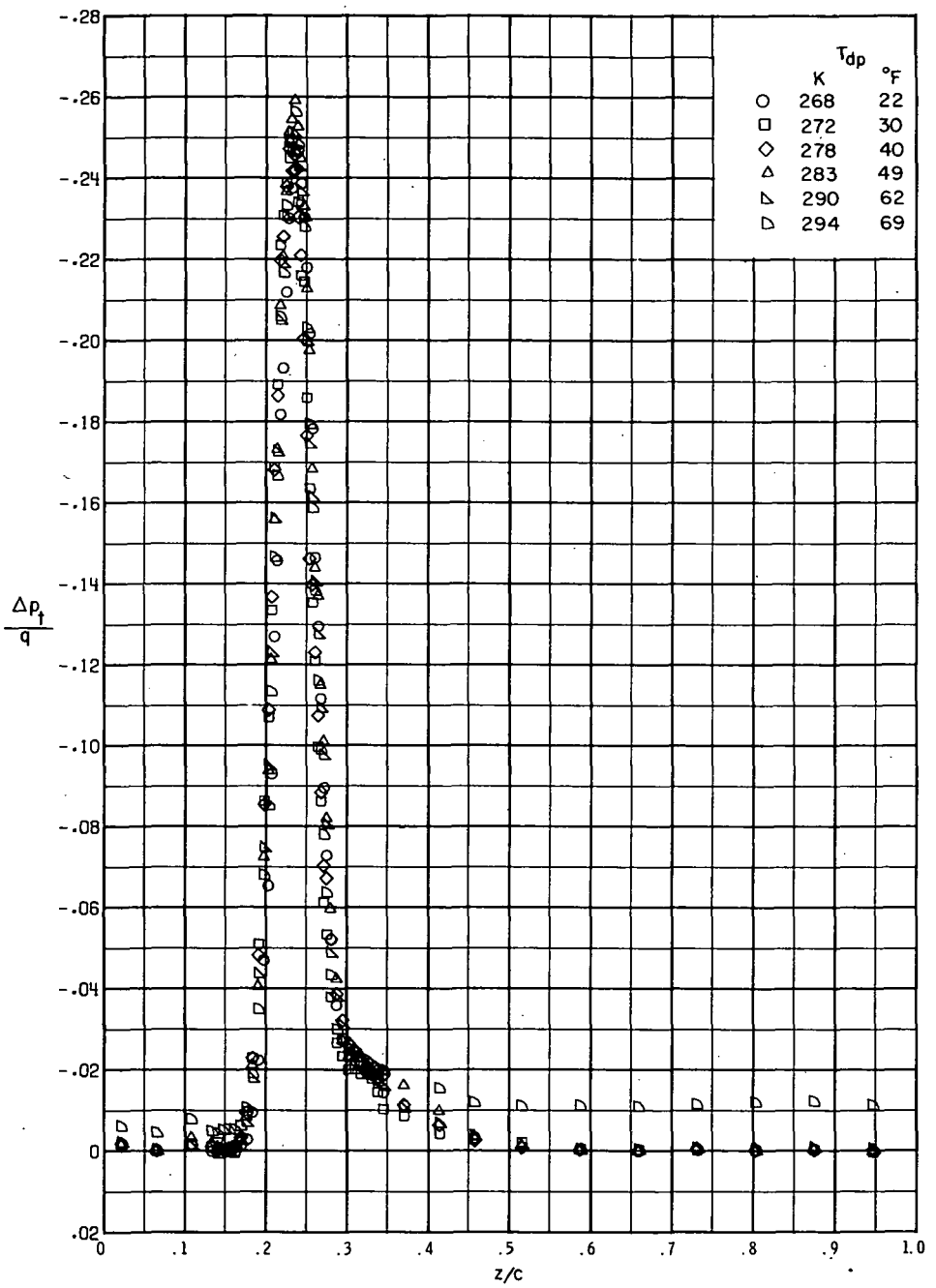

(e) M = 0.82; α = 1.0°.

Figure 10.- Continued.

[redacted]

[redacted]

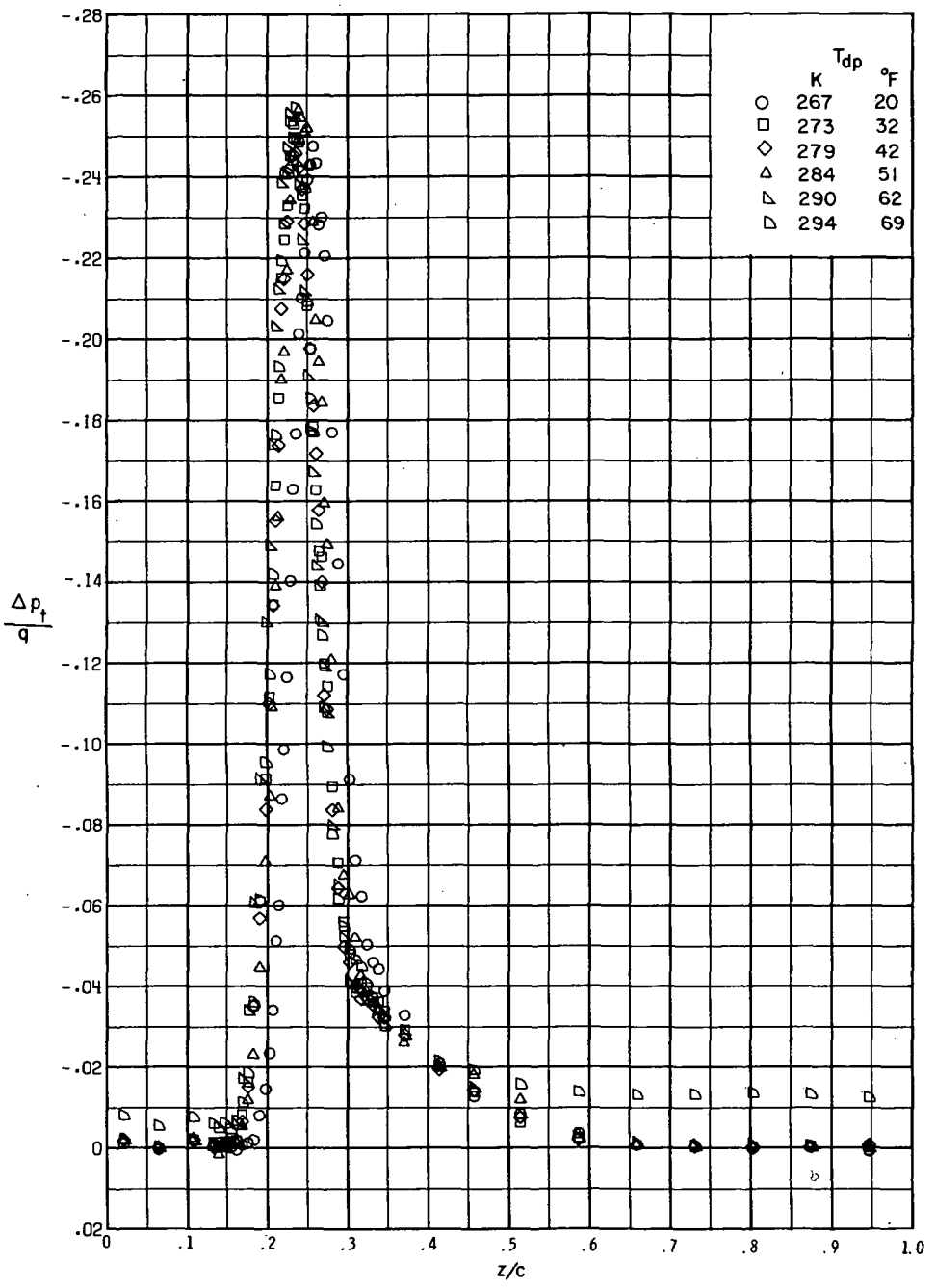

(f) M = 0.83; α = 1.0°.

Figure 10.- Continued.

[redacted]

[redacted]

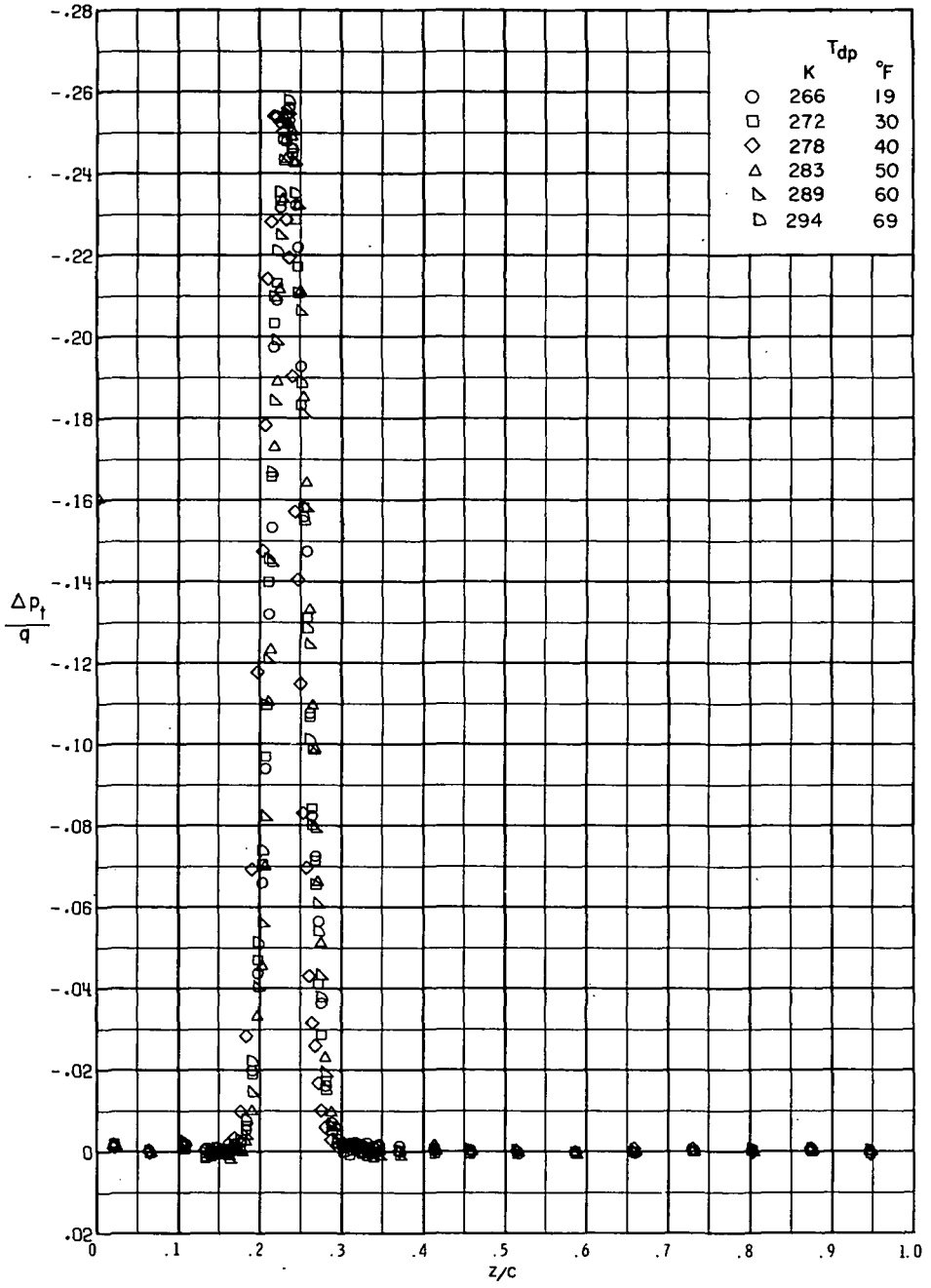

(g) M = 0.70; α = 2.0°.

Figure 10.- Continued.

[redacted]

[redacted]

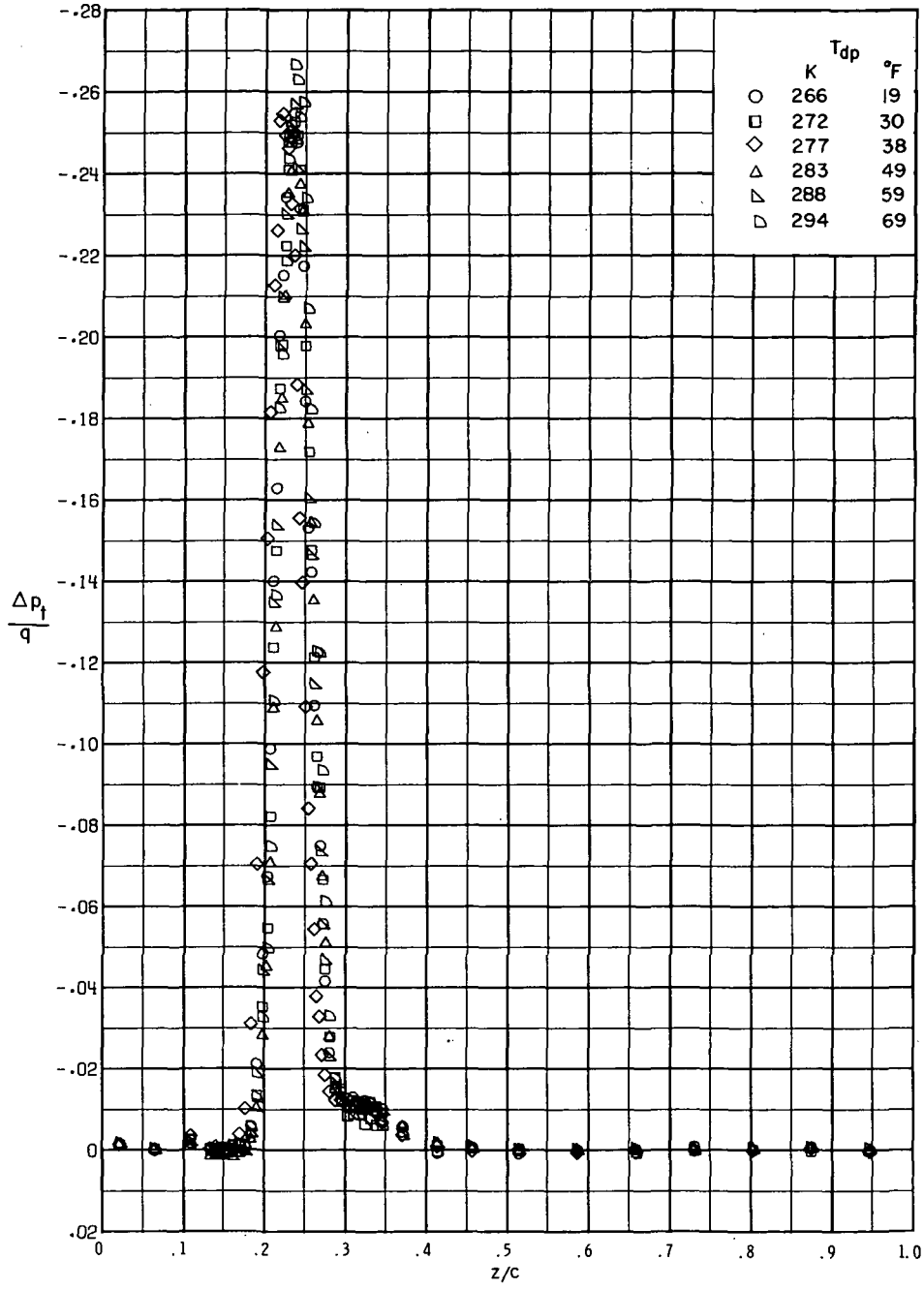

(h) M = 0.74; $\alpha = 2.0^{\circ}$.

Figure 10.- Continued.

[redacted]

[redacted]

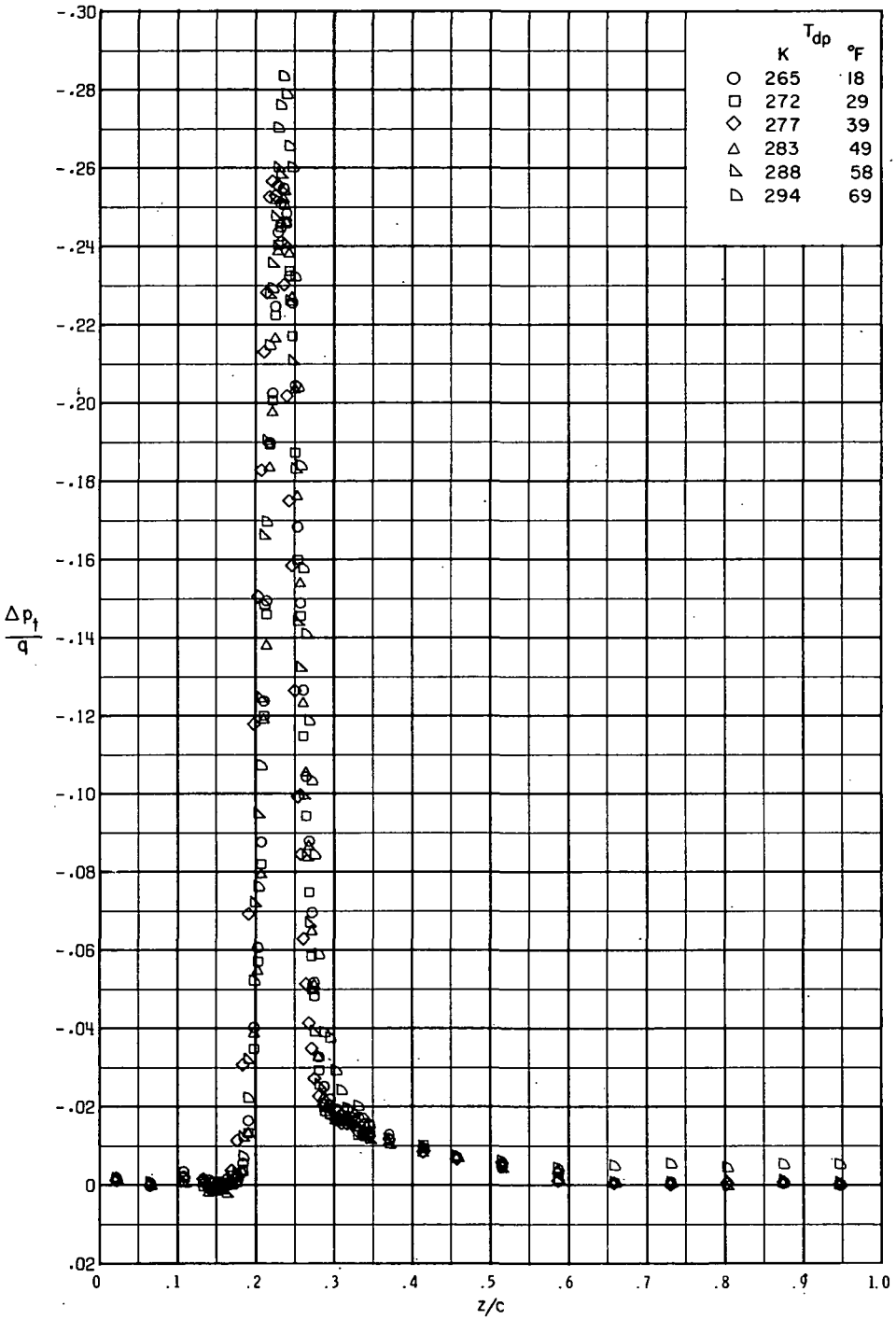

(i) M = 0.78; $\alpha = 2.0^{\circ}$.

Figure 10.- Continued.

[redacted]

[redacted]

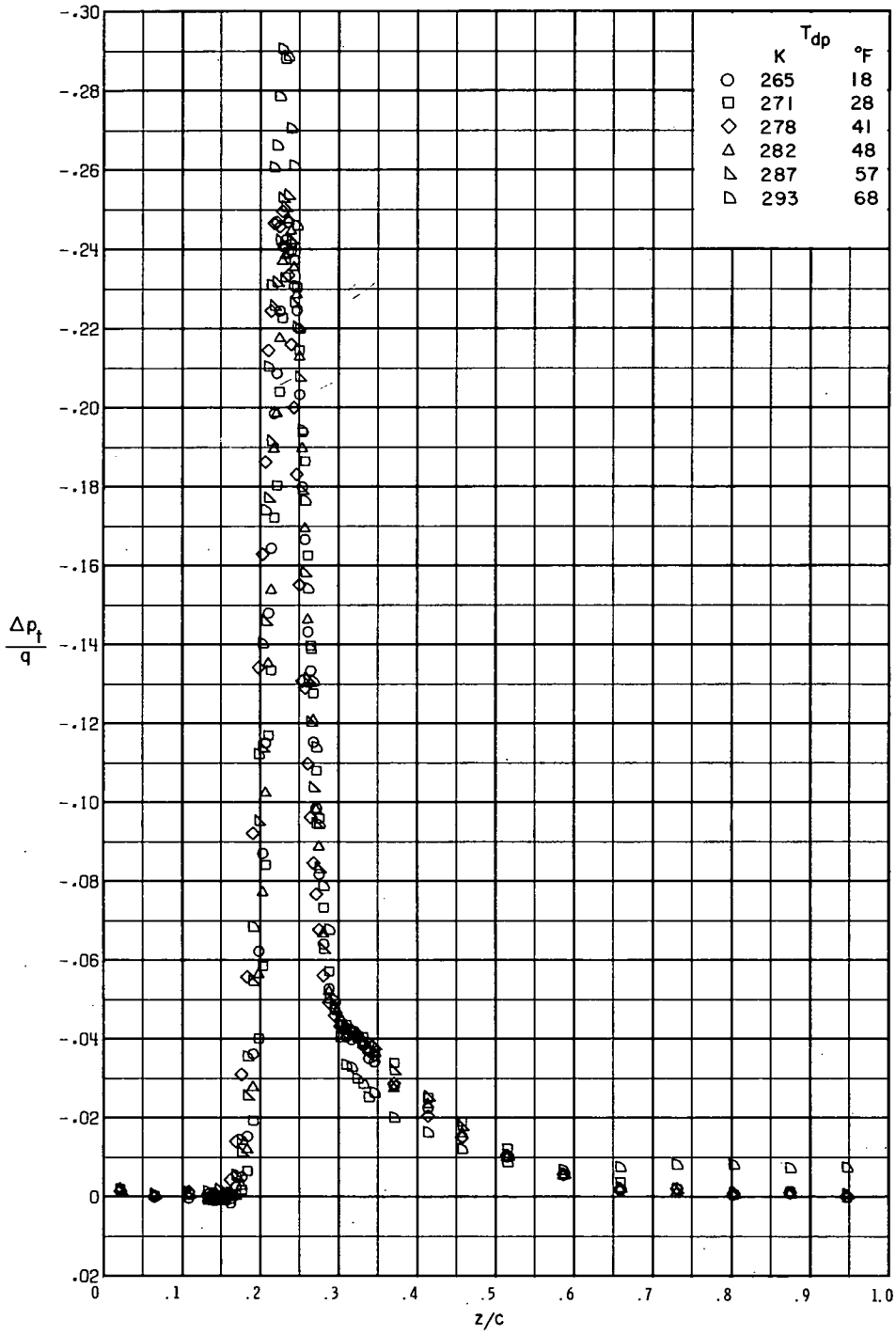

(j) M = 0.80; $\alpha = 2.0^{\circ}$.

Figure 10.- Continued.

[redacted]

[redacted]

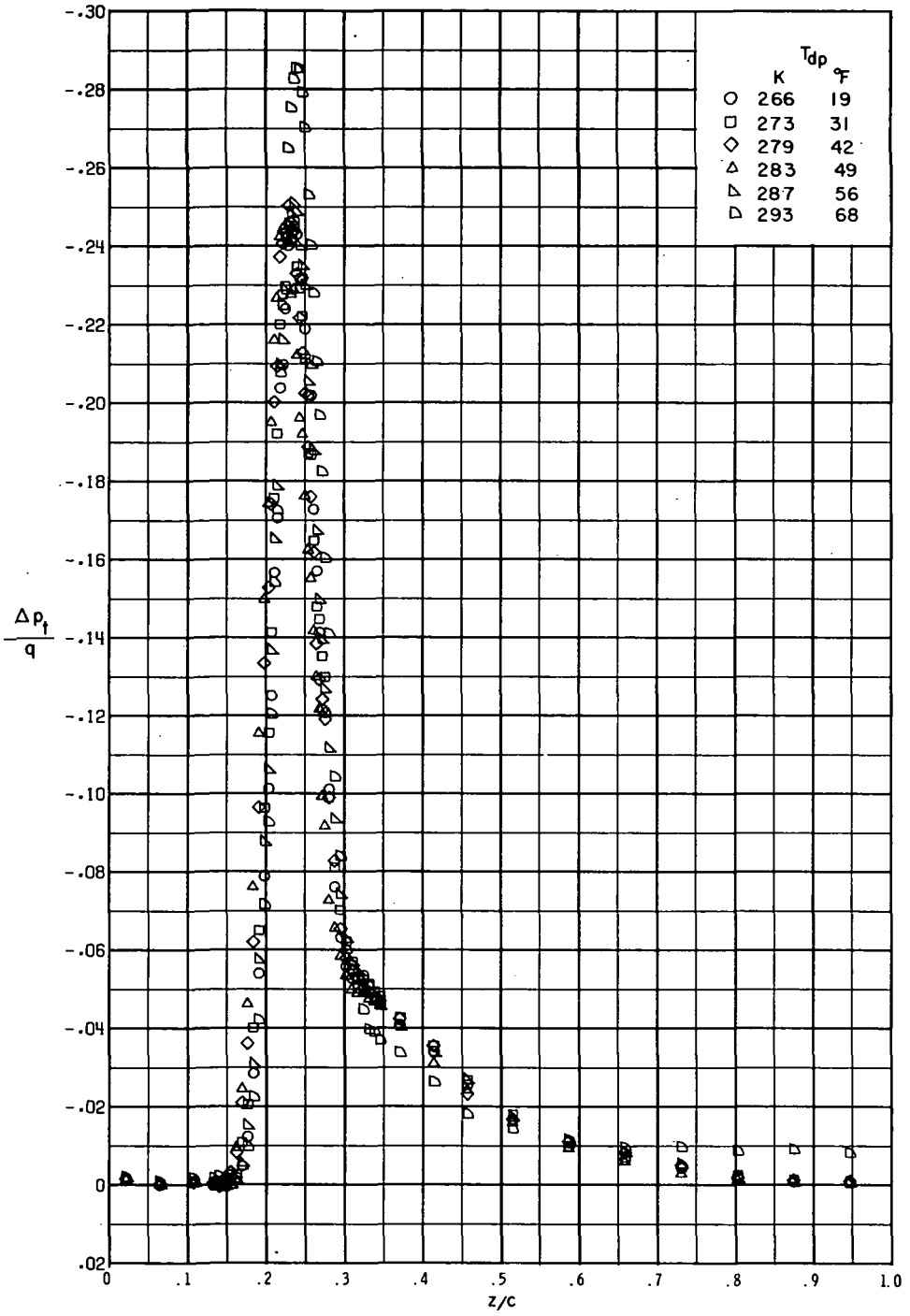

(k) M = 0.81; $\alpha = 2.0^{\circ}$.

Figure 10.- Continued.

[redacted]

[redacted]

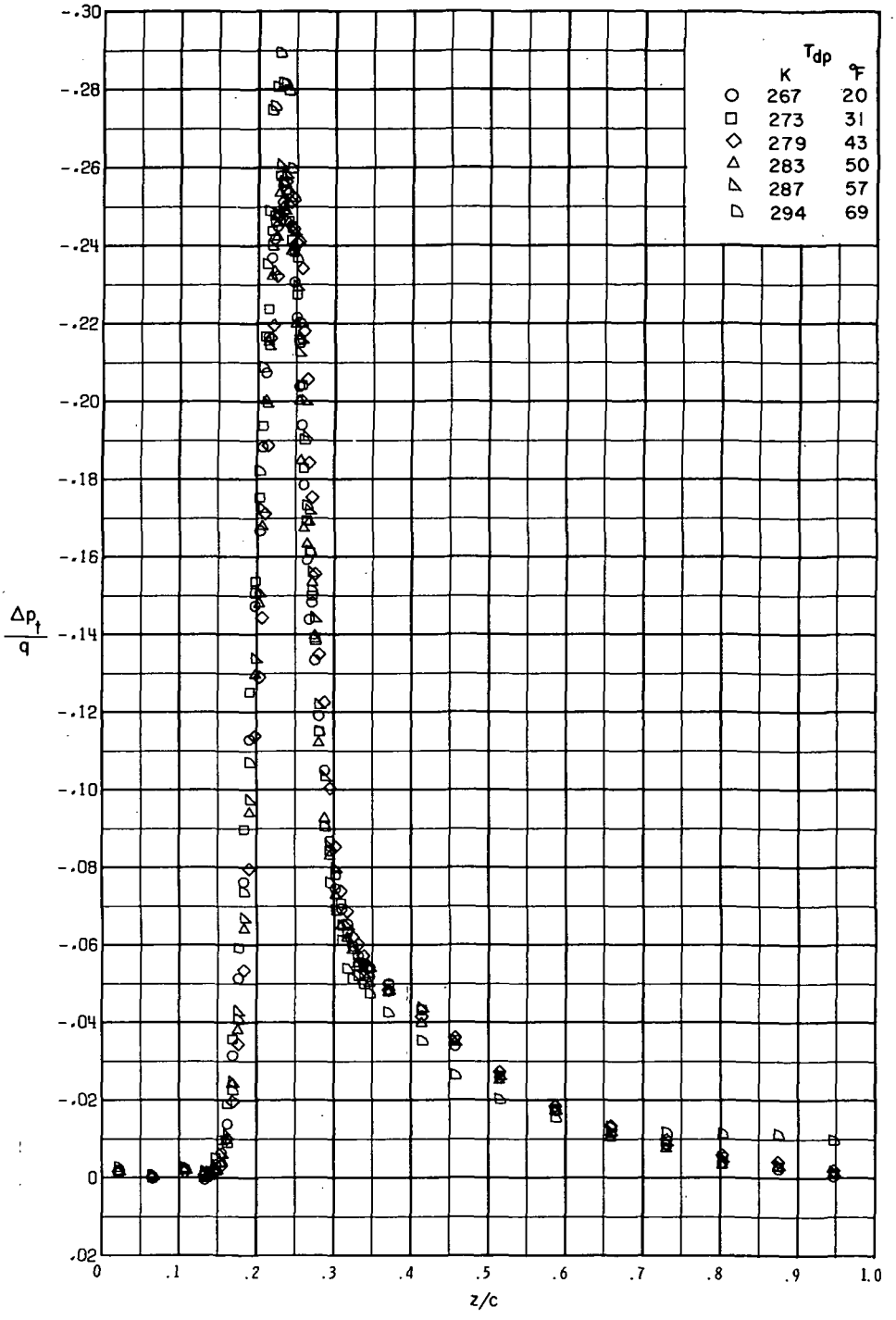

(l) M = 0.82; α = 2.0°.

Figure 10.- Continued.

[redacted]

[redacted]

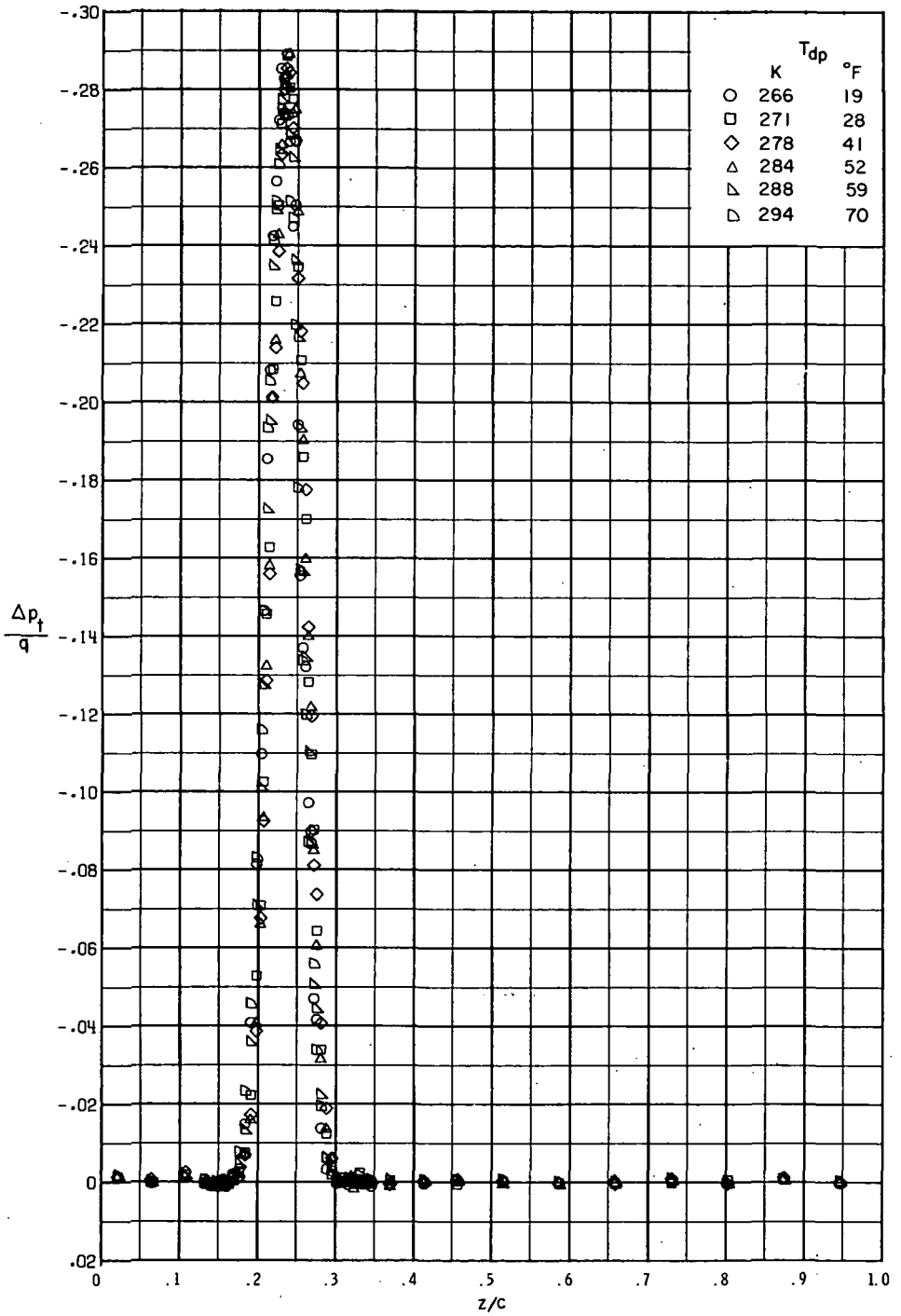

(m) M = 0.60; $\alpha = 3.5^{\circ}$.

Figure 10.- Continued.

[redacted]

[redacted]

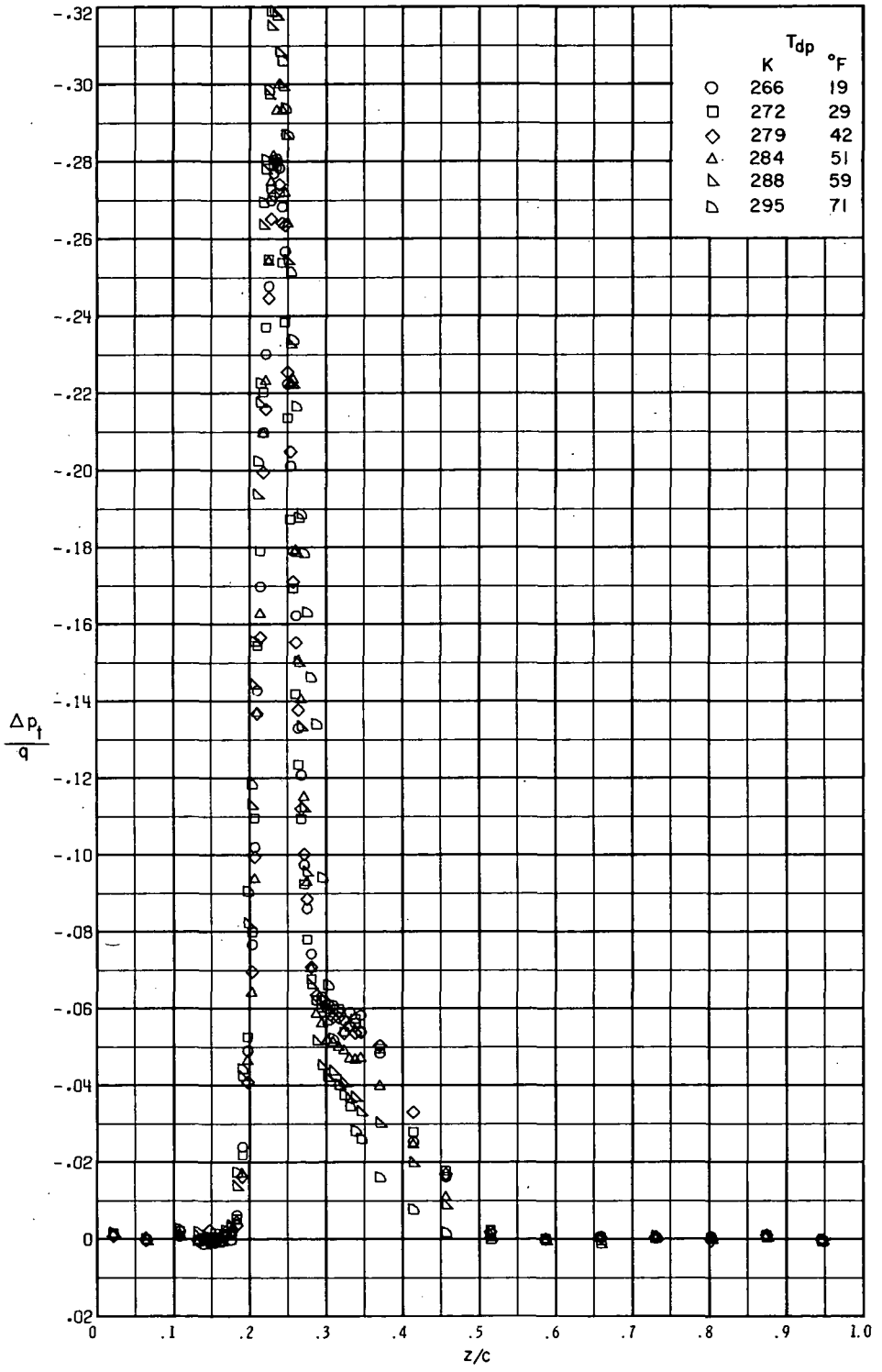

(n) M = 0.70; α = 3.5°.

Figure 10.- Continued.

[redacted]

[redacted]

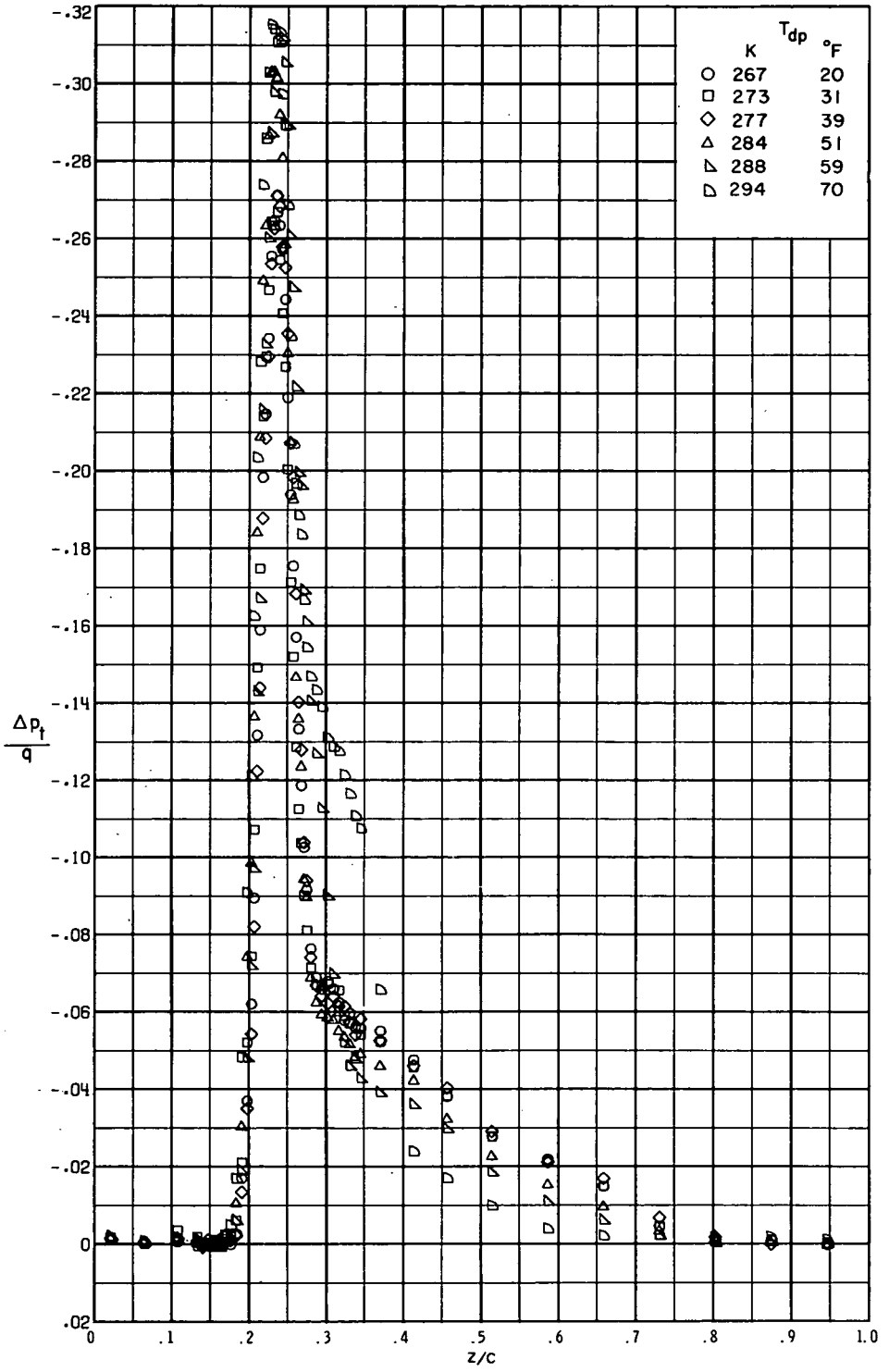

(o) M = 0.74; $\alpha = 3.5^{\circ}$.

Figure 10.- Continued.

[redacted]

[redacted]

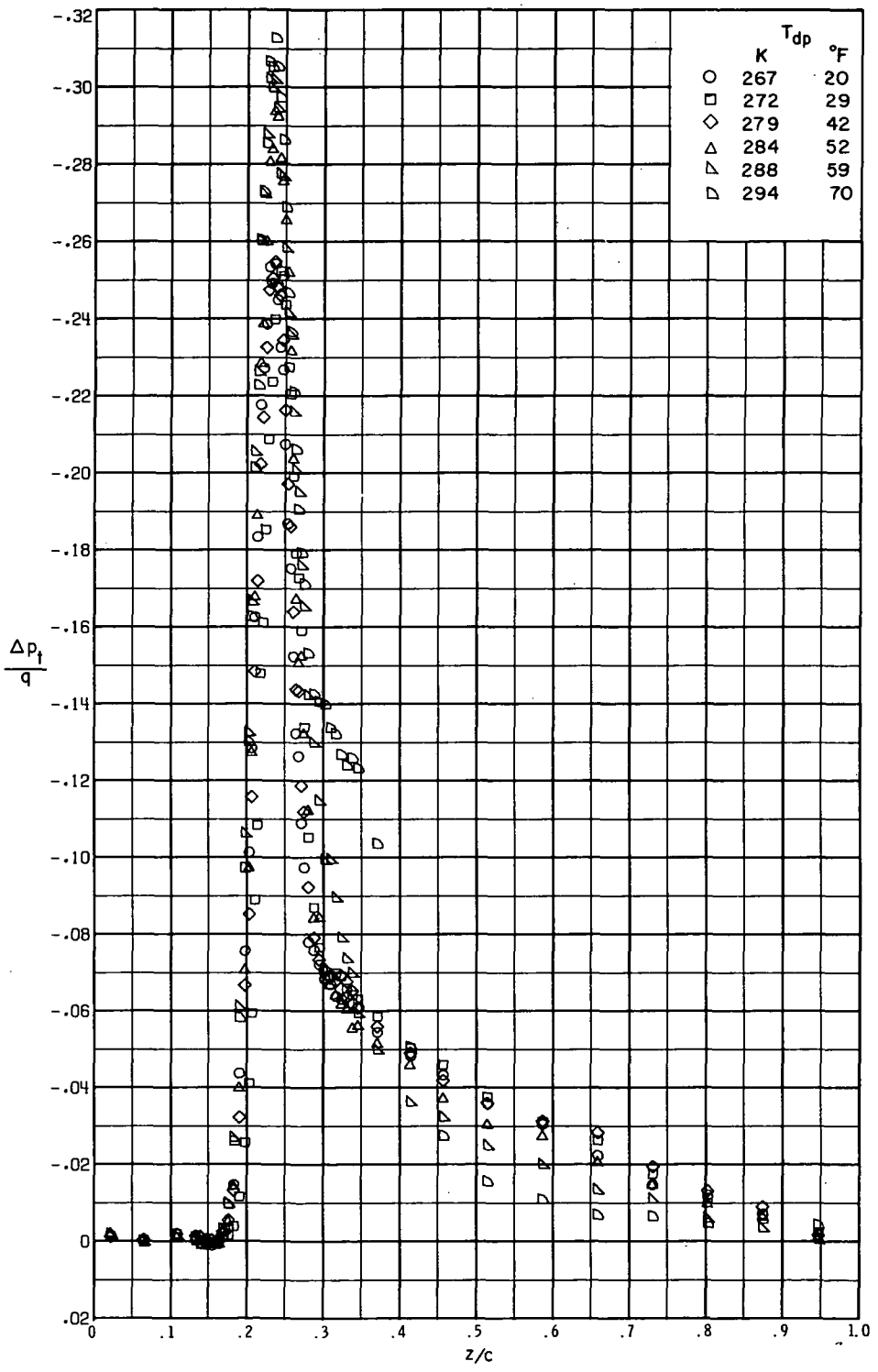

(p) M = 0.76; $\alpha = 3.5^{\circ}$.

Figure 10.- Concluded.

[redacted]

[redacted]

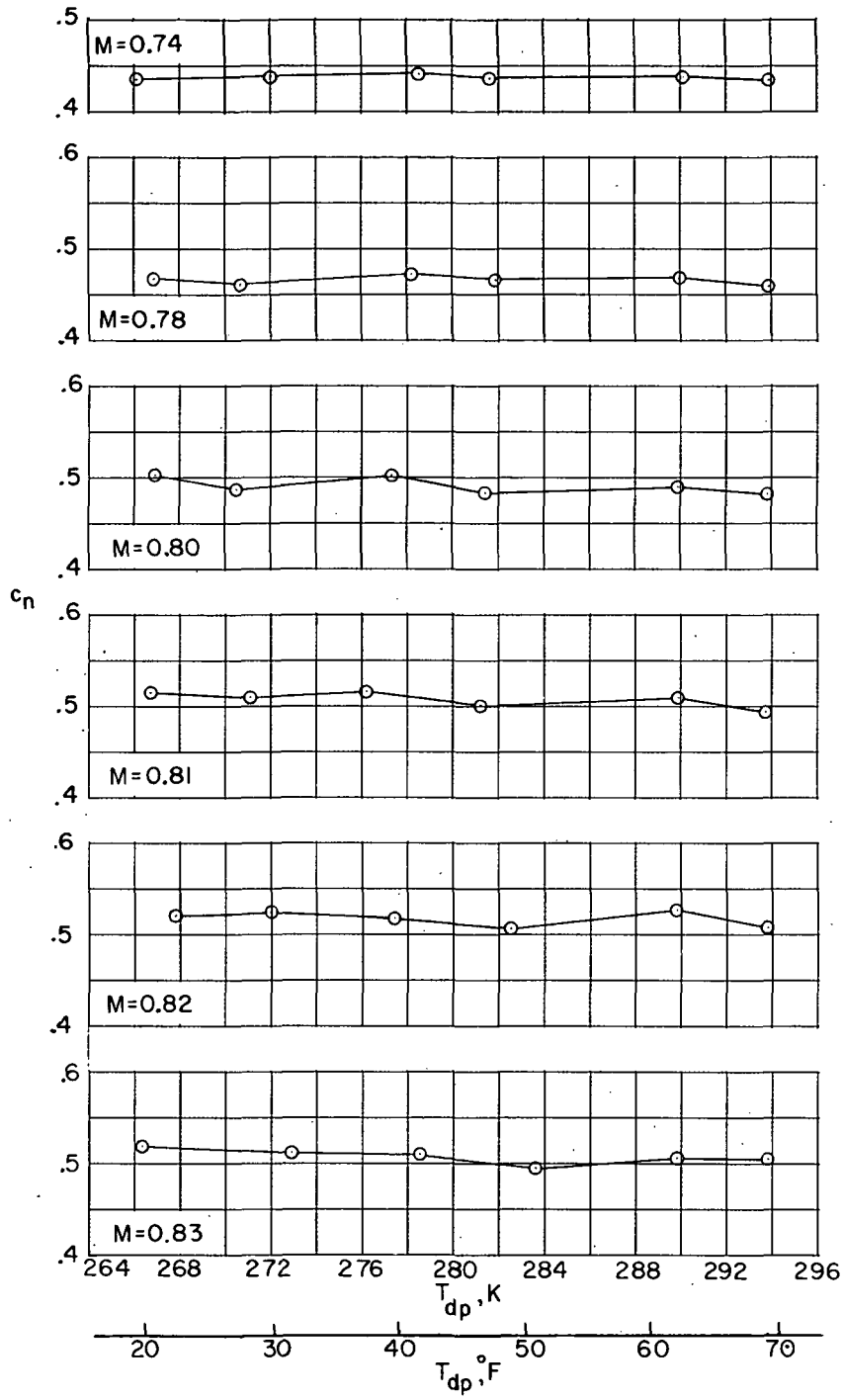

(a) $\alpha = 1.0^{\circ}$.

Figure 11.- Effect of wind-tunnel humidity on section normal-force coefficient.

[redacted]

[redacted]

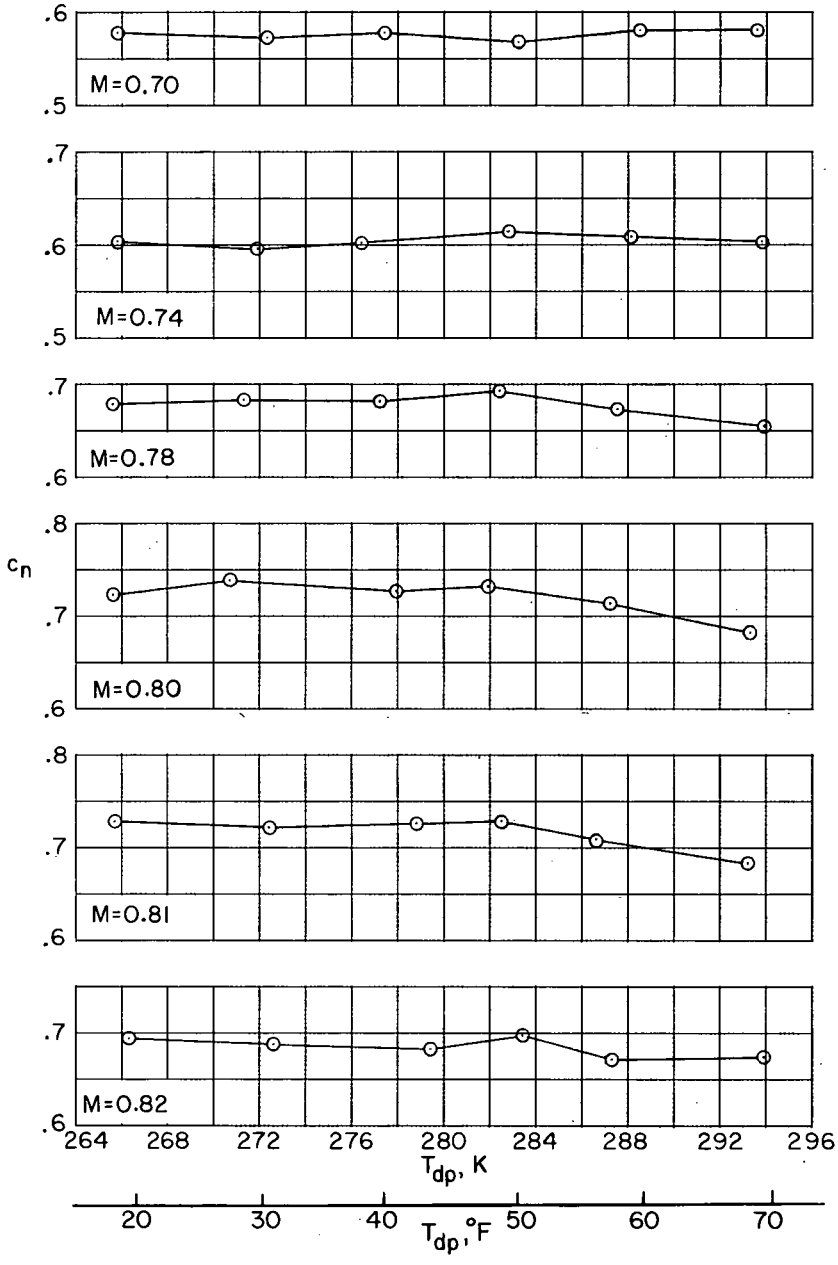

(b) $\alpha = 2.0^{\circ}$.

Figure 11.- Continued.

[redacted]

[redacted]

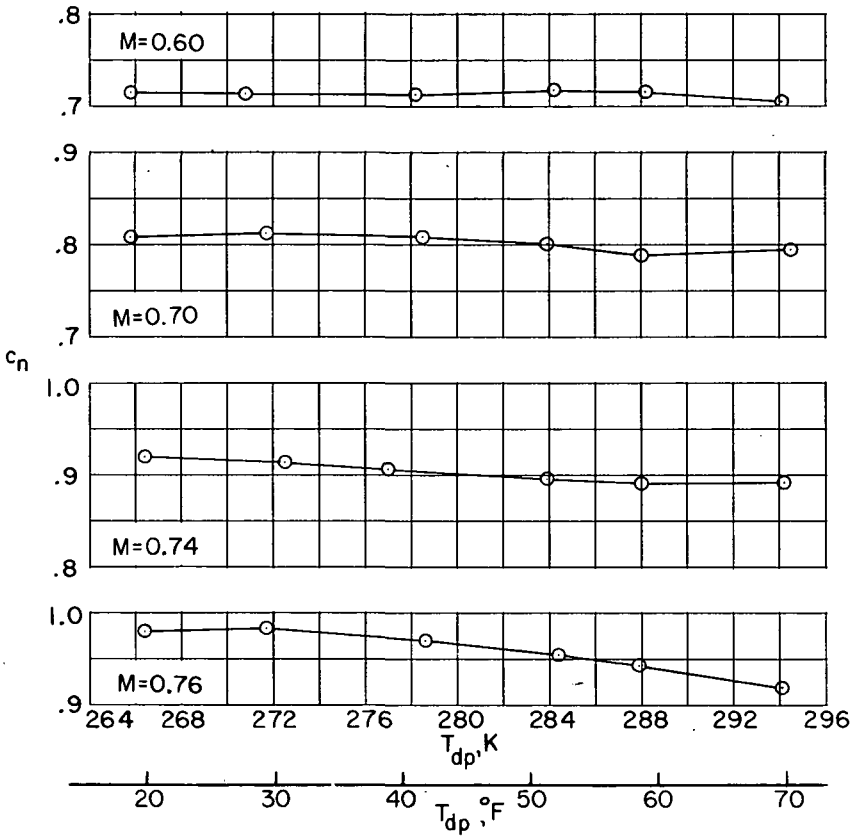

(c) $\alpha = 3.5^{\circ}$.

Figure 11.- Concluded.

[redacted]

[redacted]

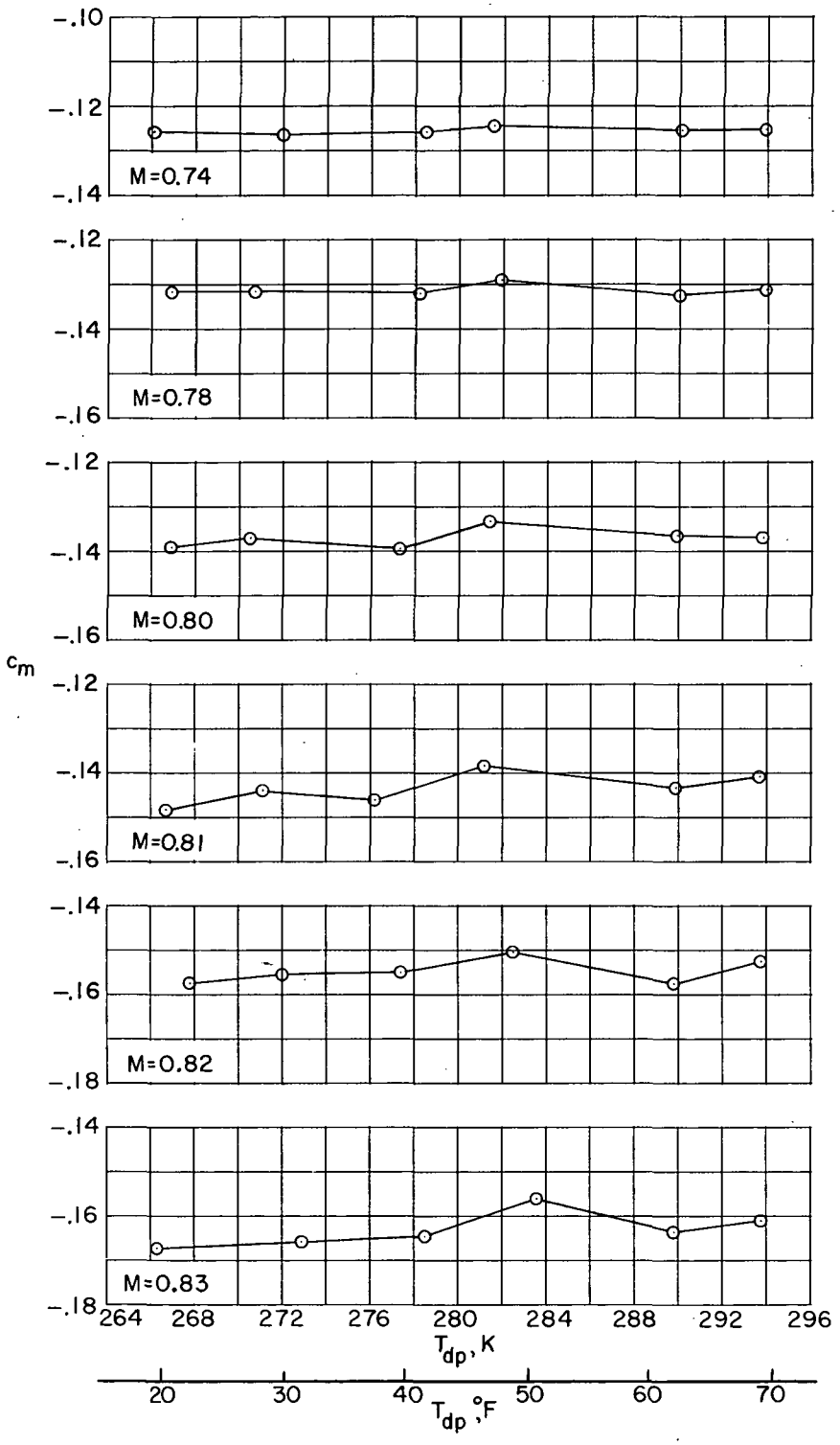

(a) $\alpha = 1.0^{\circ}$.

Figure 12.- Effect of wind-tunnel humidity on section pitching-moment coefficient.

[redacted]

[redacted]

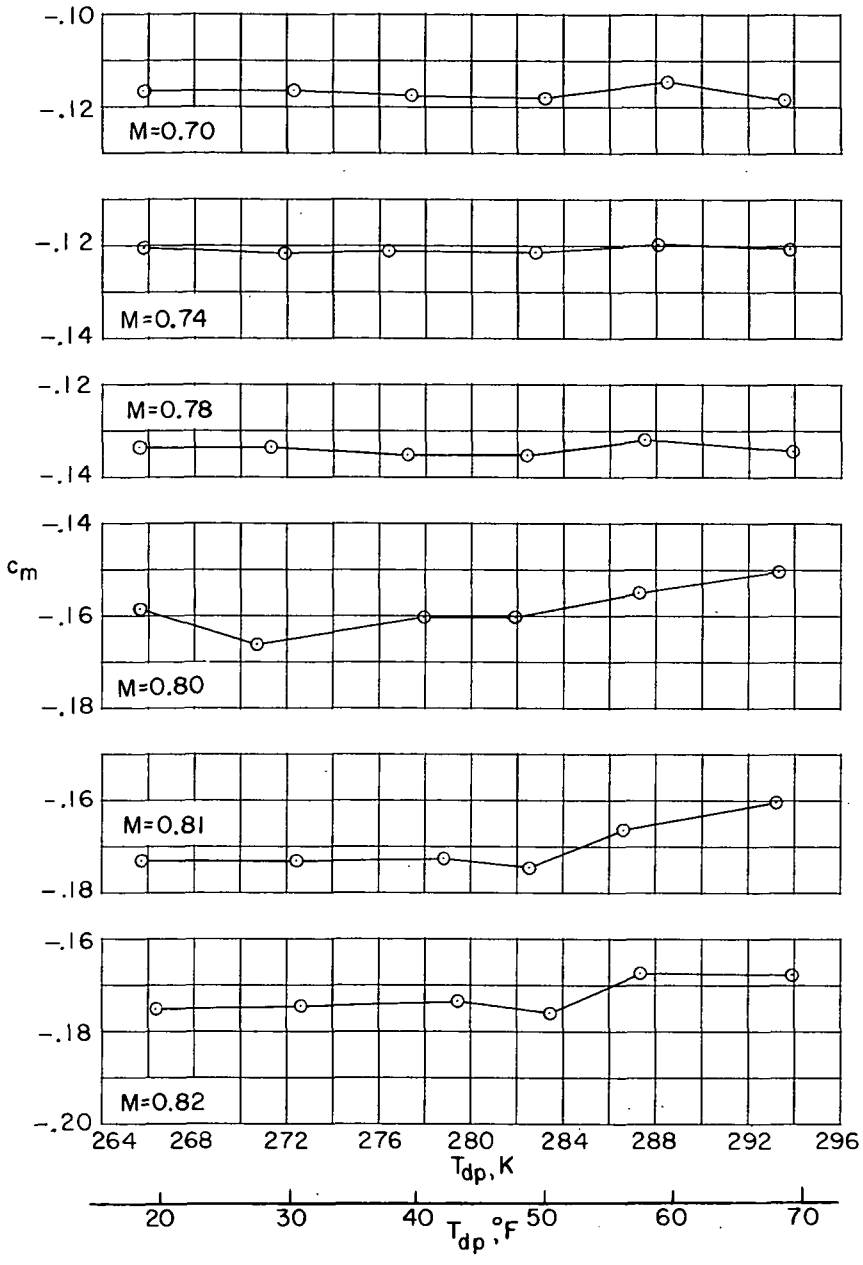

(b) $\alpha = 2.0^{\circ}$.

Figure 12.- Continued.

[redacted]

[redacted]

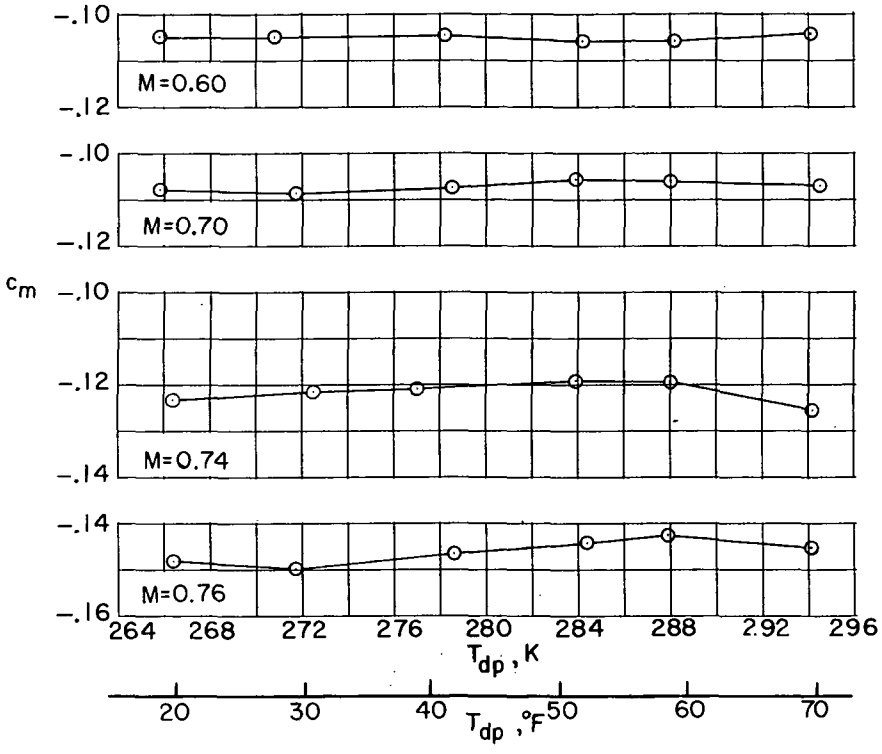

(c) $\alpha = 3.5^{\circ}$.

Figure 12.- Concluded.

[redacted]

[redacted]

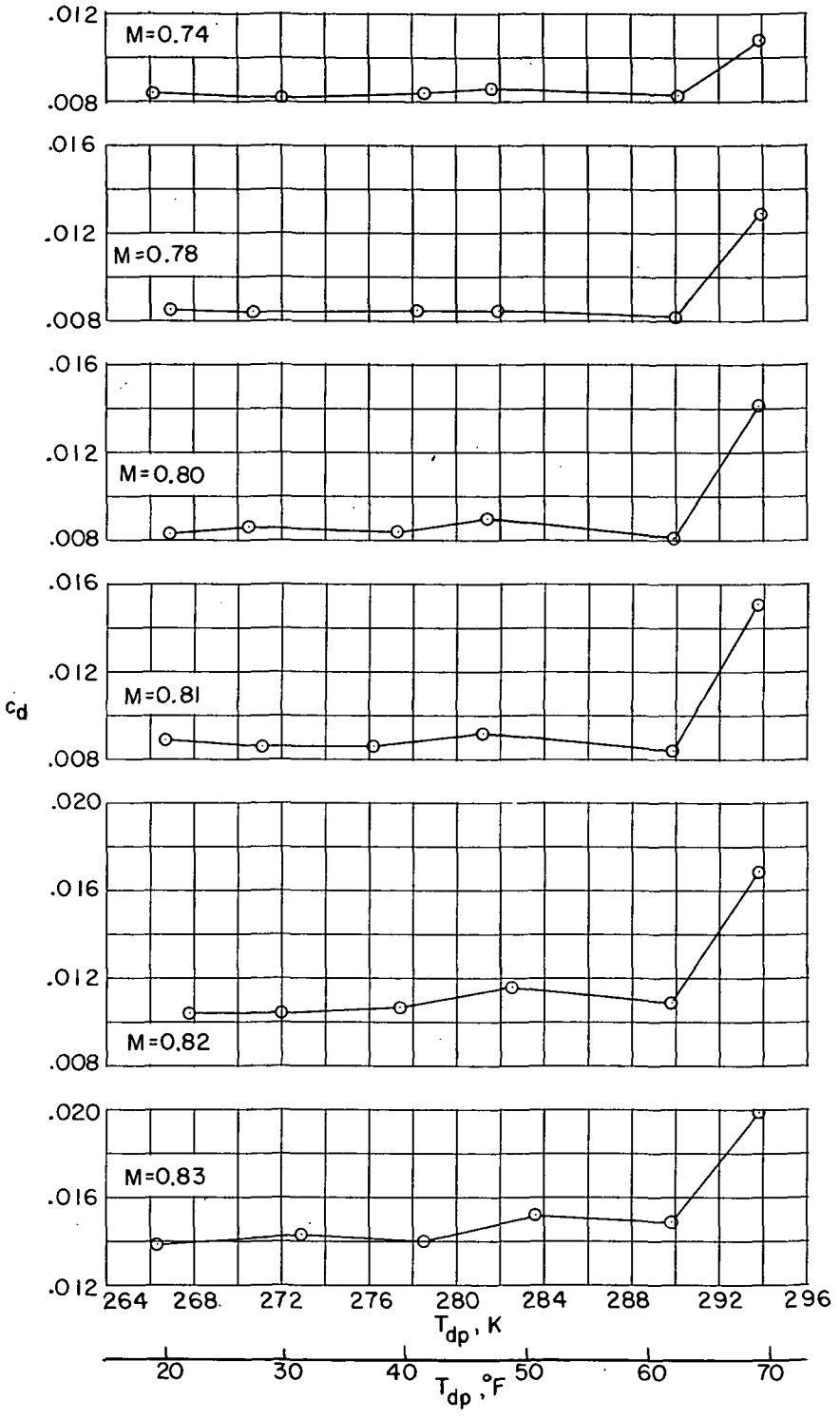

(a) $\alpha = 1.0^{\circ}$.

Figure 13.- Effect of wind-tunnel humidity on section drag coefficient.

[redacted]

[redacted]

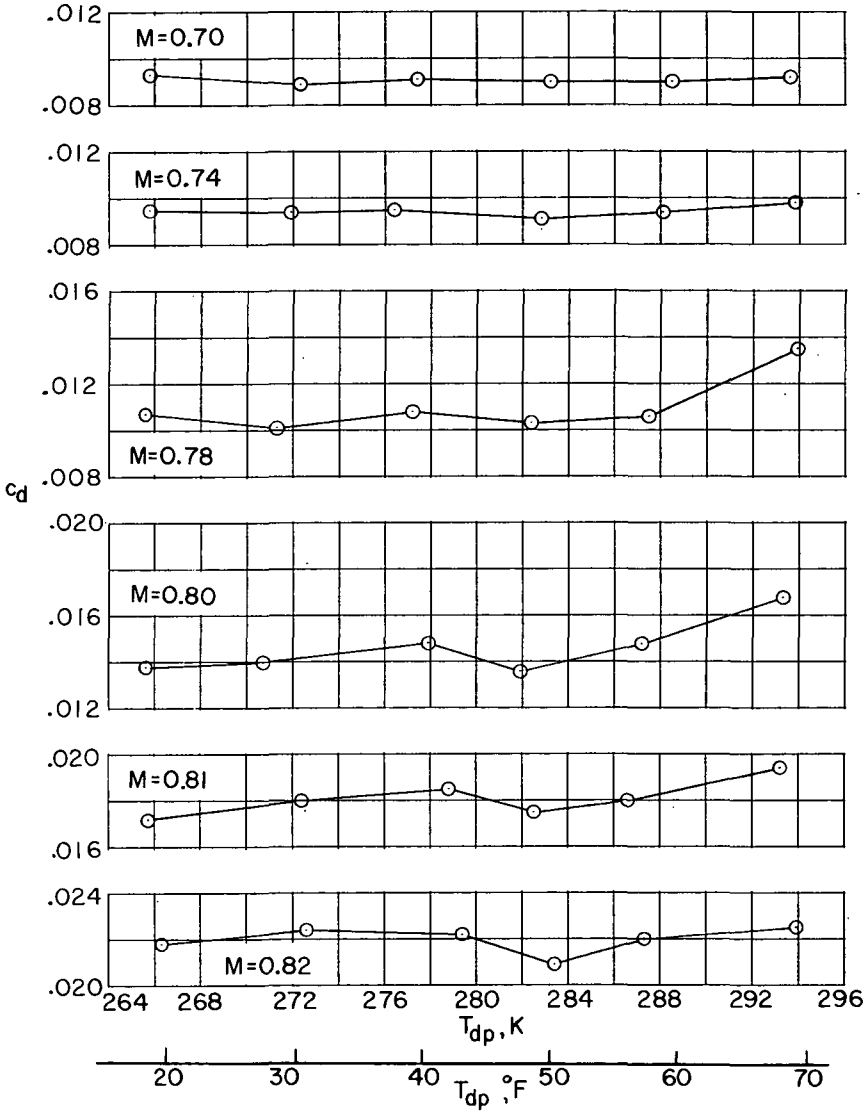

(b) $\alpha = 2.0^{\circ}$.

Figure 13.- Continued.

[redacted]

[redacted]

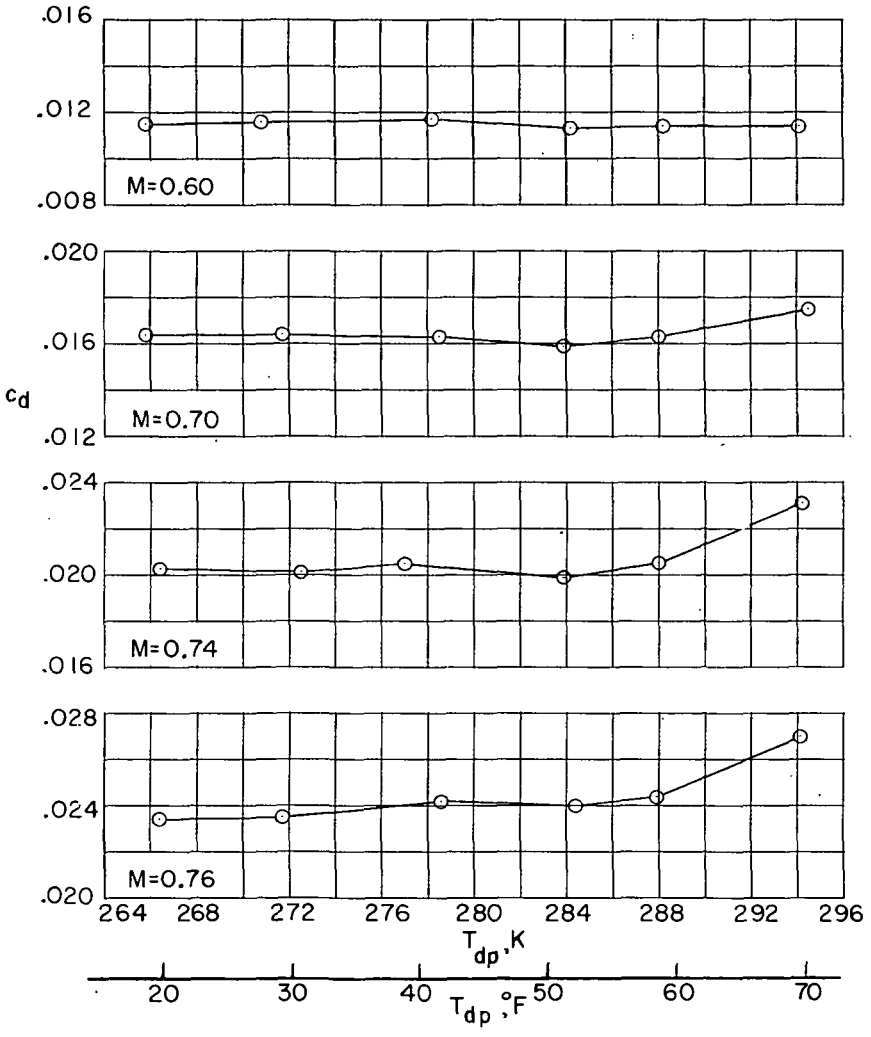

(c) $\alpha = 3.5^{\circ}$.

Figure 13.- Concluded.

[redacted]

"The aeronautical and space activities of the United States shall be conducted so as to contribute . . . to the expansion of human knowledge of phenomena in the atmosphere and space. The Administration shall provide for the widest practicable and appropriate dissemination of information concerning its activities and the results thereof."

—NATIONAL AERONAUTICS AND SPACE ACT OF 1958

NASA SCIENTIFIC AND TECHNICAL PUBLICATIONS

TECHNICAL REPORTS: Scientific and technical information considered important, complete, and a lasting contribution to existing knowledge.

TECHNICAL NOTES: Information less broad in scope but nevertheless of importance as a contribution to existing knowledge.

TECHNICAL MEMORANDUMS: Information receiving limited distribution because of preliminary data, security classification, or other reasons.

CONTRACTOR REPORTS: Scientific and technical information generated under a NASA contract or grant and considered an important contribution to existing knowledge.

TECHNICAL TRANSLATIONS: Information published in a foreign language considered to merit NASA distribution in English.

SPECIAL PUBLICATIONS: Information derived from or of value to NASA activities. Publications include conference proceedings, monographs, data compilations, handbooks, sourcebooks, and special bibliographies.

TECHNOLOGY UTILIZATION PUBLICATIONS: Information on technology used by NASA that may be of particular interest in commercial and other non-aerospace applications. Publications include Tech Briefs, Technology Utilization Reports and Notes, and Technology Surveys.

Details on the availability of these publications may be obtained from:

SCIENTIFIC AND TECHNICAL INFORMATION OFFICE

NATIONAL AERONAUTICS AND SPACE ADMINISTRATION

Washington, D.C. 20546

[redacted]